Development of a Tablet-Based Sensor for Point-of-Care Analyses Utilizing Pullulan-Stabilized Gold Nanoparticles

Muna Al-Kassawneh

A Thesis

In the Department of

Chemical and Materials Engineering

Presented in partial fulfillment

of the requirements for the degree

Master of Applied Science (Chemical Engineering) at

Concordia University

Montreal, Quebec, Canada

June 2023

© Muna Al-Kassawneh, 2023

CONCORDIA UNIVERSITY

School of Graduate Studies

This is to certify that the thesis is prepared,

By: **Muna Al-Kassawneh**

Entitled: **Development of a tablet-based sensor for point-of-care analyses utilizing pullulan-stabilized gold nanoparticles**

And submitted in partial fulfillment of the requirements for the degree of

Master of Applied Science in (Chemical Engineering)

Complies with the regulations of the University and meets the accepted standards concerning originality and quality.

Signed by the Final Examination Committee:

_____ Chair
Dr. Pantcho Stoyanov

_____ Examiner 1
Dr. Chunjiang An

_____ Supervisor
Dr. Sana Jahanshashi Anbuhi

Approved by: _____
Dr. Sana Jahanshashi Anbuhi Graduate Program Director

Date: 13th June 2023 _____ Dean of Faculty
Dean Mourad Debbabi

Abstract

Development of a tablet-based sensor for point-of-care analyses utilizing pullulan-stabilized gold nanoparticles

Muna Al-Kassawneh

The quickly expanding fields of nanotechnology and engineered nanomaterials helped solve serious issues that environments and human health suffer from for a long period of time. By accelerating the diagnoses and providing portable sensors that enable the demarcation of processes in biological systems to a previously unattainable degree, this nanotechnology will have an impact on clinical research and the detection of many analytes.

Tablet-based sensors have emerged as a powerful tool for point-of-care analyses, revolutionizing the way healthcare professionals diagnose and monitor patients. These sensors, when integrated with tablets, offer numerous advantages and play a crucial role in enhancing healthcare delivery. This advancement in tablet-based sensors for point-of-care analyses should include features such as; enabling healthcare professionals to conduct rapid and accurate diagnostics of various biomarkers, pathogens, and diseases by providing instant results. This real-time information allows for timely interventions and treatment decisions, reducing the need for sending samples to a laboratory and waiting for results, which can lead to delays in treatment. Importantly, the portability and compactness of tablets are highly required especially in remote or resource-limited settings. Furthermore, tablet-based sensors offer a cost-effective alternative to traditional laboratory-based diagnostics where the need for expensive laboratory equipment is eliminated, reducing the overall cost of diagnostics.

Additionally, portable tablet sensors do not require training, enabling healthcare professionals to perform tests without extensive specialized expertise. Notably, patients can interact with the sensors and see the results in real-time, empowering them to actively participate in their healthcare. This engagement fosters better patient-provider communication, improves treatment adherence, and increases patient satisfaction. Finally, tablet-based sensors not only aid in diagnostics but also facilitate continuous monitoring of patients by tracking vital signs, glucose levels, and drug concentrations. This routine monitoring helps healthcare professionals make

informed decisions, promptly adjust treatments, prevent health complications, and save the lives of millions of people.

Following nanotechnology and based on encapsulation of materials, in this work the fabrication of pullulan stabilized gold nanoparticles tablet (AuNPs-pTab) was used as a point-of-care (POC) analytical device utilizing pullulan-AuNPs solution (AuNPs-pSol) without the need for any extra ingredients, which were subsequently used as colorimetric sensors for glucose and cysteamine detection in human saliva and serum samples, respectively. This newly offered AuNPs-pTab sensor has demonstrated excellent peroxidase-like activity and gives an easy substitute for AuNPs solution with enhanced catalytic efficiency. Additionally, the AuNPs-pTab sensor is a promising platform for point-of-care devices due to its fulfillment of RE-ASSURED criteria (Real-time, Ease of specimen collection, Affordable, Sensitive, Specific, User-friendly, Rapid and robust, Equipment-free, and Deliverable to end users) which is considered of great importance in the field of diagnosis and detection. AuNPs-pTab sensor is an attractive tool that has the potential to open a new horizon in disease diagnosis due to its functionality in H_2O_2 detection which is a possible biomarker for many diseases. Even though a range of nanozymes has been reported to date for their enzyme-mimicking catalytic activity as a solution-based sensor. However, in remote areas, the need for portable, cost-effective, and one-pot preparation is extremely demanding. Therefore, this work is appealing to researchers working in nanotechnology, and the advancement of innovative portable bioassays as well as point-of-care devices.

List of publications and conference contributions

The following list of publications and conference proceedings shows my contribution to the annals of research in the course of this thesis. *The expected coming four publications are not presented in this thesis.*

- **Muna Al-Kassawneh**; Zubi Sadiq; Sana Jahanshahi-Anbuhi. Pullulan-stabilized gold nanoparticles tablet as a nanozyme sensor for point-of-care applications. Sensing and Bio-Sensing Research, 38, 100526, (**2022**). https://doi.org/10.1016/j.sbsr.2022.100526.

- **Muna Al-Kassawneh**; Zubi Sadiq; Sana Jahanshahi-Anbuhi. User-friendly and ultra-stable all-inclusive gold tablets for cysteamine detection. RSC Advances, 13, 19638-19650 (**2023**). https://doi.org/10.1039/D3RA03073C

- Zubi Sadiq, Seyed Hamid Safiabadi Tali, Hasti Hamijri, **Muna Al-Kassawneh,** Sana Jahanshahi-Anbuhi. Gold nanoparticles-Based Colorimetric Assay for Environmental Monitoring and Food Safety Evaluation. Critical Reviews in Analytical Chemistry, 1-36, (**2023**). https://doi.org/10.1080/10408347.2022.2162331

Conferences:

- **Muna Al-Kassawneh**; Zubi Sadiq; Sana Jahanshahi-Anbuhi. Pullulan-modified gold nanoparticles as an efficient tablet platform for colorimetric sensing of cysteamine. Oral presentation. Chemical Engineering Research Day, Montreal, Canada, March **2023**.

- **Muna Al-Kassawneh**; Zubi Sadiq; Sana Jahanshahi-Anbuhi. Tablet-based colorimetric sensor for the detection of glucose in real saliva using peroxidase mimicking the enzymatic activity of pullulan-stabilized gold nanoparticles. Oral presentation, Chemical Engineering Research Day, Montreal, Canada, March **2022**.

- **Muna Al-Kassawneh**; Seyed Hamid Safiabadi-Tali; Sana Jahanshahi-Anbuhi. Tablet-based sensor for on-site colorimetric detection of arsenic. Canadian Chemical Engineering research day, Montreal, Canada, October **2021**.

Acknowledgments

First and foremost, I would like to convey my heartfelt appreciation and acknowledge my supervisor, *Dr. Sana Jahanshahi-Anbuhi*, for her direction and boundless encouragement during my academic pursuit. Her scholarly counsel and expert tutelage have assisted me in laying firm groundwork for my study. In particular, her sagacity, foresight, commitment, and motivation have propelled me to surpass the boundaries of what I deemed unattainable.

I would also like to thank my committee members, *Dr. Pantcho Stoyanov* and *Dr. Chunjiang An* for being committee members and for the bright comments, suggestions, and valuable time.

I wish to thank my father *Dr. Osameh Al-Kassawneh*, and my mother *Mrs Doina Tecuceanu* for their encouraging words throughout my journey. All in all, I extend my deepest gratitude and appreciation to my family for their unconditional support and encouragement. Especially, my husband *Dr. Mohammad Masadeh* for encouraging me to pursue this degree which is simply impossible without his understanding, strength, and help. To my kids, *Rayan, Leen*, and *Larin* for their patience when I couldn't be with them due to lab work during stormy days. This achievement would not have been possible without their support and invaluable care.

My thanks are extended to my colleagues and friends at Concordia University, and the entire Anbuhi Research Group members; *Zubi Sadiq*, *Seyed Hamid Safiabadi-Tali*, and *Hasti Hajimiri* for the wonderful teamwork and friendship. Furthermore, many thanks go to all faculty members and staff who have impacted my development during this thesis. I am extending my sincere gratitude to the department chair *Prof. Alex de Visscher* and *Harriet Laryea* for their encouragement and inspiration. I would like to thank *Kerri Warbanski* for her invaluable help and time.

Moreover, I would like to acknowledge the Natural Sciences and Engineering Research Council of Canada (NSERC) for funding this work through a Discovery Grant and Concordia University for Concordia University Research Chair (CURC) funds for the development of Stable Bio/Chemosensors. I also thank the Centre for NanoScience Research (CeNSR) funded by Concordia University, Montreal, Canada to capture TEM images.

Table of Contents

List of Figures x
List of Tables xvii
Abbreviations xviii
Chapter 1. Introduction and Objective 1
1.1 Background 1
1.1.1 Glucose Detection 1
1.1.2 Cysteamine Detection 3
1.2 Motivation 6
1.2.1 Glucose monitoring 6
1.2.2 Cysteamine monitoring 8
1.3 Thesis objectives 10
1.4 Thesis organization 11
Chapter 2. Literature Review 12
2.1 Introduction 12
2.2 Nanozymes vs. natural enzymes 14
2.3 Peroxidase activity of different nanozymes 15
2.3.1 CdS NPs 16
2.3.2 Carbon-based NPs 16
2.3.3 CeO_2 NPs 16
2.3.4 Pd NPs 17
2.3.5 CuO NPs 18
2.3.6 Fe NPs 18
2.3.7 Pt NPs 19
2.3.8 AgNPs 20
2.3.9 AuNPs 20
2.4 AuNPs as peroxidase memetic nanozymes 21
2.5 Glucose detection 22
2.5.1 Available platforms for glucose detection 23
2.5.2 Samples for glucose detection 28
2.6 Common chemicals methods of AuNPs synthesis 32
2.6.1 Turkevich method 33
2.6.2 Burst Method 33
2.7 Green methods of AuNPs synthesis using polysaccharides 34

2.8 Some methods for Cysteamine detection 36
2.8.1 Cysteamine derivatization 36
2.8.2 Pivaldehyde 36
2.8.3 Bis (trimethylsilyl) trifluoroacetamide (BSTFA) 36
2.8.4 Ammonium 7-fluorobenzo-2-oxa-1,3-diazole-4-sulphonate (SBD-F) 36
2.8.5 Enzymatic assay 37
2.8.6 Ion-exchange chromotography 37
2.8.7 Fluorescent assay 37
2.8.8 Colorimetric method using Ellman's reagent 37
2.8.9 Ultra-high performance liquid chromatography-electrospray 37
2.8.10 Electrochemical detection of cysteamine 38
2.9 Inhibition of the peroxidase-like activity of AuNPs-pTab by amino acids 38
Chapter 3. Glucose Detection 40
3.1 Chemicals and materials 40
3.2 Synthesis of pullulan stabilized gold nanoparticles solution (AuNPs-pSol) 40
3.3 Preparation of pullulan stabilized gold nanoparticles tablet (AuNPs-pTab) 41
3.4 Preparation of McIlvaine and PB buffers 43
3.5 Preparation of catalytic activity test reagents 44
3.6 Procedure for glucose detection in buffer solution using AuNPs-pTab sensor 44
3.7 Procedure for glucose detection in artificial and real saliva using AuNPs-pTab 45
3.8 Preparation of interference materials with glucose assay using AuNPs-pTab sensor 46
3.9 Results and discussion 47
3.9.1 Principles of peroxidase-like activity of AuNPs-pTab 47
3.9.2 The characterization of the AuNPs-pSol and AuNPs-pTab 47
3.9.3 The mechanism of glucose assay using AuNPs-pTab sensor 53
3.9.4 Optimization of glucose assay using AuNPs-pTab sensor 54
3.9.5 The reaction kinetics of AuNPs-pTab using Michaelis Menten's model 57
3.9.6 Colorimetric detection of glucose using AuNPs-pTab sensor 58
3.9.7 Analysis of the interference studies 62
3.9.8 Application of AuNPs-pTab sensor in real saliva samples 62
3.9.9 Comparison of the performances of AuNPs-pTab and HRP in catalyzing the oxidation of TMB 64
3.9.10 The catalytic activity test analysis 64
3.9.11 The stability test of AuNPs-pTab 65
Chapter 4. Cysteamine Detection 67

4.1 Chemicals 67
4.2 Synthesis and fabrication of pullulan-stabilized gold nanoparticles 67
4.3 Sensing of cysteamine in Phosphate buffer 67
4.4 Sensing of cysteamine in artificial serum 68
4.5 Interference study for the colorimetric detection of cysteamine 69
4.6 Analysis of cysteamine in human serum 69
4.7 Results and discussion 69
4.7.1 Mechanism of cysteamine detection using pAuNPs-Tablet 69
4.7.2 Optimization of cysteamine ratio 72
4.7.3 Inhibition of the peroxidase-like activity of pAuNPs-Tablet in presence of cysteamine 73
4.7.4 Reaction kinetics in the presence and absence of cysteamine 73
4.7.5 Colorimetric detection of cysteamine in buffer and artificial serum 77
4.7.6 Selectivity analysis towards cysteamine detection 80
4.7.7 Determination analysis of cysteamine in human serum 80
Chapter 5. Conclusion and Future Work 82
Future work 85
References 86
Appendix 102
A1. Studying the difference between Alkali-treated and untreated pullulan 102
A2. Evaluation of AuNPs-pSol concentration on peroxidase-like activity for glucose detection 102
A3. Fabrication of AuNPs-pTab using 1 and 2% of pullulan (wt/v) 103
A4. Studying the effect of oven temperature in AuNPs-pTab formation 104
A5. Examining the effect of humidity in AuNPs-pTab 105
A6. Fabrication of AuNPs-pTab using 5% and 6% pullulan (wt/v) 106
A7. Encapsulation of TMB and McIlvaine buffer 107
A.8 List of formulas and software 107

List of Figures

Figure 2-1 Representation of the ping-pong mechanism (E: enzyme; E∗: enzyme intermediate; A: substrate one; B: substrate two; C: product one; D: product two. Adapted from (Jin et al. 2019). 13

Figure 2-2 Representation of colorimetric detection of glucose by using glucose oxidase (GOx) and GO-COOH-catalyzed reactions as reported by Song et al. Adapted from Ref. (Song et al. 2010). 16

Figure 2-3 Representation for TMB oxidation in the presence of H_2O_2 over CeO_2/NT-TiO_2. Adapted from (Zhao et al. 2015). 17

Figure 2-4 Sarcosine detection using Pd NPs. Sarcosine triggers a fast release of H_2O_2 by the catalytic action of sarcosine oxidase. Adapted from (Lan et al. 2014). 17

Figure 2-5 Representation of colorimetric detection of glucose by using GOx and Cu NCs catalyzed color reaction. Adapted from (Hu et al. 2013). 18

Figure 2-6 Based on the peroxidase activity of magnetic Fe_3O_4 nanoparticles, immunoassays. b) an immunoassay based on Fe_3O_4 MNPs. Anti-preS1 antibody identified the HBV preS1 antigen, and Fe_3O_4 MNPs conjugated to protein A, which binds exclusively to the Fc portion of the antibody, were used to detect it. c) An immunoassay for capture-detection. Target TnI in the sample was captured and separated using antibody modified Fe_3O_4 MNPs. When the substrate TMB was introduced when H_2O_2 was present, this combination interacted with the secondary anti-TnI antibody that had been coated on the plate. Adapted from (Gao et al. 2007). 19

Figure 2-7 Illustration of the formation of Pt-Ft NPs where Pt ions were reduced by adding $NaBH_4$ to yield zero-valent Pt NPs. Adapted from (Fan et al. 2011). 19

Figure 2-8 The TMB's oxidation process. Adapted from (Yuanjun Liu et al. 2014). 20

Figure 2-9 Detection of glucose using positively charged Chitosan-AuNPs. Adapted from (C. Jiang et al. 2017b). 21

Figure 2-10 Evaluation of the peroxidase-like activity of a) amino-modified, b) citrate-capped, and c) unmodified gold nanoparticles toward TMB as peroxidase substrate. Adapted from (S. Wang et al. 2012). 22

Figure 2-11 The principles of electrochemical sensors. Adapted from (Rahman et al. 2008). 23

Figure 2-12 The ZnO/AuNP/GOx/ITO electrode's electrochemical reaction and the produced sensor's design based on its 450 nm ZnO/AuNP/GOx/ITO wavelength. Adapted from (Tian et al. 2015). 24

Figure 2-13 H_2O_2 assay representation highlighting its key elements: (top) top view and (bottom) cross-section (A). The bar code enzyme test reaction technique for producing signals in a ladder bar pattern as dosage responses at various times (B). In this case, TMB was used as an enzyme substrate to produce a blue color in the presence of H_2O_2. Adapted from (Fung, Chan, and Renneberg 2009). 25

Figure 2-14 Plasmonic immunoassay readout via the naked eye. Sandwich immunoassay, avidin-biotin interaction, GOx-mediated oxidation of glucose, H_2O_2-induced oxidation of BDBA, and BDBA-triggered aggregation of citrate-capped AuNPs are all used to detect the target protein. Adapted from (Y. C. Yang and Tseng 2016). 26
Figure 2-15 Representation of the (IFE)-based assay for the histidine-glucose nanoclusters (His-GNCs) mediated fluorometric detection of glucose based on the self-catalyzed enlargement of AuNPs. Adapted from (Pezhhan, Akhond, and Shamsipur 2020b). 27
Figure 2-16 Representation of AuNPs-based colorimetric sensor with different sensing mechanisms. Adapted from (Sun et al. 2020b). 28
Figure 2-17 Movement of glucose molecules from blood vessels to saliva medium. 30
Figure 2-18 A summary of the features of AuNPs emphasizing their principal attributes. (A) Depiction of diverse configurations, dimensions, and hues of AuNPs; (B) modification of the surface of AuNPs using a range of ligands comprising diverse chemical groups; (C) various sorts of stabilizing forces and surface charge surrounding AuNPs; (D) synthetic methods grouped into top-down and bottom-up classes for generating AuNPs; (E) the primary classifications of sensors based on AuNPs. Adapted from (Sadiq et al. 2023). 34
Figure 3-1 Synthesis of AuNPs-pSol in a beaker with plastic cover. 41
Figure 3-2 Making pullulan-stabilized gold nanoparticle tablets (AuNPs-pTab) (AuNPs-pSol). First, treated pullulan was created by degrading it with NaOH for an hour at 70 °C. This step was followed by the addition of $HAuCl_4$ solution and heating the reaction media at 90 °C for another hour to synthesize AuNPs-pSol. Lastly, a 100 µL solution of AuNPs-pSol was pipette-out on a non-stick tray to cast AuNPs-pTab. The tablets took 24 hours to dry at room temperature, compared to 30 minutes in a 50 °C oven to dry them. 42
Figure 3-3 AuNPs-pTabs dried in different conditions. Oven drying at 60 °C for 30 minutes produced well-rounded circular shape tablets whereas ambient condition drying at room temperature produced quasi-round-shaped tablets. 42
Figure 3-4 Benedict's test was performed to discover the presence of reducing sugar in alkali-treated pullulan. The same procedure was followed using AuNPs-pSol or AuNPs-pTab. 44
Figure 3-5 Using an AuNPs-pTab sensor, glucose may be detected calorimetrically in saliva. First, the glucose assay involves, to release hydrogen peroxide, the saliva sample was treated with glucose oxidase (GOx) in PB solution at pH 7.4 for 15 minutes (H_2O_2). One AuNPs-pTab tablet was dissolved in TMB solution at pH 4.2, which was sustained by McIlvaine buffer, in the meantime. To see the visible color shift, both solutions were combined and incubated for 30 minutes. The H_2O_2-TMB system was employed in this procedure to assess glucose levels. The presence of glucose in saliva was detected by the blue color complex formed when the

peroxidase substrate TMB was oxidized by H_2O_2 in the presence of AuNPs-peroxidase pTab's mimicking activity (a diabetic condition). In the absence of glucose, the solution remained colorless or faint grey indicating a non-diabetic condition. 46

Figure 3-6 The reaction theory or process linked to glucose detection using synthetically produced AuNPs that are negatively charged. i) pullulan is oxidized when pullulan and NaOH are combined. ii) the emergence of a carboxylate group with a negative charge when gold nanoparticles are introduced to the mixture. iii) From AuNPs-pSol, AuNPs-pTab is formed. iv) the production of H_2O_2 from glucose when water, oxygen, and GOx are present. This process emits also gluconic acid. v) addition of AuNPs-pTab into a solution of TMB and H_2O_2 triggers the oxidation of TMB and the production of water. 47

Figure 3-7 A) AuNPs-pSol reaction development. a) after 10 minutes of adding $HAuCl_4$. b) after 20 minutes. c) after 30 minutes. d) after 40 minutes. e) after 50 minutes. f) after 60 minutes. and g) after 70 minutes. B) Absorbance at 520 nm corresponds to the peak development and particle growth of dAuNPs-pSol showing no change in absorbance was reported after 60 minutes..... 48

Figure 3-8 A) The influence of temperature on the particle size formation of AuNPs-pSol. a) the color of the solution was wine-red with a peak at 520 nm specifying smaller size particles. While b) purple color AuNPs-pSol is obtained with a peak at 540 nm signifying larger size particles. B) The hydrodynamic diameter vs the apparent zeta potential for AuNPs-pSol and AuNPs-pTab indicates almost the same features..... 49

Figure 3-9 The FTIR analysis of a) Pullulan powder. b) Alkali-treated pullulan. and c) AuNPs-pTab showing the different functional groups. 50

Figure 3-10 A) The absorption spectra of AuNPs-pSol and AuNPs-pTab show almost the same peak at 520 nm. B) Transmission electron microscopy (TEM) analysis of AuNPs-pTab showing the spherical shape and nanosize of particles. 50

Figure 3-11 The AFM images of the pAuNPs-Tablet particles show a height trace of the tablet surface. A) 2D image of height profile of pAuNPs-Tablet in an amplitude trace; B and C) 3D image of height profile of A; D) Height distribution as surface roughness and texture description along the black line area of image A. The average roughness was ~1.8 nm, the average maximum height of the roughness was ~10 nm, the average maximum roughness valley depth was ~6.6 nm, the maximum peak to valley roughness was ~18 nm and the waviness average was ~1.15 nm. The results confirmed that the strong binding between pullulan and AuNPs occurred. ... 51

Figure 3-12 Benedict's test shows the presence or absence of reducing sugars (α-hydroxy ketone and aldehyde functional groups) in pullulan polymer. The Benedict solution did not undergo any color change and remained blue (1) with untreated pullulan showing the absence of reducing sugars. The solution turned green (2) in the case of alkali-treated pullulan indicating the

presence of reducing sugars. Benedict's solution shows dark-green color (3) in the presence of AuNPs-pSol or AuNPs-pTab solution. 53

Figure 3-13 The catalytic activity of AuNPs-pTab and their comparison with AuNPs-pSol. A) The TMB-H_2O_2 solution was colorless and showed no absorption peak in the absence of AuNPs-pTab whereas an intense blue color formed having absorption peak at 652 nm in the presence of AuNPs-pTab. When 1M H_2SO_4 was added in the blue solution, the color turned to yellow having an absorption peak at 450 nm; B) The peroxidase-like activity of AuNPs-pTab was higher than AuNPs-pSol due to having concentrated AuNPs in TMB-H_2O_2 system. 54

Figure 3-14 Optimization of pH of TMB and temperature of the reaction condition. A) Effect of pH on the development of blue color; B) Effect of temperature on reaction time for TMB-H_2O_2 system showing the increase in peroxidase activity of AuNPs-pTab with increasing temperature (55-75 °C). 56

Figure 3-15 Optimization of TMB concentrations and number of AuNPs-pTabs for the detection of H_2O_2 and glucose. C) The effect of TMB concentrations in the development of blue color having absorbance maximum at 652 nm; D) The effect of a different number of tablets showing deeper blue color with increasing the concentration of AuNPs. 57

Figure 3-16 The reaction kinetics study for the TMB-H_2O_2 system involves AuNPs-pTab as a peroxidase catalyst. A) The absorbance at 652 nm was recorded for various TMB concentrations with 1M H_2O_2 over 33 minutes; B) The reaction velocity was evaluated by changing the concentration of TMB substrate with 1M H_2O_2. The points represent real experimental data while the curve was fitted with a non-linear function of the Michaelis–Menten equation. 58

Figure 3-17 Detection of H_2O_2 using AuNPs-pTab sensor. A) Absorption spectra showing a gradual increase in peak intensity with increasing H_2O_2 concentration; B) The absorbance at 652 nm showing a linear relationship between the first six peak values over-concentration of H_2O_2. . 59

Figure 3-18 Detection of glucose in buffer using AuNPs-pTab sensor. A) Glucose detection in PB using AuNPs-pTab and the absorption spectra at a variable concentration of glucose (5-500 μM); B) The calibration curve was obtained using an average absorbance of three tests which shows the relationship between the relative absorption intensities versus the concentration of glucose. The linear relationship in the first five concentrations of glucose. The error bars represent the standard deviation of three independent measurements. 60

Figure 3-19 Detection of glucose in an artificial saliva sample. A) Absorption spectra of variable concentration of glucose 0.5-500 μM in artificial saliva; B) The calibration curve showing the relationship between relative absorption intensity (blue color intensity) versus the concentration of glucose. The error bar signifies the standard deviation of three independent measurements. The linear relationship in the first four concentrations of glucose. 61

Figure 3-20 The interference study used glucose, fructose, maltose, lactose, and buffer solution. The higher absorption is detected for glucose which implies the sensor specificity for glucose detection. Testing procedure: 300 uL TMB+330 uL citrate buffer+1 tablet of AuNPs-pTab. In another tube, 20 uL glucose oxidase+(1 mM) of 80 uL (glucose, fructose, maltose, lactose, Mcilvaine buffer) + 200 uL PB (pH 7.4). 62

Figure 3-21 Detection of glucose in real saliva samples. The absorption spectra of different glucose levels in real saliva samples and inset show color change of wells with the presence and absence of glucose. 63

Figure 3-22 A comparison between peroxidase mimic activity of AuNPs-pTab and horseradish peroxidase (HRP) in catalyzing the TMB-H_2O_2 system. The absorbance at 652 nm shows that the artificial nanozyme AuNPs-pTab (>6 months old tablets) catalytic activity was similar to the natural enzyme HRP. The error bar represents the standard deviation of three independent measurements (n=3). 64

Figure 3-23 The catalytic activity test for different concentrations of AuNPs-pTab using the conversion of 4-4-nitrophenol (yellow color) into 4-aminophenol (colorless) using sodium borohydride. A) a) quarter tablet, b) half tablet, c) three-quarter tablet, and one tablet of AuNPs-pTab. B) The corresponding absorbance spectra show a high catalytic activity (high conversion of 4-nitrophenol (yellow color) into 4-aminophenol (colorless) in the presence of one tablet of AuNPs-pTab. While the catalytic activity is less when using quarter AuNPs-pTab. 65

Figure 3-24 The stability profile of AuNPs-pTab over sixteen months shows a gradual decrease in the stability of AuNPs. 66

Figure 4-1 The UV-vis spectra of pAuNPs-Tablet in the presence of (200 and 500 μM) cysteamine. A 200 μM of cysteamine could not cause the aggregation of pAuNPs-Tablet while 500 μM caused the aggregation. Considering the higher concentrations of cysteamine cause aggregation of pAuNPs-Tablet based on LSPR, the peroxidase-like activity method is the resolution for cysteamine detection to achieve lower LoD. 70

Figure 4-2 Representation of the synthesis of pAuNPs-Solution/pAuNPs-Tablet and the mechanism of cysteamine detection. A) The production of tablets containing gold nanoparticles stabilized with pullulan (pAuNPs-Tablet) was achieved by using pAuNPs-Solution. To start, pullulan was treated with NaOH-mediated degradation at a temperature of 70 °C for 60 minutes. The next step involved adding a solution of $HAuCl_4$ and heating the reaction mixture to 90 °C for another 60 minutes to synthesize the pAuNPs-Solution. Finally, pAuNPs-Solution was pipetted onto a non-stick tray to create the pAuNPs-Tablet. The tablets were then dried for 30 minutes in an oven at 50 °C or left to dry at room temperature for 24 hours. B) The mechanism of peroxidase-like activity inhibition in the presence of cysteamine. In the absence of cysteamine, the active

sites of pAuNPs surface are free so that TMB can attach easily to pAuNPs surface. Consequently, the charge transfer from the surface of pAuNPs to the H_2O_2 generates the radical $^{\bullet}OH$ resulting in the formation of oxidized TMB (oxTMB) (blue color). Upon incubating pAuNPs with cysteamine, a pAuNPs-cysteamine complex is formed which blocked the active sites on the surface of pAuNPs. When TMB is added because the surface is blocked with cysteamine, no charge transfer can leave the surface of pAuNPs causing the inhibition of the formation of oxTMB. Hence, the colorless-grey color will not develop into a blue color..... 71

Figure 4-3 Inhibition effect using various ratios (25, 50, 75, and 100) µL of 200 µM of cysteamine showing the maximum inhibition occurred using 100 µL cysteamine. Hence, this ratio was applied to the rest of the tests. 72

Figure 4-4 The TMB response in the presence and absence of cysteamine and the effect of using sulfuric acid (H_2SO_4) as a color indication for oxTMB. In the absence of cysteamine and the presence of pAuNPs-Tablet, a high absorbance peak was observed at 652 nm. While no peak was observed when 200 µM of cysteamine was added to the system. The effect of using H_2SO_4 on TMB + pAuNPs-Tablet and TMB + pAuNPs-Tablet + cysteamine. The TMB color was shifted to 450 nm in the system containing TMB + pAuNPs-Tablet. Whereas, adding H_2SO_4 to TMB + pAuNPs-Tablet + cysteamine did not cause any color change since the oxTMB was not presented in the system. 73

Figure 4-5 The reaction kinetics in the presence of (0, 60, and 200 µM) of cysteamine. A) The kinetics study shows a detection time of 20 min. The reaction in the absence of cysteamine converted into a complete blue color (higher absorbance) while the solution containing 60 µM cysteamine shows less blue color intensity (less absorbance). On the other hand, no color transformation was achieved using 200 µM cysteamine which confirms the absence of oxTMB. B) Michaelis-Menten parameters were obtained when using (0, 60, and 200 µM) of cysteamine according to three replicas. A reversible (competitive) mechanism (blue squares) was observed when using 60 µM of cysteamine while the inhibition was irreversible (non-competitive) using 200 µM of cysteamine (red triangles). 75

Figure 4-6 The FTIR analyses after centrifugal and washing of the pAuNPs-Tablet-cysteamine solutions. The FTIR spectrum of the washed pAuNPs-Tablet + 200 µM cysteamine exhibited extra strong peaks arising from the -SH bend and -NH stretch due to the presence of pAuNPs-Tablet-cysteamine complex even after washing the catalyst. The absence of -SH and -NH peaks in the pristine pAuNPs-Tablet + 60 µM cysteamine indicates the pAuNPs-Tablet-cysteamine complex formation is dependent on cysteamine concentration. 75

Figure 4-7 The DLS analyses of the pAuNPs-Tablet-cysteamine complex. A) The ζ-potential analysis displays a decrease in ζ-potential value from-9 to -2 mV. B) An increase in the hydrodynamic

diameter from 91.77 nm with PDI% of 24% to 785 nm with 46%, respectively indicating the formation of a complex of nanoparticles. 76

Figure 4-8 The catalytic activity test using the conversion of 4-Nitrophenol (4-NP) (yellow) to 4-Aminophenol (4-AP) (colorless) in the presence of pAuNPs-Tablet. A) A higher catalytic activity was observed using 100 μM pAuNPs-Solution to cast pAuNPs-Tablet. B) The catalytic activity in the presence and absence of 200 μM cysteamine. The conversion of 4-NP into 4-AP was completed using pAuNPs-Tablet. While the conversion was blocked in the presence of 200 μM cysteamine. C) The reaction rate in the presence of (0, 60, and 200 μM) cysteamine shows a very fast conversion when 0 μM cysteamine. Whereas a slower reaction was noticed in the presence of 60 μM cysteamine. Almost no conversion was achieved in the case of 200 μM cysteamine which was comparable to the color of the blank. D) The Langmuir-Hinshelwood model to calculate the apparent reaction constant (k_{app}) shows a fast reaction in the case of 0 μM cysteamine while a very low (k_{app}) was observed in 200 μM cysteamine indicating that pAuNPs-Tablet-cysteamine complex prevented the conversion of 4-NP to 4-AP. 77

Figure 4-9 Detection of cysteamine in phosphate buffer and artificial serum. A) UV-vis spectra of TMB in phosphate buffer pH=7 in the presence of a different concentration of cysteamine (0-200 μM). B) The calibration curve was obtained using various concentrations of cysteamine. C) The linear range of the curve shows good linearity between (0-40 μM) of cysteamine. The LoD was calculated using the 3σ/slope method and was found to be 69 μM. D) UV-vis spectra of TMB in artificial serum pH= 6.8 in the presence of a different concentration of cysteamine (0-200 μM). E) The calibration curve was obtained using various concentrations of cysteamine. F) The linear range of the curve shows good linearity between (0-40 μM) of cysteamine. The LoD was measured using the 3σ/slope method where the value was 80 μM. $\Delta A = (A_{652\ nm,\ absence}) - (A_{652\ nm,\ cysteamine})$. 79

Figure 4-10 The interference studies and the real sample testing. A) The selectivity of the sensor in the presence of other amino acids shows that other amino acids do not interfere with the sensor specificity for cysteamine. B) UV-vis peaks at 652 nm of the samples before spiking indicating a higher peak for (sample 1: healthy individual) while a decrease in peaks was observed for samples 2,3, and 4 which are samples taken from patients with cystinosis. (n=3). 81

Figure 4-11 Analytical performance of the tablet-based sensor in real human serum samples. The calibration curve was attained by testing the sensor with the known concentrations of 60, 70, and 100 μM cysteamine in real human serum samples. A Hill function was fit to the whole data with an R2 > 0.99, showing the compatibility of the data with a standard saturation model. Each data point is the mean ± standard deviation of the replications (n = 3). 81

List of Tables

Table 1-1 The normal and diabetic levels of glucose concentrations in (μM) in unstimulated saliva in human adults (male and female)(Jurysta et al. 2009). 3
Table 1-2 Evaluation of the colorimetric detection performance of AuNPs-pTab with other peroxide-like activity sensors for H2O2 and glucose detection. 7
Table 1-3 Comparison between this method and some previously reported methods employed in the detection of cysteamine. 9
Table 2-1 A comparison between natural enzymes and nanozymes. 15
Table 2-2 Comparison between the chemical and green methods of AuNPs synthesis. 35
Table 3-1 The results of glucose levels in real saliva samples (n = 3) are presented here. 63

Abbreviations

WHO	World health organization
AuNPs	Gold nanoparticles
AuNPs-pSol	Gold nanoparticles pullulan solution
AuNPs-pTab	Gold nanoparticles pullulan tablet
pAuNPs-Solution	Pullulan gold nanoparticles solution
pAuNPs-Tablet	Pullulan gold nanoparticles tablet
PB	Phosphate buffer solution
McIlvaine buffer	Phosphate-ctrate buffer solution
H_2O_2	Hydrogen peroxide
Hydroxyl radical	$^{\bullet}OH$
TMB	3,3′,5,5′-tetramethylbenzidine
ABTS	2,2′-azino-bis-(3-ethylbenzothiozoline-6-sulfonic acid)
OPD	o-phenylenediamine
NaOH	Sodium hydroxide
$NaBH_4$	Sodium borohydride
%R	Recovery percentage
SD	Standard deviation
%RSD	Relative standard deviation percentages
DMSO	Dimethyl sulfoxide
v_{max}	Maximum velocity
K_m	Michaelis Menten's constant
HRP	Horseradish peroxidase
GOx	Glucose oxidase
CdS NPs	Cadmiums nanoparticles
CeO_2 NPs	Cerium oxide nanoparticles
Pd NPs	Palladium nanoparticles
CuO NPs	Copper (II) oxide nanoparticles
Fe NPs	Iron nanoparticles
Pt NPs	Platinium nanoparticles
AgNPs	Silver nanoparticles
°C	Degree of Celsius

DI	De-ionized water
NaCl	Sodium chloride
UV-Vis	Ultraviolet light visible
TEM	Transmission electron microscopy
λ	Wavelength
sec	Second
min	Minutes
h	Hour
g	Gram
mL	Milliliter
mM	Millimolar
mg	Milligram
µg	Microgram
µM	Micromolar
mol	Mole
wt/v	Weight per volume

Chapter 1. Introduction and Objective

In this chapter, a brief introduction to the challenges associated with glucose and cysteamine detection is presented. This section continues with the objectives of this research project and ends up with the thesis outline.

1.1 Background

1.1.1 Glucose Detection

Point-of-care (POC) devices propose simple, speedy, accurate, low-cost, and early detection of a wide range of biomarkers such as glucose (Rossini et al. 2021), cholesterol (Alle et al. 2022), creatinine (Liang et al. 2022), and uric acid (Li et al. 2021) which help to prevent many diseases such as hyperglycemia (Jiang et al. 2021), cardiovascular diseases (Packard et al. 2021), chronic kidney diseases (Lin et al. 2021), and hypertension (Piani, Cicero, and Borghi 2021), respectively. Based on the variable size and sensing capabilities, numerous attractive detection platforms have been introduced in the past such as; microfluidic lateral flow paper-based assays (Oyewunmi, Safiabadi-Tali, and Jahanshahi-Anbuhi 2020; H. Zhang et al. 2022; Iles et al. 2022) and intelligent detection devices (Zheng et al. 2021; Khor et al. 2022; Fiore et al. 2022). Still, some challenges are associated with these platforms; for instance, microfluidic lateral flow paper-based assays suffer sample leakage complications, and less sensitivity (Qin et al. 2021) while intelligent detection devices are costly and less user-friendly because of the difficult constructions and sophisticated data analysis (Zheng et al. 2021). That is why there is a need to establish new platforms which address the current challenges of point-of-care devices whilst maintaining the ASSURED criteria. A new transformation of this criteria has been established newly which added the RE part in front of the ASSURED to form the word: (RE-ASSURED). The new RE is established as R: reader or mobile phone to provide the required data to decide about clinical management devices that facilitate the transportation of data. While E: ease of specimen collection which is designed for non-invasive collection of samples (Das et al. 2021). Therefore, researchers are keen to establish novel platforms that use non-invasive human specimens for disease diagnostics in clinical settings.

Recently, many platforms have been established for analyte detection as solution-based sensors. It is well known that analyte detection in the solution phase is more sensitive as compared to a solid-supported system, so reagent encapsulation strategies have been opted which offer quick detection

in a solution phase by releasing encapsulated reagents at the time of testing (Jahanshahi-Anbuhi et al. 2014a; Esfahani et al. 2021). This hybrid approach not only offers a sensitive detection method but also merges the advantageous features of point-of-use analytical devices. Thus, scientists and researchers are fascinated by research that can discover more new platforms and facilitate disease detection to serve end users.

The daily life application of POC devices is to monitor glucose levels in blood using a glucometer. A high concentration of blood glucose is correlated with diabetes; a disorder when insulin production in the individual is not adequate to convert glucose into energy (World Health Organization 2016). As such, diabetes mellitus triggers many health problems such as hyperglycemia and microvascular disease of the eyes and kidneys as well as clinical neuropathies (Balaji, Duraisamy, and Santhosh Kumar 2019). According to the World Health Organization, more than 422 million cases, and 1.5 million deaths are associated with diabetes worldwide till 2022 (World Health Organization 2016). Consequently, early detection and frequent observing of glucose levels in several body fluids such as blood, saliva, sweat, tear, and urine are of great significance to be informed of human health conditions. As known, glucose monitoring in a blood sample is not attractive or user-friendly because of needle fear and related pain which restrict its application in children and elderly patients (Cemeroglu et al. 2015; Al Hayek et al. 2017; Al Hayek, Robert, and Al Dawish 2017). On the other hand, glucose detection in sweat, tears, and urine are challenging because of complicated procedures to extract the sweat after long hours of exercising, small tear volumes after using tear enhancers or eye drops, and the need for a private space to take the urine sample which is difficult in public places. Therefore, these shortcomings negatively influence diabetes management and raise the need for a non-invasive and user-friendly detection assay.

In this context, glucose detection in saliva samples fascinates many researchers since the collection of saliva is easy, effortless, and suitable for a variety of populations. Besides, the correlation between mean salivary glucose concentration and mean blood glucose level has been studied recently which indicates glucose can easily pass from the blood vessel membranes of the mouth through the trans-cellular and para-cellular routes to saliva fluid as shown in Table 0-1 (Y. Cui et al. 2022; Jurysta et al. 2009). Consequently, the detection of glucose in the saliva is considered an appealing alternative for a blood sample for diabetes monitoring.

Table 0-1 *The normal and diabetic levels of glucose concentrations in (μM) in unstimulated saliva in human adults (male and female)*(Jurysta et al. 2009).

Gender	Normal	Diabetic
Male	78.7 ± 9.2	201.9 ± 34.9
Female	80.4 ± 7.9	175.0 ± 22.3

1.1.2 Cysteamine Detection

Cysteamine, a type of amino acid medication that is used to treat cystinosis, performs by interacting with crystalline cysteine to reduce the buildup of intraliposomal cystine (M. Besouw et al. 2007). According to some reports, one case per 100,000/200,000 live births suffers from cystinosis(Emma et al. 2014). In living organisms, the neuronal structure and/or function can be maintained due to cysteamine's neuroprotective and antioxidation properties to treat neurodegenerative diseases (Gibrat and Cicchetti 2011)(Wood, Khan, and Moskal 2008). The concentration of cysteamine has been documented to be in the low micromolar range in organs such as the liver, kidney, and brain (Gallego-Villar et al. 2017).

Elevated levels could develop side effects such as Ehlers−Danlos syndrome, high alkaline phosphatase, ulcers/bleeding in the gastrointestinal tract, and idiopathic intracranial hypertension (IIH) which can cause ringing in the ears, loss of vision along with dizziness and nausea (M. T. P. Besouw et al. 2011). Therefore, the daily intake of cysteamine for patients with cystinosis based on body weight is (1.3-1.95) g/m^2/day distributed over 4-2 doses (Franzin et al. 2022)(Bouazza et al. 2011). However, serum/plasma cysteamine levels in healthy cystinosis patients should be monitored to be ~150 μM after 30-60 minutes of cysteamine digestion(Stachowicz et al. 1998a). Due to the adverse effects of cysteamine in clinical settings, it is critical to improve an economic, transportable, and easy-to-operate bioanalytical approach for cysteamine detection in serum samples. Nowadays, cysteamine is used to treat a wide range of neurodegenerative diseases such as Parkinson's (Aminabad et al. 2022), Huntington's (T.-Y. Wei et al. 2018), and Alzhamier's (Zhang et al. 2023), increasing the chance for cysteamine overdoses. Thus, establishing a sensor for cysteamine monitoring will help prevent the side effects of consuming this drug.

The detection and quantification of cysteamine is a challenging task due to the lack of a chromophore in its structure and its susceptibility to oxidation before or during the analysis (Atallah, Charcosset, and Greige-Gerges 2020). Consequently, several conventional methods have been used to detect cysteamine such as electrochemical (Raoof, Ojani, and Chekin 2009), HPLC (Ogony et al. 2006), and liquid chromatography(Y. Kim and Na 2019). However, these platforms suffer from some disadvantages such as expensive, required multi-step preparations, and the need for trained workers to perform the tests. Hence, the detection of cysteamine using a tablet-based sensor is considered an attractive substitute for the previous detection methods.

Recently, significant focus has been given to colorimetric techniques that rely on the localized surface plasmon resonance (LSPR) feature of gold nanoparticles (Yu et al. 2021). The ease of use, and relatively quick signal reading make colorimetric methods appealing. The interaction between analytes and nanoparticles affects the color difference between dispersed and aggregated nanoparticles, which is fundamental to colorimetric detection (Li et al. 2009). Nonetheless, accurate control of nanoparticle size and inter-particle distance, which are challenging variables in LSPR-based colorimetric techniques (Chang et al. 2017), is necessary to generate colorimetric signals for analyte detection. Additionally, the stability of nanoparticles linked to aggregation is another limitation of colorimetry based on the LSPR of gold nanoparticles (Aldewachi et al. 2018).

Consequently, catalysis-based colorimetric techniques for identifying various analytes are gaining interest as they overcome these limitations (Yan et al. 2020). This is because, the catalytic performance of gold nanoparticles is usually monitored calorimetrically via the redox properties of gold, which allows it to act as an electron acceptor and donor, facilitating the transfer of electrons between H_2O_2 and the substrate. The production of a single type of product from this reduction reaction simplifies monitoring the reaction's progress through UV-visible spectrophotometric measurements (Qiu, Ma, and Hu 2014).

A variety of substances are available for the fabrication of POC devices as many detection parameters such as sensitivity, speed, and accuracy of the assay are highly dependent on the choice of functional material. Among different substances, nanomaterials particularly gold nanoparticles (AuNPs) are considered smart sensing materials due to tunable physical and chemical characteristics suitable for many different detection methods (Marin, Nikolic, and Vidic 2021; Qiao and Qi 2021). However, the catalytic property of AuNPs also called ‘nanozyme’ offers an

easy and user-friendly detection method for several analytes analysis. The nanozyme activities of AuNPs is due to its catalytic capability to oxidize the chromogenic agent at the interface of nanoparticles (S. Liu, Leech, and Ju 2003). Common chromogenic substances are 3,3′,5,5′-tetramethylbenzidine (TMB), 2,2'-azino-bis(3-ethylbenzothiazoline-6-sulphonic acid (ABTS), and o-phenylenediamine dihydrochloride (OPD) that are crucial to generate color read-out in nanozyme sensors. Many AuNPs-based nanozyme sensors such as chitosan-AuNPs(C. Jiang et al. 2017a), cytidine-Au nanoclusters (C. Jiang et al. 2021), and AuNPs coated with mexene nanosheets (X. Cui et al. 2022) have been used for disease diagnosis due to their high sensitivity and comparable activity to natural enzymes like horseradish peroxidase (HRP), galactose oxidase (GOase), and xanthine oxidase (XO) which has restricted use due to their high cost and stringent storage requirements (Jeevanandam et al. 2022; Alvarado-Ramírez et al. 2021).

The intrinsic peroxidase-like activity of AuNPs is dependent on surface modifications that make nanoparticles either positively or negatively charged. Citrate-capped AuNPs are negatively charged that show high peroxidase activity as compared to positively charged amino-modified AuNPs (S. Wang et al. 2012). The negative surface charge significantly increases the affinity of nanoparticles for peroxidase substrate (TMB) through electrostatic attraction in slightly acidic conditions (Yanping Liu et al. 2014) compared to positively charged AuNPs. Besides this, AuNPs and TMB remain functional over a wider temperature range (5-90 °C) which makes them attractive materials over natural enzymes (Yanping Liu et al. 2014). Additionally, negatively charged AuNPs can be easily synthesized with high colloidal stability and monodispersity using natural biocompatible ligands like plant extracts (R. S. Li et al. 2016a) and carbohydrates such as chitosan (F. Li et al. 2021), dextran (Tang, Fu, et al. 2018), and pullulan (Laksee et al. 2017a). Among other carbohydrates, pullulan is favorable due to its highest preserving ability which can prolong the shelf life of materials. Pullulan is used for the synthesis of gold nanoparticles solution (AuNPs-pSol) where synthesized pullulan is employed as a reducing, stabilizing, capping, and encapsulating agent (Laksee et al. 2017a). The alcoholic groups (C-OH) in the polymeric chain of pullulan are oxidized to carboxylate functionality ($C\text{-}OO^-$), resulting in the formation of negatively charged AuNPs (Laksee et al. 2017a). This negatively charged AuNPs-pSol can be used to detect many diseases and drugs using a positively charged substrate for color readout.

1.2 Motivation

1.2.1 Glucose monitoring

The common route for glucose monitoring is by using the glucometer based on donating blood samples. This method suffers from many disadvantages such as the machine being expensive and hard to use when it comes to a specific group of people such as elders and children. Furthermore, the huge emotional and psychological impacts when donating blood samples are still the main concern for many diabetic patients. On the other hand, saliva samples are considered convenient, cost-effective, suitable for frequent monitoring, and reduced risk of infection. Collecting saliva samples is a simple and quick process that can be done almost anywhere. Usually, patients can collect their own saliva samples and do not need to go to a medical facility or have a healthcare professional collect the specimen for them.

In addition, saliva samples collections are cost-effective and less expensive compared to blood samples. There is less waste and less need for specialized equipment, which can make the overall process more economical. Moreso, saliva samples can be collected more frequently than blood samples, which can be beneficial for individuals who need to monitor their glucose levels regularly. Because saliva collection is a non-invasive procedure, there is a reduced risk of infection or contamination, which can be important for individuals who have compromised immune systems. Therefore, to meet the RE-ASSURED criteria, prevent the use of painful needles, and reduce fear while monitoring glucose levels among children and elders, many methods have been established in the literature to monitor blood glucose levels. However, these methods present accurate results while requiring expensive instruments, multi-step preparation, and need trained labor to perform the tests. Nonetheless, the large amount of samples for operation is considered challenging when dealing with other human specimens such as tears, sweat, and saliva which do not allow for dynamic POC testing. These features limit the use of these testing methods in remote areas and some developing countries. However, testing can be made easily and readily available by fabricating simple, portable, and cheap devices that can also perform the required test with high accuracy. Thus, the development of a tablet-based analytical device will be of great advantage for daily glucose monitoring.

Table 0-2 Explains why this work is distinctive by comparing other recently available platforms for glucose detection. Most of the glucose sensors are not portable and are hard to handle and perform while AuNPs-pTab is completely portable and one person can perform the test.

Table 0-2 *Evaluation of the colorimetric detection performance of AuNPs-pTab with other peroxide-like activity sensors for H_2O_2 and glucose detection.*

Materials	Analyte	Sample	LOD	Linear range	Concerns	Ref.
IrO_2@NiO nanowires	glucose	saliva	0.31 µM	0.5 µM to 2.5 mM	Need multistep synthesis and complicated equipments to take the reading, solution-based sensor	(J. Wang et al. 2016)
µPADs	glucose	saliva	27 µmol L^{-1}	0-2.0 mmol L^{-1} and 0-400 µmol L^{-1}	Need multi-layer µPAD paper preparation	(de Castro et al. 2019)
CuO	glucose	saliva	0.41 µM	(5µM-0.225 mM)	Need electrochemical work station, solution-based sensor	(Chakraborty et al. 2020)
cobalt phthalocyanine-carbon nanotube-reduced graphene oxide	glucose	saliva	0.12 µM	(0.30 µM - 0.50 mM) and (0.50–5.0 mM)	Multistep preparation of the sensing electrode needs specific equipment to take the readings	(Adeniyi et al. 2021)
AuNPs-pTab	**H_2O_2 and glucose**	**saliva**	**163.04 µM**	**0-5 µM**	**-**	**This work**

To offer low-cost analytical testing platforms for POC analysis, AuNPs have, over the last decade, become common in the research community. These solution-based sensors use AuNPs as a colorimetric indication, which can change the color due to surface plasmon resonance (SPR) in the presence of analytes (Chu et al. 2008). Many researchers have discovered other features of AuNPs such as peroxidase and oxidase (Deshmukh, Aloui, and Kim 2021) to detect various biomarkers such as glucose and cholesterol. However, most of these AuNPs based sensors are solutions-based as well as require the use of multi-step preparation, toxic chemicals for the synthesis, and need special requirements for transportation. To allow for the simplicity of transportation, recent research has encapsulated AuNPs which produced a tablet-based sensor (Sadiq, Safiabadi Tali, and Jahanshahi-Anbuhi 2022). This encapsulation not only permitted easy shipping but also protects the AuNPs from fungus attack and preserves them for at least one year. This encapsulation

technique using pullulan or dextran emerged in 2014 from the idea of enzyme conservation and preservation without manipulating their activities or features (Jahanshahi-Anbuhi et al. 2014b).

Glucose sensors have attracted more researchers in the last few years (Galant, Kaufman, and Wilson 2015). Many available platforms have been developed to provide diabetic patients with comfort while monitoring their glucose levels. Even though blood is the most extensively investigated biological fluid for clinical diagnostics, its collection can cause pain, phobia, fright, and discomfort for patients (Orenius et al. 2018). Recent psychological studies highlighted the fear of needles as one of the most worrying problems among diabetic patients, especially children, and elders (Kalra, Jena, and Yeravdekar 2018).

1.2.2 Cysteamine monitoring

Cysteamine detection plays a crucial role in diagnosing and monitoring various medical conditions, such as cystinosis and cysteamine therapy efficacy. However, the accurate detection of cysteamine often requires the use of expensive equipment and mult-steps preparations, which presents both advantages and challenges. Expensive equipment used for cysteamine detection often incorporates specialized methodologies and techniques. These may include high-performance liquid chromatography (HPLC), mass spectrometry (MS), or other sophisticated analytical techniques. These methodologies offer enhanced separation, identification, and quantification of cysteamine, enabling a comprehensive analysis of samples. Despite their advantages, expensive equipment for cysteamine detection can pose challenges in terms of accessibility and cost implications. Not all healthcare facilities or research institutions may have access to such equipment due to their high cost and specialized requirements. This limited accessibility can hinder the widespread use of accurate cysteamine detection methods, particularly in resource-limited settings. Moreover, the acquisition, maintenance, and operation costs associated with expensive equipment can impose financial burdens on healthcare systems, laboratories, or researchers.

Furthermore, the use of expensive equipment for cysteamine detection often demands specialized expertise and training. Skilled personnel are required to operate and maintain the equipment correctly, as well as to interpret the obtained results accurately. The training and expertise necessary for utilizing expensive equipment can be a barrier, especially in regions or institutions

where access to such training opportunities is limited. It is essential to ensure that there is a sufficient number of trained professionals to handle and interpret the data generated by expensive equipment. As such, the development of affordable, portable, and easy to perform tests for cysteamine detection is considered of high importance in resource limited areas. This shows that our catalysis-based method using pAuNPs-Tablet has high sensitivity and wide range of linearity comparable to previously reported methods for the cysteamine detection as shown in Table 0-3.

Table 0-3 *Comparison between this method and some previously reported methods employed in the detection of cysteamine.*

No	Material	Medium	LoD	Linear range	Concerns	Ref.
1	Polydentate Aromatic Nanoparticles Complexed with Cu^{2+}	Serum/ urine	(0.02 - 0.05) µM	(0.1-10) µM	Solution based/ multistep preparation	(Singh et al. 2019)
2	Label-free AuNPs	water	0.01 µg mL^{-1}	(0.01-0.05) µg mL^{-1}	Solution-based	(Apyari et al. 2012)
3	N-doped carbon do	buffer	75.6 nM	(10–210) µM	Solution-base/ multistep preparation	(Konar et al. 2019)
4	bovine serum albumin protected Au_{25} nanoclusters	serum	150 nM	(500–10,000) nM	Solution-based/ multistep preparation	(Shu et al. 2015)
5	Cysteine-stabilized silver nanoparticles	serum	0.37 µM	(0.6-1.8) µM	Solution-based/ multistep preparation	(Diamai and Negi 2019)
6	**pAuNPs-Tablet**	**serum**	**82.9 µM**	**(0-40) µM**	**-**	**This work**

The invention of tablet-based sensors for cysteamine detection offers significant benefits in terms of accessibility, cost-effectiveness, and patient empowerment. These sensors enable POC diagnostics, reduce the cost of cysteamine detection, and actively involve patients in their own healthcare. By leveraging the power of tablet technology, healthcare professionals can enhance cysteamine detection, improve patient care, and advance medical diagnostics in the field of cysteamine-related conditions.

Overall, colorimetric tablet-based sensors are attractive tools as a replacement for solution-based and paper-based platforms due to their portability and cost-effectiveness. The prolonged shelf life of tablets is another advantage compared to the solution and paper-based devices since the chemicals lose sensitivity with time. To provide low-cost analytical testing platforms for POC analysis, tablet-based analytical devices have become popular in the research community. These devices use a substrate that is impregnated with reagents for systematic testing of analytes through colorimetric readout. Thus, the first tablet-based colorimetric sensor for glucose and cysteamine monitoring, as an easy-to-use platform, has been developed. The fabricated tablets are made of AuNPs captured with pullulan (AuNPs-pTab) that demonstrate catalytic activity revealed by the oxidation of the TMB substrate. This approach to detecting glucose and cysteamine levels in saliva and serum media using a tablet sensor is simple and consists of two steps: synthesis and colorimetric detection assay. Moreso, many biomarkers such as cholesterol and glutathione can be detected easily and accurately using this tablet sensor (Feng et al. 2017).

1.3 Thesis objectives

Employing the same features of reagent encapsulation and searching for challenging diseases to monitor such as glucose and cysteamine, an innovative peroxidase tablet-based sensor has been established. As such, the objective of this work is to fabricate a portable peroxidase tablet for the detection and routine monitoring of glucose using non-invasive human saliva. Likewise, to monitor cysteamine overdoses in human serum samples using simple and portable tablet sensors that can replace the types of specified tests using expensive equipment. This work could be achieved by the combination of gold nanoparticles and pullulan polymer in the synthesis which will produce high catalytic activity AuNPs-pTab. This AuNPs-pTab can catalyze the reaction of glucose into gluconic acid, and hydrogen peroxide (H_2O_2). H_2O_2 can be indirectly used to quantify glucose concentrations by the oxidation of the TMB substrate into blue product. Thus, this approach can facilitate not only the detection of glucose but also other biomarkers that can be quantified according to H_2O_2 productions such as cholesterol (Guan et al. 2020), creatinine (Serafín et al. 2013), and uric acid (J. Zheng et al. 2022). While using the inhibition of the peroxidase-like activity of AuNPs-pTab in the presence of cysteamine can be used to quantify cysteamine concentrations in human serum samples. Furthermore, to overcome the loss of activity

and sensitivity of AuNPs while storage and to conquer the special packaging of AuNPs during transportation.

1.4 Thesis organization

The content of this thesis is categorized into five chapters as the following:

- Chapter 1 gives an introduction platform that includes the background knowledge of peroxidase, glucose, and cysteamine detection, the motivation to produce this research, and the objectives of this research work.

- Chapter 2 provides a comprehensive literature review including the history of nanozymes and their advantages over natural enzymes and the principles of peroxidase-like activity. A list of the most common peroxidase nanozymes, the available platforms and media for glucose and cysteamine detection, and the fabrication of glucose and cysteamine assay using gold nanoparticles.

- Chapter 3 aims at the preparation of the reagents that were used during the experiments, the experimental techniques that were employed, and the synthesis procedures that were utilized for the analytical testing platforms. The results obtained from each experiment for glucose detection using the highest catalytic activity presented by peroxidase-like activity of pullulan stabilized gold nanoparticles.

- Chapter 4 outlines the procedure utilized for cysteamine detection along with the experiments and results using the inhibition of peroxidase-like activity of pullulan stabilized gold nanoparticles.

- Chapter 5 gives a conclusion on the research work and future recommendations.

Chapter 2. Literature Review

In this chapter, some general information is provided about the peroxidase-like activity of different inorganic nanoparticles and different methods of gold nanoparticle synthesis. This part continues with an overview of glucose detection in different human fluids and ends up with some methods for cysteamine detection and the inhibition of the peroxidase-mimetic activity of gold nanoparticles using amino acids.

1.5 Introduction

The term "nanozymes" was first been used by Manea, Houillon, Pasquato, and Scrimin ("Angewandte Chemie - 2004 - Manea - Nanozymes Gold-Nanoparticle-Based Transphosphorylation Catalysts.Pdf," n.d.) and particularly refers to an outstanding enzyme-like activity (Shivakumar, BG, and MR 2017). Linosier and colleagues first named peroxidase after it which was isolated from the cells of the bloodstream. According to Raveendran et al., peroxidase is an oxidoreductase that catalyzes the breakdown of H_2O_2 by an electron donor leading to the oxidation of a variety of organic and inorganic compounds (Raveendran et al. 2018).

$$3H_2O_2 + \text{peroxidase mimetic enzymes} \longrightarrow 6HO^{\bullet}$$

$$6HO^{\bullet} + 2\text{peroxidase substrates (TMB/OPD/ABTS)} \longrightarrow 2(\text{TMB/OPD/ABTS}) + 6H_2O$$

In these reactions, organic hydroperoxides or hydrogen peroxide are reduced while working with an oxidized redox substrate as an electron donor. The type of electron donor varies depending on the structure of the enzyme. The ping-pong mechanism is the documented phenomenon for peroxidase activity. The double-displacement response is another name for this non-sequential process. Similar to a ping-pong ball, the enzyme will switch to an intermediate form when the initial substrate transforms into the final product and return to its initial form without being consumed during the reaction as shown in (Figure 0-1). Additionally, one product must be produced and released in an enzymatic reaction based on the ping-pong process before the second substrate attaches.

$$E + A \rightarrow EA \rightleftharpoons E^{*}C \xrightarrow{\uparrow C} E^{*} + B \rightarrow E^{*}B \rightleftharpoons ED \xrightarrow{\uparrow D} E$$

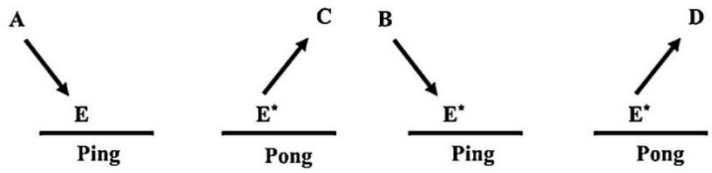

Figure 0-1 *Representation of the ping-pong mechanism (E: enzyme; E∗: enzyme intermediate; A: substrate one; B: substrate two; C: product one; D: product two. Adapted from* (Jin et al. 2019).

There are two popular catalysis routes for nanozymes in a peroxidase mimic reaction: an electron transfer path and a hydroxyl radical creation path based on the Fenton reaction. For a very long time, it was thought that the Fenton reagents' reaction with H_2O_2 was the primary source of the peroxidase-like activity of nanomaterials. For instance, H_2O_2 could be converted into •OH radicals when ferrous ions are present on the surface of iron oxide. The resulting •OH radicals would then interact with the redox substrate. The reactive sites in nanocarbon oxides' carboxyl groups have also been discovered (Z. Chen et al. 2012). First, peroxycarboxyl groups could be created by oxidizing the carboxyl groups. Second, the homolytic homocarboxylic cleavage of the peroxycarboxyl groups yields hydroxyl radicals. The redox substrate is finally oxidized by hydroxyl radicals, which results in a color shift. However, it was discovered that some types of nanozymes did not have peroxidase-like activity because of the Fenton reaction as the field of study continued to deepen and develop. For example, Co_3O_4 NPs demonstrated increased peroxidase-like activity when compared to Fe_3O_4 NPs.

The strong redox potential of Co^{3+}/Co_2 prevented Co_3O_4 NPs from effectively enhancing •OH production. An electron transport path was suggested in this regard (Dong et al. 2014). Due to the transfer of electrons from lone-pair electrons in amino groups to the nanomaterials in this pathway (Co^{3+} becoming Co_2), the substrate could be directly oxidized. Then, it would encourage the transfer of electrons to H_2O_2 (converting Co_2 back into Co^{3+}). H_2O_2 receives two electrons as a result, and it then breaks down into OH^-. By keeping an eye on both, the creation of oxidized products and the consumption of H_2O_2, their peroxidase-like activities can be assessed. Some specific chromophores, (TMB), (ABTS), (OPD), and others, can change color in the presence of H_2O_2. The absorbance intensity can be monitored to detect this shift, or it can be seen with the

naked eye. The Michaelis-Menten equation is used to calculate several parameters for enzyme kinetics investigations, such as the maximum turnover number (K_{cat}), reaction velocity (v_{max}), and Michaelis-Menten constant (K_m).

Previous studies report an intrinsic peroxidase-like activity of nanoparticles to be pH sensitive where a mildly acidic condition (pH 4.0) is considered as one of the fundamental necessities. Thus, driving the oxidation of peroxidase substrates (TMB, OPD, ABTS), which finally results in subsequent colorimetric product formation used in the detection of a variety of analytes. Therefore, the detection sensitivity is significantly dependent on the capability of oxidation of peroxidase substrate by nanoparticles in the presence of hydrogen peroxide.

1.6 Nanozymes vs. natural enzymes

Peroxidases have been extensively used in pharmaceutical and health, food, agriculture, paper and printing, and chemical industries (Sellami et al. 2022). However, similar to proteins, peroxidase enzymes are extremely sensitive to environmental conditions such as temperature, pH, ionic strength, etc., and their control is not always cost-effective (Ashrafi et al. 2021a). With the change in the above factors, the catalytic activity of peroxidase enzymes is lost due to protein denaturation. Furthermore, the peroxidase enzyme displays several activities due to fluctuations in the substrate concentration, enzyme affinities, optimum pH, and so on.

The enzyme activity can also be stopped significantly by inhibitors such as heavy metals, drugs, minerals, or other compounds by competing in binding to the active site or reducing the affinity of the enzyme to the substrate by altering the structure of the enzyme (BHOOLA 1969). To reduce the challenges ahead, researchers have recommended the use of substances that have similar activity with enzymes. One of the most important compounds used is nanozymes, which greatly reduce the problems in industries. Table 0-1 provides a comparison between natural enzymes and nanozymes.

Table 0-1 *A comparison between natural enzymes and nanozymes.*

Type	Advantages vs. disadvantages
Natural enzymes (Ashrafi et al. 2021a)	denature quickly at a particular pH and temperature. Required to be freshly prepared, challenging to transport (need specialized conditions of at most 4°C), pricey, demand special handling and skilled staff.
Nanozymes (J. Wu et al. 2019a)	high activity, high stability against changes in temperature and pH, high tunability, multifunctionality, affordability, high susceptibility to the substrate, and compatibility with Michaelis-Menton and Ping-Pong processes.

Over the past few decades, studies have concentrated on nanomaterials with enzyme-like characteristics (nanozymes) as simple, stable, high-performance substitutes for natural enzymes in a broad selection of applications. Gao et al. discovered the intrinsic peroxidase activity of ferrous nanoparticles in 2007 (Gao et al. 2007). After this breakthrough, a series of research has been followed to find the peroxidase mimetic activity of other materials and nanoparticles. A variety of inorganic nanomaterials including Cd, carbon-based nanomaterials, CeO_2, Co_3O_4, CuO, Au, Fe, Mn, Pd, Pt, SiO_2, Ag, VO_2, and Zn NPs have been considerably used to mimic the activity of naturally occurring enzymes. These nanomaterials have been shown to mimic widely enzyme-like activities, and good improvements have been made in these approaches due to the immense progress in nano-research and the unique states of nanomaterials.

1.7 Peroxidase activity of different nanozymes

As of now, numerous nanomaterials have been created to produce nanozymes systems. Nanomaterials utilized in intrinsic peroxidase mimics can be loosely divided into four groups based on the various catalytic compositions and active sites of peroxidase-mimic systems: noble metal-based nanomaterials, transition metal-based nanomaterials, carbons, and other inorganic materials. This section will give a thorough introduction to the fundamental peroxidase-like characteristics and enzyme mimics systems design approaches of these four categories of intrinsic peroxidase mimics applications. The enzyme mimetic properties of the most common inorganic nanomaterials “nanozymes” have been listed below.

1.7.1 CdS NPs

Maji et al. have synthesized cadmium nanoparticles (CdS NPs) with tunable shapes (rods and spheres) and sizes which were synthesized through the decomposition of a newly synthesized precursor complex [$Cd(SOCPh)_2Lut_2$] utilizing structure-directing solvents such as dimethylsulfoxide (DMSO), ethylenediamine (EN), and ammonia (NH_3). In addition, CdS NPs are also prepared by the thermal decomposition of the precursor complex under the N_2 atmosphere (Maji et al. 2012). The peroxidase-like activity of CdS NPs was analyzed based on the degradation of TMB and H_2O_2 substrates. Kinetic analysis showed that the catalysis reaction by CdS NPs shows typical Michaelis–Menten kinetics. Moreover, regardless of the long period time of preparation, the synthesized CdS NPs exhibited substantially greater catalytic activity for the substrate TMB than HRP and were applied for some wastewater treatments.

1.7.2 Carbon-based NPs

Song et al. suggested that GO-COOH showed intrinsic peroxidase-like activity and its activity is greatly improved by physiological constraints similar to HRP (Song et al. 2010). In the presence of H_2O_2 and TMB, GO-COOH generated a diamine blue color. The sensor possesses high surface-to-volume ratios and a high affinity to organic substrates due to hydrophobic interactions as shown in Figure 0-2. The sensor was able to detect glucose in blood, orange, and apple juice samples.

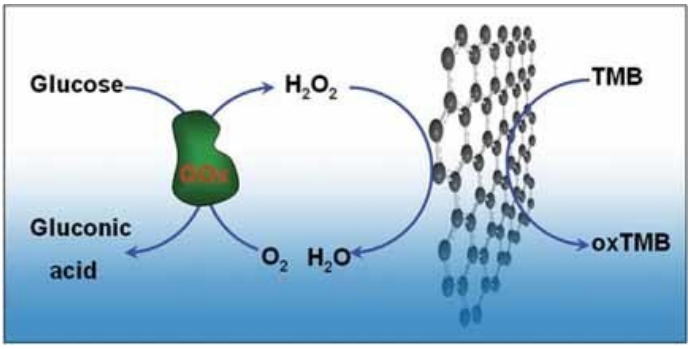

Figure 0-2 *Representation of colorimetric detection of glucose by using glucose oxidase (GOx) and GO-COOH-catalyzed reactions as reported by Song et al. Adapted from Ref.* (Song et al. 2010).

1.7.3 CeO_2 NPs

Nanocomposites of dispersed Cerium oxides (CeO_2) on a TiO_2 nanotube have been synthesized by Zhao et al. (Zhao et al. 2015). The strong peroxidase-like activity was calculated for the

CeO_2/nanotube-TiO_2, which was better than those for CeO_2/nanowire-TiO_2, CeO_2/nanorod-TiO_2, or CeO_2/NPs-TiO_2 with a similar molar ratio of Ce/Ti. Regardless of the time of preparation of these nanoparticles (>20 h), these nanocomposites exhibit a very high catalytic activity. Ce^{3+} sites were established as the catalytic active locations for the catalytic reaction. The first interaction of surface CeO_2 with H_2O_2 chemically changed the surface state of CeO_2 by transforming Ce^{3+} sites into surface peroxide species causing adsorbed TMB oxidation as indicated in (Figure 0-3). The sensor was applied to the detection of glucose in human serum.

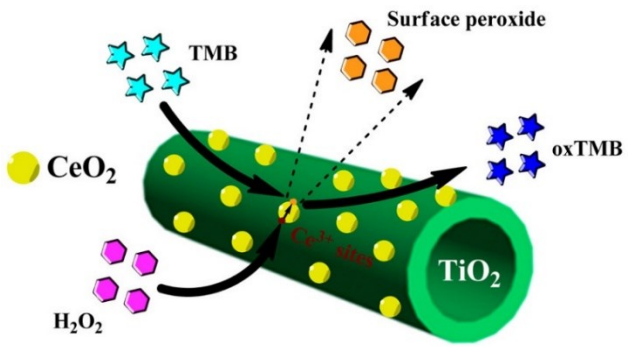

Figure 0-3 *Representation for TMB oxidation in the presence of H_2O_2 over CeO_2/NT-TiO_2. Adapted from* (Zhao et al. 2015).

1.7.4 Pd NPs

Palladium nanoparticles (PdNPs) have been synthesized by Lan et al. and proved to be an effective catalyst for the H_2O_2-mediated oxidation of TMB (Lan et al. 2014) as depicted in (Figure 0-4). The suggested Pd NPs have a catalytic activity similar to the HRP enzyme which can be seen by the formation of blue color in urine samples containing sarcosine and was applied for the diagnosis of prostatic carcinoma. The Pd NPs were synthesized using $NaBH_4$ as a reducing agent.

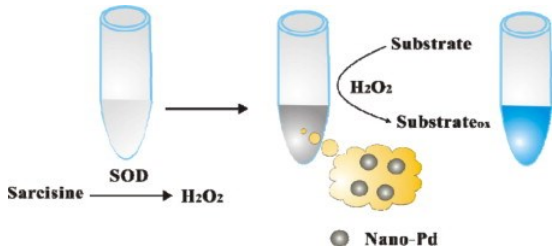

Figure 0-4 *Sarcosine detection using Pd NPs. Sarcosine triggers a fast release of H_2O_2 by the catalytic action of sarcosine oxidase. Adapted from* (Lan et al. 2014).

1.7.5 CuO NPs

Hue et al. synthesized water-soluble Cu NCs by using bovine serum albumin (BSA) as a stabilizer and reducer (Hu et al. 2013). The peroxidase-like activity of Cu NCs can catalyze the oxidation of TMB by H_2O_2 to produce a blue-color product as shown in (Figure 0-5). Then, by coupling GOx with Cu NCs, glucose detection can be easily applied. It is noteworthy that the BSA-Cu NCs have stronger activity around neutral pH than horseradish peroxidase, which is advantageous for biological applications.

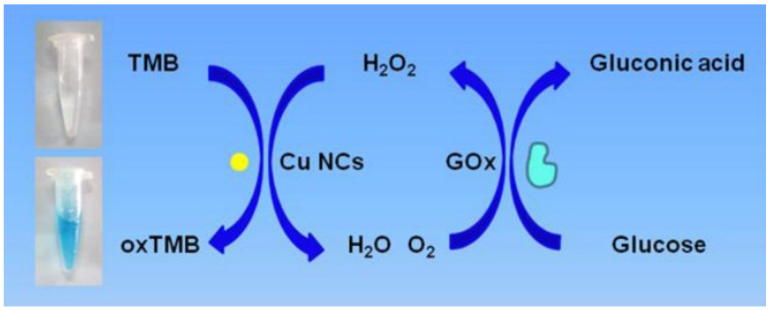

Figure 0-5 *Representation of colorimetric detection of glucose by using GOx and Cu NCs catalyzed color reaction. Adapted from* (Hu et al. 2013).

1.7.6 Fe NPs

Gao et al. reported ferromagnetic nanoparticles of different sizes (30, 150, and 300 nm) and spherical shapes (Fe NPs) can catalyze the oxidation of TMB to produce a blue color. These nanoparticles have an intrinsic enzyme mimetic activity similar to natural peroxidases, which was extensively employed to oxidize organic substrates in the remediation of wastewater or as detection systems (Gao et al. 2007). The group has the following findings: (1) the peroxidase-like activity of Fe_3O_4 MNPs was also H_2O_2, pH, and temperature dependent; (3) catalysis by Fe_3O_4 MNPs showed typical Michaelis-Menten kinetics; and (4) catalysis by Fe_3O_4 MNPs was consistent with a ping-pong mechanism. Fe_3O_4 MNPs catalyzed the reaction of various peroxidase substrates such as TMB, DAB, and OPD. Based on their data, they developed a novel immunoassay with triple functions Fe_3O_4 MNPs in which antibody-modified Fe NPs possess three outcomes: capture, separation, and detection. In order to make the Fe_3O_4 MNPs (30 nm) more biocompatible for use in these tests, they first treated them using substances such as SiO_2, 3-aminopropyltriethoxysilane (APTES), polyethylene glycol (PEG), or dextran. They applied immobilized protein A on Fe_3O_4 MNPs in replacement of an enzyme-conjugated secondary antibody in the original immunoassay. Similar to a traditional ELISA, they coated a plate with the hepatitis B virus surface antigen (preS1)

and then incubated the plate with an anti-HBV preS1 antibody. Non-specific binding was eliminated after multiple washes. Following the addition of the substrate TMB and immobilized protein A-containing Fe_3O_4 MNPs, protein A attached to the primary anti-preS1 antibody, and the H_2O_2-induced color reaction was catalyzed by the MNPs as displayed in (Figure 0-6). An ELISA reader was used to measure the response at 652 nm.

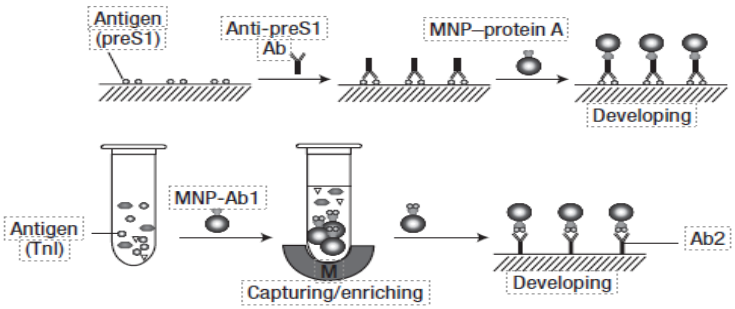

Figure 0-6 *Based on the peroxidase activity of magnetic Fe_3O_4 nanoparticles, immunoassays. b) an immunoassay based on Fe_3O_4 MNPs. Anti-preS1 antibody identified the HBV preS1 antigen, and Fe_3O_4 MNPs conjugated to protein A, which binds exclusively to the Fc portion of the antibody, were used to detect it. c) An immunoassay for capture-detection. Target TnI in the sample was captured and separated using antibody modified Fe_3O_4 MNPs. When the substrate TMB was introduced when H_2O_2 was present, this combination interacted with the secondary anti-TnI antibody that had been coated on the plate. Adapted from* (Gao et al. 2007).

1.7.7 Pt NPs

Platinum nanoparticles (Pt NPs) were synthesized by Fan et al. using apoferritin (apoFt) as a nucleation substrate in the size of (1–2 nm) to form (Pt–Ft NPs). Pt–Ft NPs possessed both catalase and peroxidase activities (Fan et al. 2011). With H_2O_2 as substrate, oxygen gas bubbles were produced from H_2O_2 decomposed by Pt-Ft; the production of oxygen gas effectively supports Pt-Ft reacts as catalase, other than peroxidase. While with organic dye and H_2O_2 as substrates, unique color results were produced catalyzed by Pt-Ft, which signifies a peroxidase-like activity as indicated in (Figure 0-7). These nanozymes showed variance reaction to pH and temperature which was optimal at physiological temperature and acidic pH.

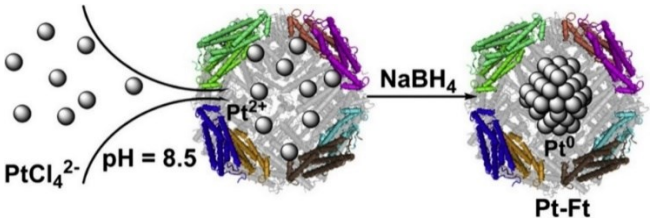

Figure 0-7 *Illustration of the formation of Pt-Ft NPs where Pt ions were reduced by adding $NaBH_4$ to yield zero-valent Pt NPs. Adapted from* (Fan et al. 2011).

1.7.8 AgNPs

Liu et al. have synthesized the mono-dispersed silver nano colloids Ag_3PO_4 with a size of 10 nm through a colloidal chemical preparation method (Yuanjun Liu et al. 2014). It was indicated that the produced Ag_3PO_4 NPs exhibit intrinsic peroxidase-like activity and perfectly follow the Michalis-Mentons equation of enzyme activity. Peroxidase-like activity of the Ag_3PO_4 nanocrystals was evaluated in the catalysis oxidation of a commonly used peroxidase substrate TMB, in the presence of H_2O_2. TMB is colorless and can be oxidized slowly by H_2O_2 as explained in (Figure 0-8). Two colored compounds are the visible by-products of oxidation. A blue charge-transfer complex of diamine, which is formed in quick equilibrium with the radical cation, is the initial end product. Its maximum wavelengths of absorption are between 370 and 652 nm. Another by-product of further oxidizing the diimine with too much H_2O_2 or under strongly acidic conditions is yellow diimine. The diimine product has a maximum absorption wavelength of 450 nm and is stable in acidic environments.

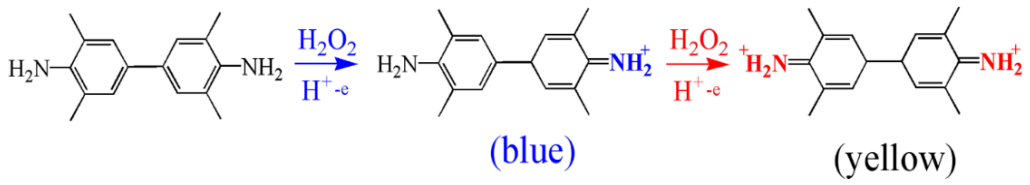

Figure 0-8 *The TMB's oxidation process. Adapted from* (Yuanjun Liu et al. 2014).

1.7.9 AuNPs

AuNPs are excellent metals that exhibit a unique surface plasmon resonance and catalytic activity. The easy synthesis and long stability of AuNPs made this metal an attractive material for researchers in the field of detection. The catalytic activity of different AuNPs has been investigated by Wang et al. (S. Wang et al. 2012). The bare AuNPs exhibited higher catalytic activity than the negatively and positively charged types. Moreover, Jiang et al. have demonstrated that the positively charged gold nanoparticles functioned as a peroxidase mimic enzyme (C. Jiang et al. 2017b). The synthesis includes the addition of a polysaccharide called “Chitosan” under vigorous stirring and reflux. The positive amine group of chitosan produced the positively charged AuNPs. It was found that surface functionalization is responsible for the production of surface charge

which corresponds to the catalytic activity of AuNPs. The detection glucose mechanism is demonstrated in (Figure 0-9).

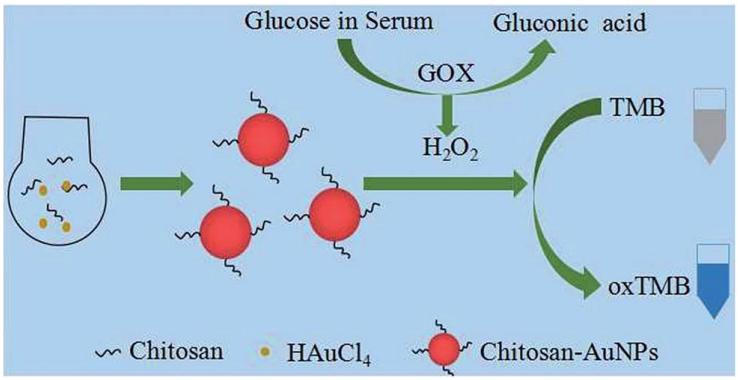

Figure 0-9 *Detection of glucose using positively charged Chitosan-AuNPs. Adapted from* (C. Jiang et al. 2017b).

1.8 AuNPs as peroxidase memetic nanozymes

Gold nanoparticles (AuNPs), a huge potential functional nanoparticle in scientific research, have attained tremendous interest for their unique physical and optical property since they have been discovered. They have been very popularly used as labels in diagnostics, sensors, etc. The application of AuNPs in sensor construction is pervasive, and so several papers have been stated throughout the past years. The peroxidase mimetic activity of AuNPs used in the sensor has been explained in the literature. Most of them tend to explain a certain kind of specific size and surface charge using one kind of synthesis technique. However, few of this research include the synthesis of positively and negatively charged AuNPs using multistep and complicated methods. Turkuvitch method was widely used to produce the negatively charged gold nanoparticles when using sodium citrate as a reducing and stabilizing agent. While the positive AuNPs were synthesized by $NaBH_4$ reduction of $HAuCl_4$ in the presence of cysteamine or chitosan. The negatively charged demonstrated higher catalytic activity than the positively charged (S. Wang et al. 2012) as explained in (Figure 2-10). However, the method needs multi-step preparation and used sodium citrate in the synthesis of AuNPs. On the other hand, polysaccharides such as pullulan are a great choice for the green synthesis of AuNPs using a one-step preparation in less than an hour. To overcome the challenges of aggregation and loss of sensitivity of liquid AuNPs during transportation, encapsulation of AuNPs using polysaccharides is of great choice.

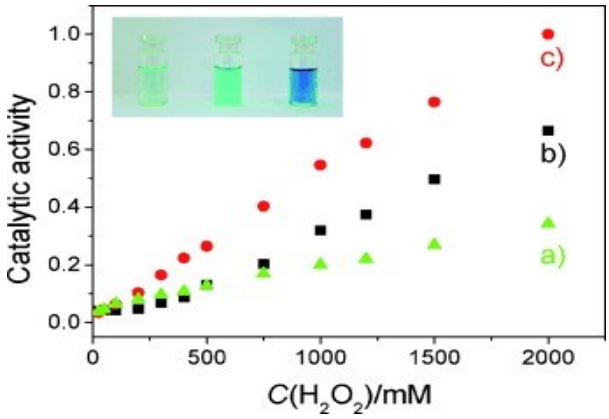

Figure 0-10 *Evaluation of the peroxidase-like activity of a) amino-modified, b) citrate-capped, and c) unmodified gold nanoparticles toward TMB as peroxidase substrate. Adapted from* (S. Wang et al. 2012).

1.9 Glucose detection

The peroxidase mimetic activity of AuNPs has been previously employed for glucose and cholesterol detection using unmodified AuNPs. The positively and negatively charged AuNPs were discovered to exhibit different peroxidase activity in the solution form only. However, recent studies did not emphasize the development of their peroxidase feature in transportable tablet platforms. Furthermore, the intricate synthesis procedure and the multi-step preparation of nanozymes encourage researchers to find more methods as a one-step process.

Glucose is one of the life-threatening biomarkers that is responsible for hundreds of deaths every year. The waiting time in clinics for diagnostic and monitoring of glucose is so long and sometimes can exceed hours. Additionally, the pain of needles while giving blood samples can add an extra burden to the patients, especially young children. While giving saliva samples is preferable, painless, and effortless and everybody can do it without hesitation. Starting from these inspirations, the fabrication of transportable and easy-to-use tablets sensor can facilitate the detection and monitoring of glucose for diabetic patients.

As such, the common glucose sensors based on AuNPs are using the solution platforms which is problematic in handling and transportation. Besides, the deterioration of catalytic activity due to loss in sensitivity over time and the difficulties of preserving the particles well dispersed emphasized the need to find alternatives for the solution-based platforms. Likewise, AuNPs become more attractive for fungus invasions and aggregation (Ramasamy, Lee, and Lee 2017). Hence, changing the platforms will be of great benefit to the detection systems. Using pullulan as

a reducing and stabilizing agent (all at once) in the synthesis and as an encapsulation agent will preserve the AuNPs for a longer time while maintaining their catalytic activity and contribute to the fast detection and diagnosis of glucose in clinical and home usage.

1.9.1 Available platforms for glucose detection

At present, many methods have been reported for the detection of glucose, including electrochemical (M. Chen et al. 2021), lateral flow devices (Jingjing Zhang et al. 2016), immunoassays (Yingshuai Liu, Lei, and Zhang 2017), fluorescence (Hammami et al. 2021), and optical/colorimetric assays (Kap et al. 2021). Between these, colorimetry has the benefits of a simple procedure, low cost, elevated speed, and robust practicability. Moreover, it can be read out by the naked eye without complicated instruments or professional knowledge and skills and is suitable for POC tests. The routine colorimetric detection of glucose is based on enzymes and chromogenic agents. While the more complicated equipment and materials are involved when it comes to the other platforms for glucose detection. Below is a list of some common platforms for glucose detection.

1.9.1.1 Electrochemical assays

Following the process of recognizing analytes, chemical information is transformed into an electrical or optical signal as presented in (Figure 0-11). It generates an electrical potential from the action of a particular ion in a solution (Rahman et al. 2008). An electrochemical sensor makes use of electrical signals that are produced as output changes by the target material. Two processes underlie the electrochemical biosensing of glucose: (1) the redox reaction of mediators bound to the electrode surface together with the enzyme, and (2) the electrochemical oxidation of H_2O_2 produced by the enzyme. In this instance, it entails the enzyme GOx reducing oxygen to H_2O_2 (S. Zhang et al. 2005).

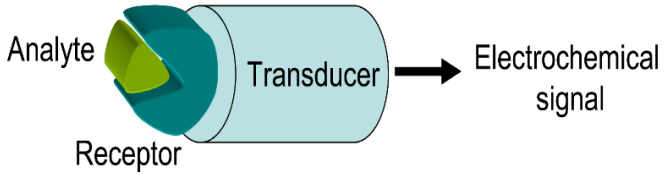

Figure 0-11 *The principles of electrochemical sensors. Adapted from* (Rahman et al. 2008).

Another electrochemical glucose sensor was developed by employing a composite film of plant-like Zinc oxide (ZnO) and chitosan-stabilized spherical gold nanoparticles (AuNPs) on which GOx was immobilized. The ZnO was placed on an indium tin oxide (ITO) coated glass and the AuNPs of an average diameter of 23 nm were stacked on ZnO as the second layer. The presence of AuNPs provides significant enhancement of the electron transfer rate during redox reactions. A substantial protective protein shell surrounds the redox center of GOx, flavin adenine dinucleotide (FAD), which catalyzes the glucose oxidation processes and prevents the transfer of electrons. The inclusion of AuNPs surrounding the GOx lessens the protein shell's insulating effect, creates an electrical route for enhanced electron transfer, and therefore boosts the electrode's sensitivity. Another theory is that the AuNPs operate as a redox mediator, much like the FAD does in natural systems. This would increase the FAD's surface area and improve the process of electron transfer between the GOx and the electrode surface. Thus, uniformly dispersed AuNPs on the reactive surface improve the transport of electrons from glucose oxidation toward the electrode as shown in (Figure 0-12) (Tian et al. 2015).

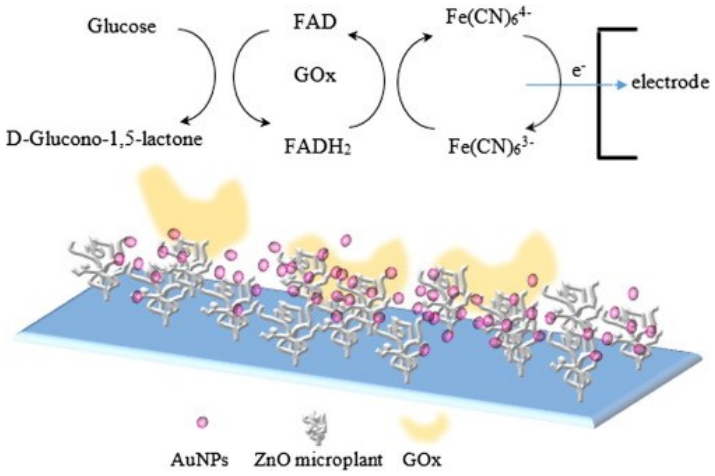

Figure 0-12 *The ZnO/AuNP/GOx/ITO electrode's electrochemical reaction and the produced sensor's design based on its 450 nm ZnO/AuNP/GOx/ITO wavelength. Adapted from* (Tian et al. 2015).

1.9.1.2 Lateral flow paper-based devices

Due to the benefits of visible readout, simple operation, and improved stability, colorimetric detection has been the most extensively used approach for paper-based analytical devices (PAD). The most popular bi-enzyme system for catalyzing the reaction between glucose and the color indicator in PADs is GOx and HRP. H_2O_2 and gluconic acid are the products of the catalytic reaction between glucose and GOx. The interaction of H_2O_2 with the color indicator is then

catalyzed by peroxidase, resulting in a visible color shift. One of the important aspects in the development of PADs for the detection of glucose concentrations is choosing a suitable color indication. One type of color indicator frequently employed was potassium iodide (KI). Iodide is converted to iodine by H_2O_2 when HRP catalyzes the process, changing the substance's color from colorless to brown. The same procedure is implied using other substrates such as TMB as shown in (Figure 0-13).

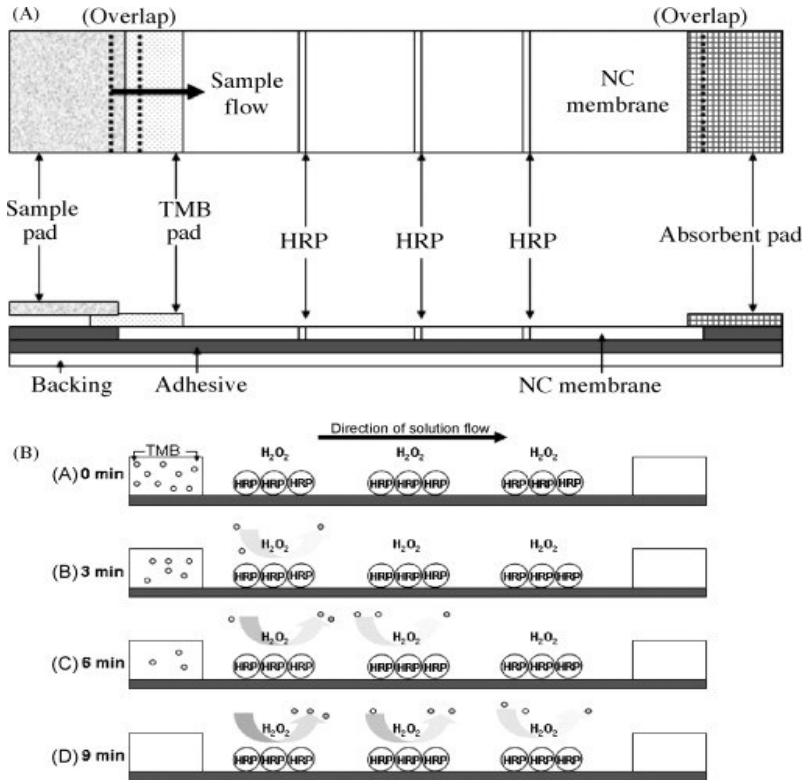

Figure 0-13 *H_2O_2 assay representation highlighting its key elements: (top) top view and (bottom) cross-section (A). The bar code enzyme test reaction technique for producing signals in a ladder bar pattern as dosage responses at various times (B). In this case, TMB was used as an enzyme substrate to produce a blue color in the presence of H_2O_2. Adapted from* (Fung, Chan, and Renneberg 2009).

1.9.1.3 Immunoassays

The unique antigen-antibody interaction is the basis of immunoassays, which are highly specific biochemical techniques. Today, immunoassays boost their sensitivity by labeling either the antigen or the antibody, or both. A radioisotope, enzyme, fluorescence, or chemical can be used as a labeling agent. Labeling enzymes and substrate degradation catalyze the process to produce the colored end product for spectrophotometric and ocular examination.

Citrate-capped AuNPs were successfully aggregated by benzene-1,4-boronic acid (BDBA) due to the interaction between the -hydroxy carboxylate of citrate and the boronic acids of BDBA. The boronic acid groups in BDBA were changed into phenol groups by H_2O_2-mediated oxidation. Citrate-capped AuNPs could not aggregate when the oxidized BDBA was present. A colorimetric probe for glucose may be created by combining the GOx-glucose system with the BDBA-induced aggregation of citrate-capped AuNPs. In addition, a sandwich immunoassay, biotinylated antibody, and avidin-conjugated GOx were merged with an H_2O_2BDBAAuNP probe for the selective detection of rabbit immunoglobulin G (IgG) and human-prostate-specific antigen with the naked eye (PSA)(Y. C. Yang and Tseng 2016). This idea is presented in (Figure 2-14).

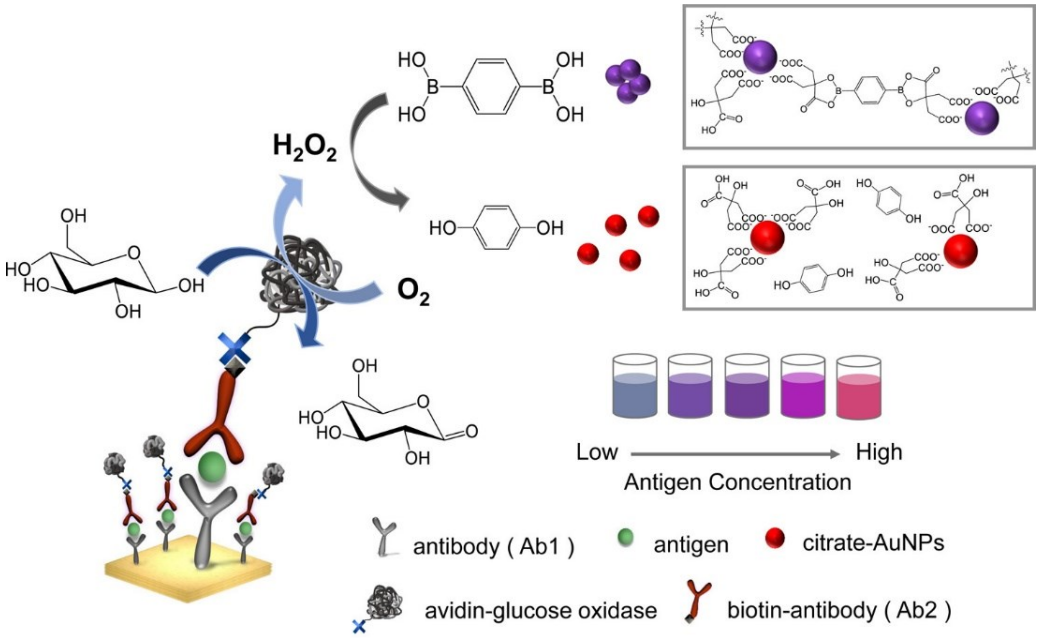

Figure 0-14 *Plasmonic immunoassay readout via the naked eye. Sandwich immunoassay, avidin-biotin interaction, GOx-mediated oxidation of glucose, H_2O_2-induced oxidation of BDBA, and BDBA-triggered aggregation of citrate-capped AuNPs are all used to detect the target protein. Adapted from* (Y. C. Yang and Tseng 2016).

1.9.1.4 Fluorescence assays

The literature is rich with several types of fluorescence sensors for glucose detection. Most fluorescence assays based on AuNPs take advantage of the inner filter effect of AuNPs on the fluorescence properties of various fluorophores or metal nanoparticles (Jing et al. 2021). In these procedures, the target analytes are determined by using enzymatic systems that create H_2O_2, such as glucose/GOx, uric acid/urease, or cholesterol/cholesterol oxidase, which have been employed as effective fluorescence quenchers. The spectroscopic characteristics of the expanded AuNPs in

such applications are strongly influenced by the analyte concentration (Pezhhan, Akhond, and Shamsipur 2020a). A fluorescent test for glucose detection has been created by Pezhhan et al. based on the self-catalyzed, enzyme-free growth of nanosized AuNPs as described in (Figure 0-15). The bare AuNPs can oxidize glucose to create gluconate and react with $HAuCl_4$ to make Au^0 species. Then, the Au^0 particles settle on the AuNP cores, increasing the size of the AuNPs. The color of the solution changes from colorless to red as a result of the increased size of AuNPs produced by higher glucose concentrations, with an absorbance maximum occurring at 530 nm. Then, they employed the inner filter effect (IFE) to detect both H_2O_2 and glucose utilizing His-AuNCs as IFE fluorophores and AuNPs as IFE absorbers. Due to the overlap between the surface plasmon resonance (SPR) band of the AuNPs and the emission band of His-AuNCs, the self-catalyzed expansion of AuNPs affects the emission of His-AuNCs.

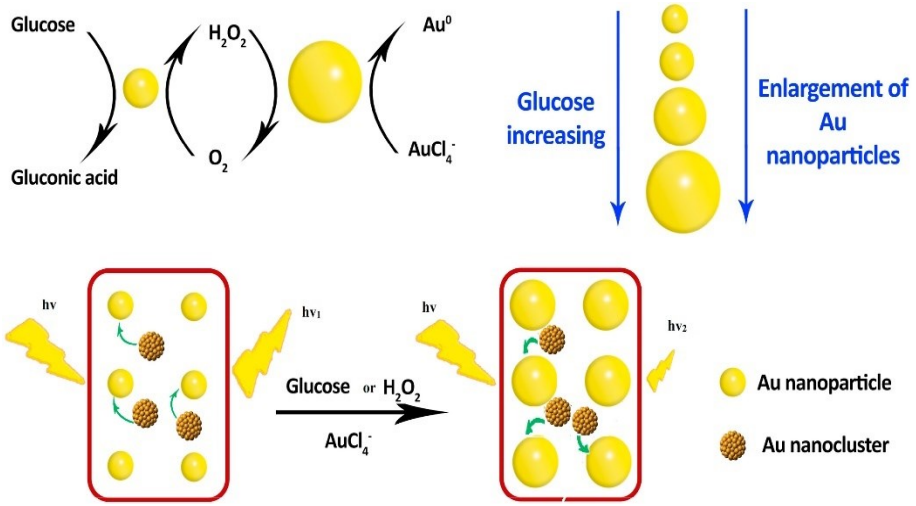

Figure 0-15 *Representation of the (IFE)-based assay for the histidine-glucose nanoclusters (His-GNCs) mediated fluorometric detection of glucose based on the self-catalyzed enlargement of AuNPs. Adapted from* (Pezhhan, Akhond, and Shamsipur 2020b).

1.9.1.5 Optical/colorimetric sensors

AuNPs show great capability of construction as a colorimetric sensor. AuNP morphologies, aggregation behavior, and catalytic activity are just a few examples of the alterations brought on by the many interactions between sensing units and various analytes. Highly cross-reactive and non-specific receptors are used in the generation of the color signals of pattern response for the analytes. Utilizing statistical tools or imaging techniques makes it simple to identify different analytes. AuNPs-based colorimetric sensor arrays may be split into three major types based on the

various sensing processes (SPR alterations, catalytic activity variations, and multidimensional sensor array) (Sun et al. 2020a).

In addition to their exceptional optical properties, AuNPs have been used to create sensing devices due to their exceptional artificial enzymatic activity. Optical signals are also produced by the peroxidase-like action toward diverse substrates. Surface coating, functional ligands, or binding agents can modify the morphology, distance between particles, and even the enzymatic activity of AuNPs, which can vary the colorimetric signals that are produced. (Figure 0-16) is a representation of the basic principles of the AuNPs colorimetric sensor.

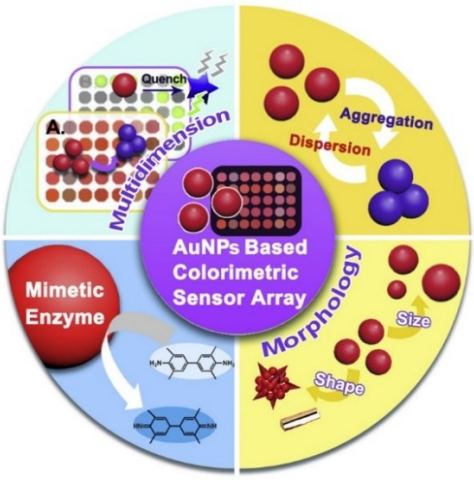

Figure 0-16 *Representation of AuNPs-based colorimetric sensor with different sensing mechanisms. Adapted from* (Sun et al. 2020b).

1.9.2 Samples for glucose detection

Routine glucose monitors for the non-invasive monitoring of diabetes are consistently being developed and enhanced. Although there are several biosensing platforms for monitoring glucose offered on the market, there is still a strong demand to enhance their accuracy, repeatability, and accessibility to end-users. Moreso, biosensing technologies are being increasingly studied that use different body fluids such as saliva, sweat, and tear fluid, etc., that can be calibrated to and therefore used to measure blood glucose concentrations accurately. To improve the applicability of these devices, exploring different fluids as testing mediums is crucial and opens the door for the development of various sensor platforms. Recent improvements have surfaced in the form of wearable sensors such as contact lenses (Jin Zhang et al. 2011) or mouthguards (Arakawa et al.

2016). Challenges still present themselves in the form of sensitivity, especially at very high or low glucose concentrations, which is critical for a diabetic person to monitor.

1.9.2.1 Blood

Blood is the most often used biofluid for diagnostic purposes, followed by urine, while saliva has only lately attracted substantial interest, for example in relation to quick diagnostic tests for COVID-19 (Pasomsub et al. 2021). While blood samples are the most accurate method for measuring blood glucose, it still causes discomfort for the majority of patients. Diabetic patients are exposed to needles during health care routine checkups. Therefore, needles are reported as one of their most feared and painful experience during daily glucose monitoring (Orenius et al. 2018). Many glucose sensors have been used to measure glucose in blood samples. Chen et al. used Tungsten disulfide (WS2) nanosheets which were discovered to possess the intrinsic peroxidase-like activity and catalyze the peroxidase substrate TMB to produce a color change in the presence of H_2O_2. Centered on this result, a colorimetric procedure and a transportable test kit for the visual detection of blood glucose have been established by using glucose oxidase (GOx) and WS2 nanosheet-catalyzed reactions (Q. Chen et al. 2015).

1.9.2.2 Urine

Urine is a fluid naturally yielded by the body, the analysis of which does not expect imposed extraction from the body, nor an implant to access it, such as in the case of blood. Therefore, this solution permits the practical and non-invasive detection of glucose levels, which has been demonstrated to relate to blood glucose levels, by utilizing the shifting refractive index of urine concerning glucose concentration (Robinson and Dhanlaksmi 2017). Nevertheless, the detected glucose concentration is an average of the glycemia for the period that urine stays in the bladder before being expelled, where it is collected. Therefore, the measurement will be more accurate and the association with blood glucose variation will be stronger the shorter the collection intervals. For example, Prasad et al. have developed a glucose monitoring system that takes advantage of copper's capacity to stimulate catalytic reactions with high efficiency (Naveen Prasad et al. 2021). The catalytically active copper nanoparticles were applied to cotton fabric thread. Cu Nanozyme's high catalytic efficiency was demonstrated by its capacity to encourage the oxidation of TMB to its second oxidation product (yellow), as opposed to the more typical blue charge-transfer complex product.

1.9.2.3 Saliva

Due to the vast sample collection and relative lack of interfering molecules compared to blood plasma, saliva has attracted the attention of numerous researchers. The ease of collecting saliva samples (even in quite large amounts) and the nature of the stress-free method for glucose testing make it perfect for daily glucose monitoring and in-home testing. When the glucose levels increase in blood vessels, it will be secreted into the capillary membranes of the mouth causing its diffusion into saliva. Hence, saliva medium is considered a huge advantage for glucose monitoring. (Figure 0-17) shows the transportation of glucose from blood vessels (when glucose concentration is high) into saliva causing an increase in salivary glucose.

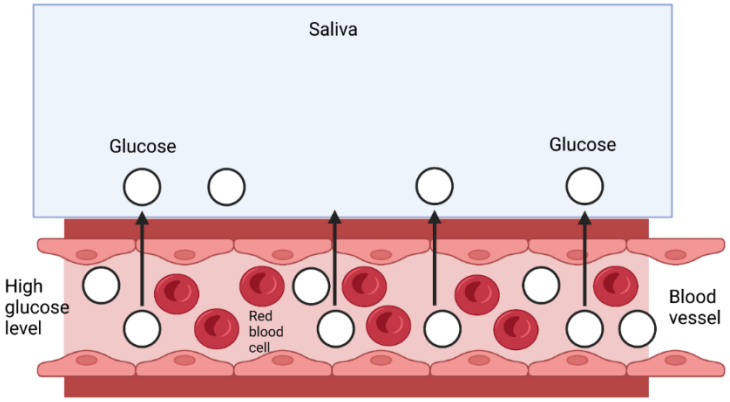

Figure 0-17 *Movement of glucose molecules from blood vessels to saliva medium.*

The use of saliva as a medium for detecting glucose was first presented as a bienzyme and carbon nanotubes combined with a thin film (W. Zhang, Du, and Wang 2015). The detection mechanism uses a combination of GOx and HRP working in parallel with multi-walled carbon nanotubules and AuNPs by entrapping the enzymes in a chitosan matrix, whose role is to house the bienzymatic reactions. Polyphenol is employed as a semipermeable membrane whose function is to reject any interferences that would otherwise hinder accurate glucose measurement and shows extremely good selectivity.

1.9.2.4 Tears

Tear fluid, because of its easy accessibility and possible correlation to blood glucose, is becoming increasingly used as a fluid medium in glucose testing (J. Kim et al. 2019). However, major disadvantages of tear sample collection include difficulty in tear pooling and a relatively low

volume of the gathered sample. In addition to the requirement of using stimulants for tear production such as specific eye drops.

Many studies have proved a relationship between blood glucose and tear glucose. Golamari et al. investigated the glucose concentration between the blood and the tear and found these two values have positive correlations (Golamari et al. 2019). Other studies focused on the development of biosensors that utilizes the properties of oxygen (O_2) sensing membrane and an immobilized layer of GOx on supporting materials to produce an enzymatic sensor displaying high sensitivity to low concentrations of glucose (Duong, Sohn, and Rhee 2020). Based on the oxygen levels used in the glucose oxidation reaction, which was catalyzed by GOx, ratiometric fluorescent glucose-sensing membranes were created. An O_2-sensitive fluorescent dye, such as platinum meso-tetra (pentafluorophenyl) porphyrin (PtP), was used to quantify the O_2 concentration by quenching the fluorescence of the dye. In the ratiometric fluorescence measurements, coumarin 6 (C6) was utilized as a reference dye.

1.9.2.5 Sweat

Given that most people produce sweat passively, sweat is a very suitable medium for measuring glucose levels (Johnston et al. 2021). However, the way of obtaining the sample is complicated as it needs lots of exercises to achieve a good amount of sample for detection. Furthermore, many other factors should be considered when taking the sweat samples such as the availability of contaminants in the skin, the quantity of sweat readily available, deviations in results because of pH differences, sweat gland's periodic activation, skin topography, sweat rate per gland, and the number of active sweat glands, as well as between measurement locations on the same person (Zafar et al. 2022).

Much research was done on sweat samples for glucose detection. A single-layer graphene-based sensor coated in gold nanoparticles that contain GOx and take advantage of the characteristics of a glassy carbon electrode and 6-hexanethiol as an electron transfer medium is used to detect glucose in sweat (Yuan et al. 2019). The manufacturing of the sensor was made easier due to the use of chemical vapor deposition for the AuNPs. A clean surface also improved the immobilization ability of GOx and made the ductility monolayer graphene ideal for the detection of low glucose concentrations.

1.9.2.6 Serum

The medium of serum is effective for the detection of glucose. Although caution must be considered due to the various proteins and biomarkers contained in the fluid, it is frequently accurate and trustworthy. However, the need for a machine to separate blood hemoglobin to extract the serum makes this method complicated. Taking into consideration the fact that obtaining the serum sample must pass through the fear of needles which is painful and bothersome.

Human blood serum samples have been used with a device based on functionalized reduced graphene oxide to detect glucose molecules. The electrocatalytic activity of glucose serves as the basis for this sensor (Guler, Turkoglu, and Kivanc 2017). The sensor was fabricated based on a modified glassy carbon (GC) electrode and functionalized reduced graphene oxide (rGO-APTES) with rGO-APTES immobilized GOx. Another invention uses polypyrrole nanowires and graphene oxide technology to create fiber electrochemical transistors (Y. Wang et al. 2017).

Overall, the use of saliva samples for glucose detection can be a more comfortable, convenient, and cost-effective alternative to other sampling, with the added benefit of potentially allowing for more frequent monitoring of glucose levels.

1.10 Common chemicals methods of AuNPs synthesis

Many different synthesis methods have been developed to produce gold nanoparticles (AuNPs). The "bottom-up" method and the "top-down" method are two categories into which techniques for creating various AuNPs can be divided. The bottom-up strategy comprises chemical, photochemical, and nanosphere thermal, sonochemical, electrochemical, and templating reducing strategies. This technique entails the assembly of atoms (resulting from ion reduction) into sought-after nanostructures. Top-down techniques, like electron beam lithography and photolithography, need that matter to be removed from the bulk material to have the nanostructure that is wanted.

While both approaches can produce Each AuNP has its ideal shape and size. limitations, such as weak monodispersity in bottom-up model approaches, as well as significant material waste in top-down methods). The simplest and most used method of synthesis is this technique which involves turning gold ions (Au^{3+}) chemically into AuNPs Au^0. The production of gold nanoparticles depends on two processes: reduction and stabilization. $NaBH_4$, sodium citrate, sugars, and polymers are a few examples of reducing agents. While the stabilizing agents include trisodium

citrate, polymers, dendrimers, and surfactants such as cetyltrimethylammonium bromide (CTAB). The Turkevich method and Brust method are the most common methods used for the chemical synthesis of AuNPs (Shah et al. 2014).

1.10.1 Turkevich method

The Turkevich method, which was first introduced in 1951, uses chemicals to synthesize AuNPs. It is one of the most well-known methods for creating spherical AuNPs with a size between 10 and 30 nm. The foundation of this technique is the reduction of the gold precursor utilizing reducing agents like polymers, ascorbic acid, trisodium citrate, and ascorbic acid. The gold precursor is heated until it boils, and then, while being vigorously stirred, 1% trisodium citrate solution is quickly added. The transition of the solution's color from pale yellow to wine red indicates the creation of AuNPs. This approach produces AuNPs that are roughly 20 nm in size. The role of sodium citrate is to provide stability for the colloidal gold (Kimling et al. 2006).

1.10.2 Burst Method

Brust first presented this technique in 1994. This technique was used to produce smaller (1.5–5 nm), low dispersal, and thermally stable AuNPs by adjusting the proportion of thiol to gold in organic solvents. The aqueous gold precursor is moved to an organic solvent like toluene using the phase transfer agent tetraoctylammonium bromide (TOAB) in this two-phase method. The reduction is then carried out by ($NaBH_4$) in the presence of alkanethiol. After the addition of reducing agents, the organic phase's color changed from orange to brown, signaling the synthesis of AuNPs (E et al. 2014). The general approach for the gold nanoparticles synthesis is presented in detail in (Figure 0-18).

In general, as this procedure involves gradual enlargement of the dimension, it enables the regulated production of AuNPs in the preferred shape and size. However, the considerable quantity of significant variables poses a challenge to the management and enhancement of the process, such as the degree of warmth, the concentration of the reducing agent and precursor, the seed density, and the pace of the reducing agent's inclusion (Sadiq et al. 2023).

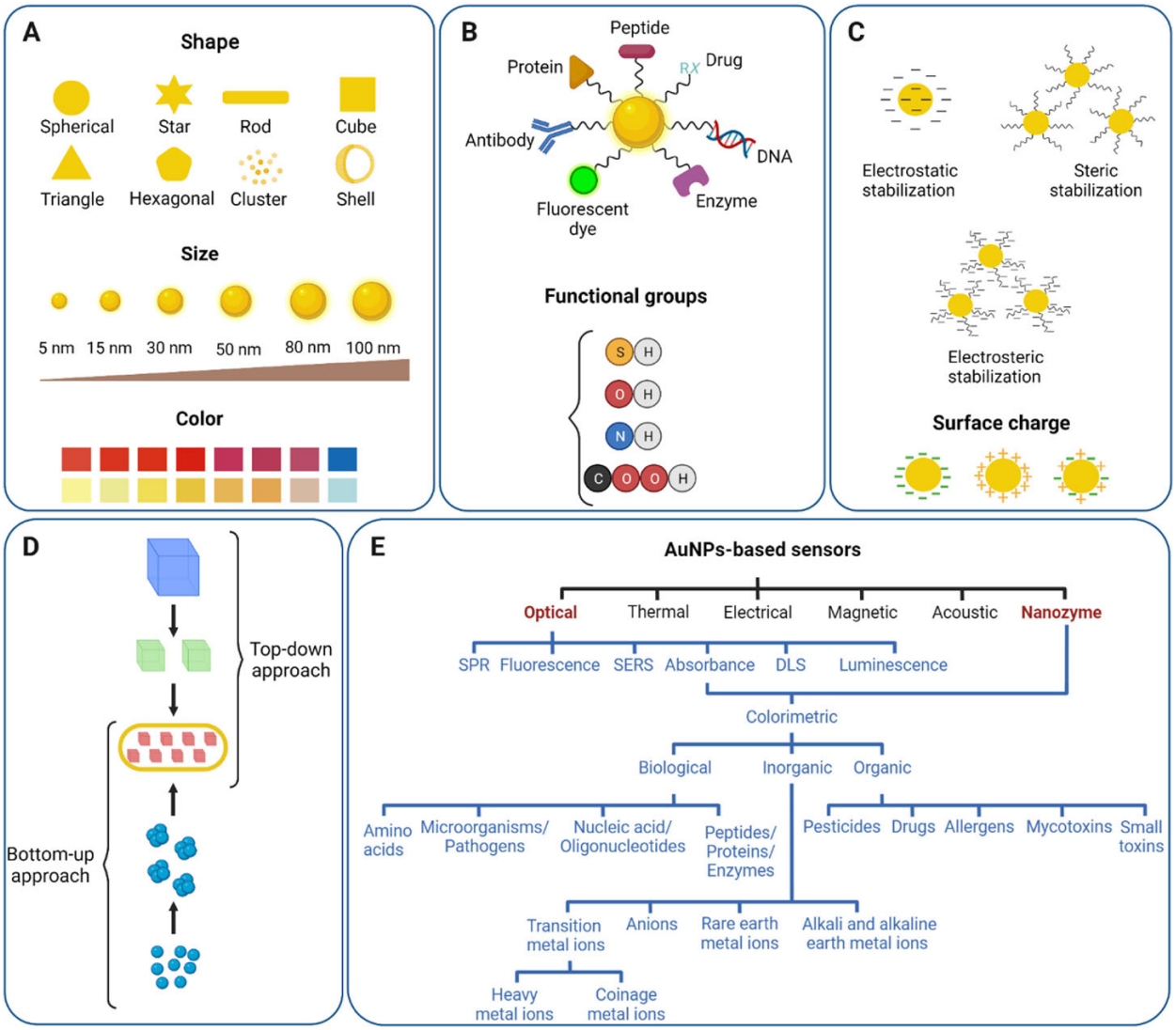

Figure 0-18 *A summary of the features of AuNPs emphasizing their principal attributes. (A) Depiction of diverse configurations, dimensions, and hues of AuNPs; (B) modification of the surface of AuNPs using a range of ligands comprising diverse chemical groups; (C) various sorts of stabilizing forces and surface charge surrounding AuNPs; (D) synthetic methods grouped into top-down and bottom-up classes for generating AuNPs; (E) the primary classifications of sensors based on AuNPs. Adapted from* (Sadiq et al. 2023).

1.11 Green methods of AuNPs synthesis using polysaccharides

Compared to conventional chemical approaches, a green biosynthesis strategy for noble metal nanoparticles has many advantages. These include bio-resources that are safe, simple, and affordable; don't require the usage of high pressure or temperature; don't consume dangerous or poisonous chemicals; and don't need any artificial ligands, cappings, or stabilizing agents for the biosynthesis of AuNPs. Most of these reducing and stabilizing agents were obtained from plants, algae, bacteria, and fungi (Bambo, Marcedo Krause, and Moutloali 2017).

Usually, plant extracts or microorganisms are used as reducing agents to reduce gold ions during the green production of Au NPs from Au^{3+} into Au^{0}. Typically, the extracts are made by soaking green materials in water under favorable climatic conditions (different green substances have different optimum conditions). Then, heat is applied (60-90) °C to enhance the reaction in the solution. The extracts are then combined with a gold ion solution, and when the solution turns red, AuNPs start to form (Ying et al. 2022). Table 0-2 explained the difference between using the chemical and the green synthesis of AuNPs.

Table 0-2 *Comparison between the chemical and green methods of AuNPs synthesis.*

Synthesis method	**Advantage**	**Disadvantage**
Chemical (Shabnam and Behboodi 2016)	- Uniform size and shape - Straightforward and fast preparation - Excellent quality of nanoparticles - Long shelf life of the nanoparticles	- Multi-step preparation - Needs stabilizing agents - Harmful, and toxic for human health and the environment - Not degradable by nature
Green using polysaccharides (Lee et al. 2020)	- Safe, simple, and facile - Easy to control the size and shape - Rapid and cost-effective - Eco-friendly, organic/easily degradable by nature	- Precise preparation steps are needed - The shelf life of the particles is short

Furthermore, other several polysaccharides, such as dextran, guar gum, cellulose, chitosan, carrageenan, and heparin, have been investigated for the manufacture of AuNPs. However, some of these polysaccharides and biopolymers cannot be used in large-scale production due to their inherent issues with high viscosity and low solubility, which necessitate derivatization (Rotureau, Dellacherie, and Durand 2006). In contrast, due to its high-water solubility and low viscosity, biocompatibility, and biodegradability, pullulan is utilized in a wide range of industrial applications, including as a food additive, a blood plasma substitute, a film, and an adhesive. Other numerous commercial and industrial uses for pullulan, including in the sectors of medicine, food science, biotechnology, and healthcare (Prajapati, Jani, and Khanda 2013). The rich structure of pullulan which is made of maltotriose, in which the three glucose units are connected by α -(1,4) glycosidic bond and the maltotriose units are connected by α -(1,6) glycosidic bond made it an attractive research polymer (H Moubasher 2014). Overall, pullulan is an attractive encapsulation material that was used to create a simple, eco-friendly, effective process for producing stable

AuNPs in a mild environment (Uryupina et al. 2011). Hence, the use of pullulan will be of great advantage in the field of sensors and detection.

1.12 Some methods for Cysteamine detection

Several analytical techniques have been proposed in the literature to identify and measure cys in biological specimens such as plasma and urine. These methods encompass enzymatic analysis, high-voltage electrophoresis, ion-exchange column chromatography, high-performance liquid chromatography (HPLC) with UV and fluorescence detection, and gas chromatography with photometric and flame ionization detection. This section will introduce a summary of some of these methodologies.

1.12.1 Cysteamine derivatization

As cysteamine lacks a chromophore in its structure, conventional analytical techniques that rely on UV absorbance or fluorescence detection pose a formidable task when it comes to quantifying this compound. Hence, the separation or quantification of cysteamine is accomplished through its derivatization. In order to achieve this, a multitude of derivatization agents have been employed and fine-tuned based on the analytical approach employed(Stachowicz et al. 1998b).

1.12.2 Pivaldehyde

Cysteamine is modified with pivaldehyde prior to its examination via gas chromatography (Lépinay et al. 2012).

1.12.3 Bis (trimethylsilyl) trifluoroacetamide (BSTFA)

The specimen, which includes cysteine, is deposited into a reaction vial with a threaded cap. Then, dimethylformamide and BSTFA are introduced. The amalgamation is permitted to settle for the duration of the night before the examination(Atallah, Charcosset, and Greige-Gerges 2020).

1.12.4 Ammonium 7-fluorobenzo-2-oxa-1,3-diazole-4-sulphonate (SBD-F)

SBD-F was formulated in a solution of borate buffer. The cysteamine sample solution was supplemented with borate buffer (125 mM; pH 9.5) that also contained 4 mM EDTA. The mixture was subjected to vortex-mixing for 30 seconds, and then the reaction mixture was subjected to heat at 60°C for 60 minutes. Finally, the labeling reaction was halted by cooling the mixture at 4°C for 15 minutes(Stachowicz et al. 1998b).

1.12.5 Enzymatic assay

This test involves hindering the D-amino acid oxidase enzyme function by the outcome of the response that arises between cysteamine and bromopyruvate. The enzyme function is in direct proportion to the quantity of cysteamine employed in the reaction, which is calculated by the decline in absorption at 324 nm. The test is advantageous for quantifying the obstruction of D-amino acid oxidase by diverse substances(Atallah, Charcosset, and Greige-Gerges 2020).

1.12.6 Ion-exchange chromotography

Hsiung et *al*. conducted research on identifying cysteamine through ion-exchange column chromatography employing an amino acid analyzer that included a brief column from Beckman analyzer. The detection of cysteamine was accomplished after 268 minutes, a duration that could result in product oxidation during analysis and consequently, an underestimation of the product's concentration (Hisung et al. 1978).

1.12.7 Fluorescent assay

Fluorescent sensing. HPLC employing fluorescent sensing is extensively utilized for sensing.cysteine. Numerous derivatizing agents are employed to induce distinct analysis conditions and elution duration(Stachowicz et al. 1998b).

1.12.8 Colorimetric method using Ellman's reagents

Ellman devised a quick and straightforward technique for measuring sulfhydryl groups using colorimetric analysis. The process involves a reaction between DTNB and sulfhydryl groups, which yields a yellow product (2-nitro-5-thiobenzoic acid). The concentration of cys is determined by measuring the absorbance of this product at a wavelength of 412 nm using a spectrophotometer (Atallah, Charcosset, and Greige-Gerges 2020).

1.12.9 Ultra-high performance liquid chromatography-electrospray

5-Aminoisoquinolyl-N-hydroxysuccinimidyl carbamate (5-AIQC) and N-(acridin-9-yl)-2-bromoacetamide (AYBA) were employed as derivatization agents for cysteamine quantification utilizing UHPLC-ESI-MS/MS (Xiao et al. 2019).

1.12.10 Electrochemical detection of cysteamine

Chemical reactions that entail the loss or acquisition of electrons are succeeded by ensuing reorganizations or responses. When these reactions transpire on metals that are physically isolated in a conductive environment, an electrical potential discrepancy is produced. The electrical indication is subject to the concentration of the analyte(Lépinay et al. 2012).

1.13 Inhibition of the peroxidase-like activity of AuNPs-pTab by amino acids

Nanozymes are inorganic nanomaterials that are credited to mimic the catalytic activity of natural enzymes. Up to now, various nanozymes including metal, metal-oxide, metal sulfide, and carbon-based materials have been documented for their catalytic activity that mimics enzymes(W. Chen et al. 2019). A recent assessment revealed that more than 200 research facilities worldwide are engaged in enhancing the development of novel nanozymes and broadening their scope of use(J. Wu et al. 2019b). Among the various uses and basic research, a particular aspect that is receiving quick recognition is the capacity to regulate the catalytic function of nanozymes to either improve or block and temporarily or permanently hinder their catalytic activity.

To this end, metal ions(Lien et al. 2013; Tseng et al. 2012), biomolecules such as ATP(Lv et al. 2020), cysteine(R. S. Li et al. 2016b), and glutathione(Zou et al. 2017) have all been effectively devoted to modulating the catalytic activity of nanozymes. As observed, ATP enhanced the catalytic efficiency of nanozymes(Vallabani, Karakoti, and Singh 2017), whereas cysteine, an amino acid, hindered their catalytic performance(W. Li et al. 2016).

Usually, inhibitory molecules attach either to the enzyme's active site or near it, leading to a reduction (temporary) or total loss (permanent) in catalytic effectiveness(Dill 1997). When it comes to temporary inhibition, the inhibitor molecule attaches reversibly to the enzyme causing a temporary reduction in the catalytic rate. In contrast, irreversible inhibitors bind to the enzyme and obstruct its activity permanently(Walther et al. 2019). Moreover, reversible inhibition has provided a profound understanding of the reversible inhibition mechanism (competitive, uncompetitive, or non-competitive) by computing the steady-state kinetic parameters, namely Michaelis Menten's constant (K_m) and maximum reaction velocity (V_{max})(Amine et al. 2014).

Overall, the use of gold nanoparticles as an enzyme mimic offers a promising alternative to traditional enzyme-based assays, addressing some of the limitations associated with natural

enzymes, such as stability and cost. Therefore, the detection of amino acids such as cysteamine using the inhibition of the peroxidase-like activity of gold nanoparticles holds significant importance in advancing various applications that rely on accurate and efficient amino acid analysis.

Chapter 3. Glucose Detection

This chapter focuses on the experimental and results analyses carried out on glucose detection in human saliva and explains the gold synthesis and the tablet fabrications in detail.

1.14 Chemicals and materials

The following chemicals were purchased from different resources to perform the synthesis and the overall experiments for the detection of H_2O_2 and glucose:

Gold (III) chloride solution (30 wt.% in dilute HCl), 3,3',5,5'-tetramethylbenzidine (TMB), sodium carbonate (Na_2CO_3), copper (II) sulfate pentahydrate ($CuSO_4 \cdot 5H_2O$), sodium citrate ($C_6H_5Na_3O_7$), and sodium borohydride ($NaBH_4$), Horseradish peroxidase (HRP) were purchased from Sigma-Aldrich, USA. Pullulan (average Mw. ~200 kDa) was obtained from Polyscience, Inc, USA. Trisodium citrate ($C_6H_5Na_3O_7$), sodium phosphate monobasic monohydrate ($NaH_2PO_4 \cdot H_2O$), sodium phosphate dibasic (Na_2HPO_4), hydrogen peroxide (H_2O_2 30%), maltose, fructose, lactose, glucose, glucose oxidase (GOx) from *Aspergillus niger,* sodium hydroxide (NaOH), Sodium borohydride ($NaBH_4$), 4-Nitrophenol ($C_6H_5NO_3$), sulphuric acid (H_2SO_4), citric acid ($C_6H_8O_7$), hydrochloric acid (37%), and nitric acid (65%) were purchased from Sigma Aldrich, Canada. Artificial unstimulated saliva (99.99% purified) was obtained from Biochemazone, USA. Deionized water from Sigma Aldrich, USA was used to prepare all solutions. A carbon steel tray (Betty Crocker) was purchased from a local store, in Canada.

1.15 Synthesis of pullulan stabilized gold nanoparticles solution (AuNPs-pSol)

With few adjustments, monodispersed AuNPs-pSol was created using the literature-reported method described by (Laksee et al. 2017a). In a beaker, a mixture of 3% (w/v) pullulan (30 mL) and 1% (w/v) NaOH (12.5 mL) was heated at 70 °C for an hour to obtain the treated pullulan solution. To this solution, 2.5 mM $HAuCl_4$ solution (7.5 mL) was added, and the reaction mixture was stirred at 90 °C for another hour to get the red wine color pullulan stabilized gold nanoparticles (AuNPs-pSol). The full synthesis was accomplished in a beaker with a plastic cover as displayed in (Figure 0-1). The concentration of AuNPs-pSol was estimated to be ~22 nM using Beer's law ($A = c\varepsilon l$) where A is the absorbance recorded at 520 nm using a UV-vis spectrophotometer (BioTek, Cytation 5, imaging reader), ε is the molar extension coefficient of 10 nm diameter gold nanoparticles, and l is the path length of one well of the 96-well plate. The extinction coefficient (ε) of 10 nm AuNPs is 9.4 X 10^7 M^{-1} cm^{-1} (Tang, Gao, et al. 2018).

Figure 0-1 *Synthesis of AuNPs-pSol in a beaker with plastic cover.*

1.16 Preparation of pullulan stabilized gold nanoparticles tablet (AuNPs-pTab)

To determine how temperature affects tablet production, the synthetic AuNPs-pSol was utilized to cast the tablets under two distinct settings. In order to obtain AuNPs-pTab, a pre-measured encapsulated AuNPs colloidal solution, (100 L) AuNPs-pSol was pipetted out and dropped in a carbon-steel tray. The first batch of tablets was dried in a laboratory oven (Thermo Scientific, Model# PR30525G, USA) without forced air convection at 50 °C for 30 minutes while the second batch was dried in an ambient condition for 24 hours. Both batches of tablets were collected and stored at room temperature in a glass vial for further use.

Particle size and zeta potential of AuNPs-pTab were evaluated applying Litesizer 500 Particle Size Analyzer on a zeta universal dip cell and polystyrene cuvettes in a Malvern Zetasizer Nano ZS equipment (Malvern, England) at 25 °C. An infrared spectrum of AuNPs-pTab was achieved from a Nicolet™ iS20 FTIR Spectrometer (Thermo Scientific Instrument Co., USA) in the range of 4000 to 400 cm^{-1} to identify potential chemical interactions or the formation of new bonds. Transmission electron microscopy (TEM) was performed using an FEI Titan Krios Cryo-STEM system (working at 200 kV) for particle morphology and size. (Figure 0-2) exhibited the whole synthesis and fabrication method of AuNPs-pSol and AuNPs-pTab.

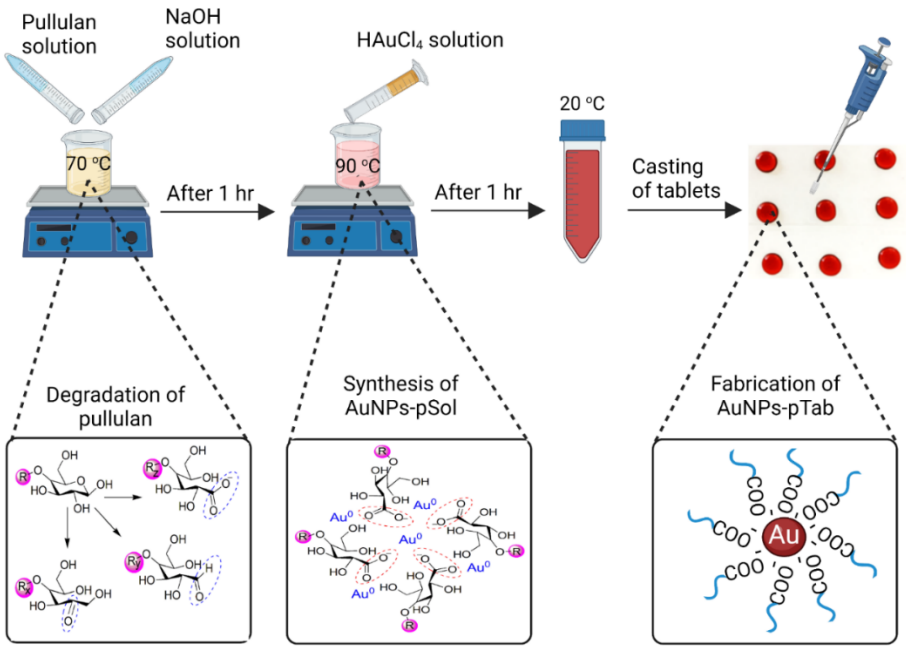

Figure 0-2 *Making pullulan-stabilized gold nanoparticle tablets (AuNPs-pTab) (AuNPs-pSol). First, treated pullulan was created by degrading it with NaOH for an hour at 70 °C. This step was followed by the addition of $HAuCl_4$ solution and heating the reaction media at 90 °C for another hour to synthesize AuNPs-pSol. Lastly, a 100 µL solution of AuNPs-pSol was pipette-out on a non-stick tray to cast AuNPs-pTab. The tablets took 24 hours to dry at room temperature, compared to 30 minutes in a 50 °C oven to dry them.*

The assessment of various methods of drying such as oven and room temperature drying is displayed in (Figure 0-3). The AuNPs-pTab's formation and shape were much affected by the drying method. It was observed that the tablets produced in the oven have a more circular-round shape than the ones obtained from drying in ambient air. However, the shape of AuNPs-pTab does not affect the sensitivity of tablets toward glucose detection.

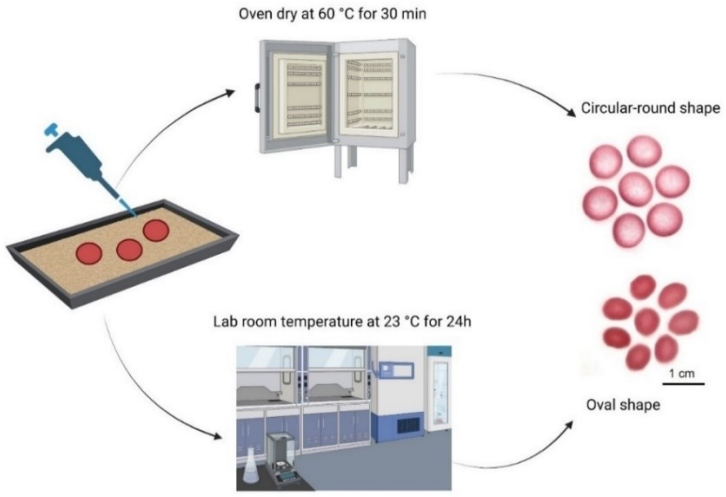

Figure 0-3 *AuNPs-pTabs dried in different conditions. Oven drying at 60 °C for 30 minutes produced well-rounded circular shape tablets whereas ambient condition drying at room temperature produced quasi-round-shaped tablets.*

1.17 Preparation of McIlvaine and PB buffers

McIlvaine buffer is a mildly acidic buffer that ranges between (pH= 2-5) and is necessary when using the TMB as a substrate and enhancing the blue color. While PB is the medium suitable for GOx enzyme and required to perform glucose detection.

McIlvaine (citrate-phosphate) buffer preparation (0.15 M):

First, in a beaker, 0.2 M of sodium phosphate dibasic was added to 25.7 ml water followed by a vortex of the produced solution. Second, in a separate beaker, 0.1 M of citric acid was combined into 24.3 ml water and vortex. Third, 12.85 ml of the sodium phosphate dibasic was taken and mixed with the previously prepared solution of 12.15 ml citric acid followed by the addition of 25 ml water. The pH of the solution was adjusted by adding either sodium phosphate dibasic or citric acid solutions. A pH meter was used to measure the pH until obtaining the required pH value.

PB solution preparation (10 mM):

To prepare 10 mM PB solution, in a beaker, 8.36 g of sodium phosphate monobasic and 19.6 g of sodium phosphate dibasic were dissolved in 10 L distilled water. The final pH was adjusted using the pH meter to obtain 7.2 ± 0.2.

Preparation of TMB substrate:

First, 1 mg of TMB was added to 1 ml of DSMO solution until completely dissolved. Second, 9 ml of McIlvaine buffer was added to the previous solution of TMB/DSMO until completely mixed. Finally, the obtained solution was kept in the fridge at 4 °C for further use.

Preparation of Benedict's reagents:

To perform the test that can indicate the presence of reducing sugar and proof the existence of reduced sugar in alkali-treated pullulan, Benedict's test is applied. Therefore, the following method of reagent preparation was followed. A 17.3 g of copper sulfate ($CuSO_4$), 173 g of sodium citrate ($Na_3C_6H_5O_7$), and 100 of anhydrous sodium carbonate (Na_2CO_3) were weighed. Then, placed in a volumetric flask of 1000 mL of distilled water. The solution was vortexed properly to make sure that all the chemicals are completely dissolved.

For the test of reducing sugar, 1 mL of the sample solution of alkali-treated pullulan or AuNPs-pSol or AuNPs-pTab) was added to a clean test tube. Second, 2 mL of Benedict's reagents were

poured over the sample. Finally, the test tube containing the reagents was warmed up and submerged in a beaker that contains boiling water for (3-5) minutes. The color change was observed by the naked eye as shown in (Figure 0-4).

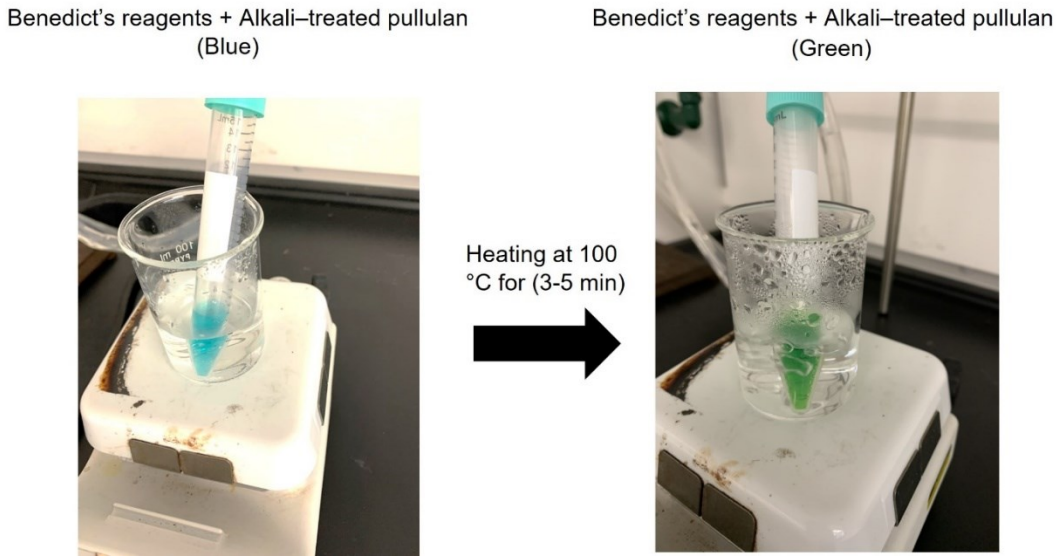

Figure 0-4 *Benedict's test was performed to discover the presence of reducing sugar in alkali-treated pullulan. The same procedure was followed using AuNPs-pSol or AuNPs-pTab.*

1.18 Preparation of catalytic activity test reagents

The catalytic activity test reagents were prepared according to the literature procedure indicated by Qiu et al. with some modification (Qiu, Ma, and Hu 2014); 500 µL of 0.1 mM of 4-nitrophenol was prepared and added to 250 µL 0.1 M $NaBH_4$. The solution of (4-nitrophenole+ $NaBH_4$=4-nitropheloate). Typically, a volume of 100 µL of pAuNPs-Solution was dispensed to form a single tablet, but for optimization investigations, quantities of 25, 50, 75, and 100 µL of AuNPs-pSol were also employed to produce quarter, half, three-quarter, and one tablet. A different portion of AuNPs-pTab (1/4, 1/2, 3/4, and 1 tablet) was added to the solution of 4-nitrophenolate. The estimated weight of AuNPs-pTab was measured to be 1.2 mg using a Sartorius digital scale. UV-vis spectroscopy was used to measure the resulting color transformation from yellow (peak at 400 nm) to colorless (peak at 298 nm).

1.19 Procedure for glucose detection in buffer solution using AuNPs-pTab sensor

The catalytic activity of AuNPs-pTab was assessed by first testing its potential to oxidize TMB substrate to its blue-colored product using H_2O_2 as an oxidizing agent. The reaction scheme

composed of 100 μL of H_2O_2 in 5-500 μM concentrations, 330 μL of McIlvaine buffer (citrate-phosphate buffer) (pH 4.2), one AuNPs-pTab (100 μL), and 300 μL TMB incubated at 25 °C for 30 minutes followed by UV-vis (BioTek, Cytation 5, imaging reader) spectroscopic measurements on Costar plate reader (Ulti Dent Scientific, Canada) as a function of time. The buffer pH was measured using a pH meter (AB200 pH/mV/conductivity made from Fisher Scientific accumet, Singapore). Reaction conditions such as the AuNPs-pTab nanozyme concentration, buffer pH, and reaction temperature were optimized. This experiment was followed by the detection of glucose concentrations (0.5-500 μM) in a phosphate buffer (PB) solution (pH 7.4). In a typical procedure, 80 μL glucose and 20 μL GOx were incubated in 200 μL PBS solution whereas one AuNPs-pTab (100 μL), 300 μL TMB and 330 μL McIlvaine buffer (pH 4.2) were incubated separately for 15 minutes at room temperature.

Finally, both the solutions were mixed using vortex (Model# 945FIALUS, 50/60 Hz Fisher brand, USA), and the absorption spectra at 652 nm were measured after 30 minutes to record the color intensity of the solution. To confirm the enzymatic activity of AuNPs-pTab, catalytic parameters were calculated by fitting the absorbance values to the Michaelis Menten kinetics model.

1.20 Procedure for glucose detection in artificial and real saliva using AuNPs-pTab

The peroxidase-mimicking catalytic activity of AuNPs-pTab was evaluated in an artificial saliva solution (pH 6.8) using different glucose concentrations (0.5-500 μM) as described in section 3.8. Detection of glucose in the real saliva of diabetic patients (pH 6.5-7.0) was also conducted to show the practical application of tablet sensors in real situations. The limit of detection (LOD) was calculated using the formula $3\sigma/\mu$, where σ and μ are the relative standard deviation of absorbance measurements and the slope of the linear calibration plot, respectively. Further, a spiking test was performed and percent recovery (% R) was calculated to validate the method. The full detection procedure in the saliva sample is shown in (Figure 0-5).

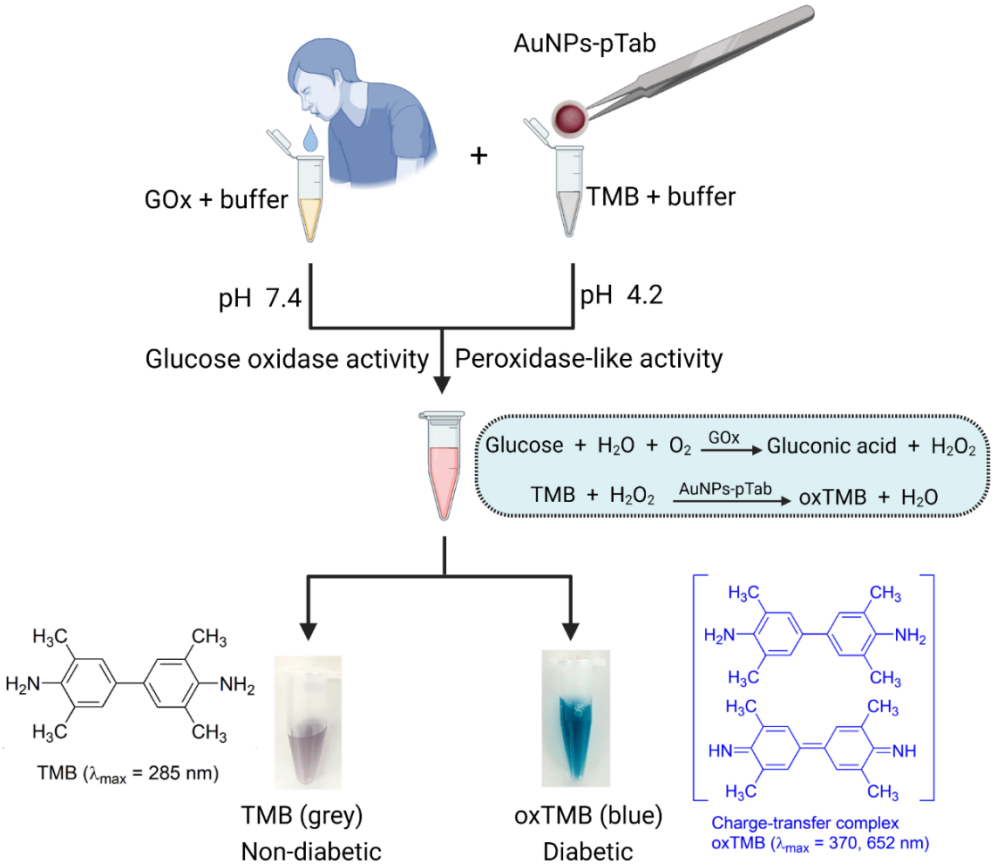

Figure 0-5 *Using an AuNPs-pTab sensor, glucose may be detected calorimetrically in saliva. First, the glucose assay involves, to release hydrogen peroxide, the saliva sample was treated with glucose oxidase (GOx) in PB solution at pH 7.4 for 15 minutes (H_2O_2). One AuNPs-pTab tablet was dissolved in TMB solution at pH 4.2, which was sustained by McIlvaine buffer, in the meantime. To see the visible color shift, both solutions were combined and incubated for 30 minutes. The H_2O_2-TMB system was employed in this procedure to assess glucose levels. The presence of glucose in saliva was detected by the blue color complex formed when the peroxidase substrate TMB was oxidized by H_2O_2 in the presence of AuNPs-peroxidase pTab's mimicking activity (a diabetic condition). In the absence of glucose, the solution remained colorless or faint grey indicating a non-diabetic condition.*

1.21 Preparation of interference materials with glucose assay using AuNPs-pTab sensor

Other than glucose, the effect of potential interferants that might exist in saliva such as fructose, maltose, and lactose was examined. The same procedure mentioned in section 3.7 was followed for this proposed glucose assay. A 1 mM of interferants was used in this experiment and the absorption spectra were recorded at 652 nm using UV-vis spectroscopy.

1.22 Results and discussion

1.22.1 Principles of peroxidase-like activity of AuNPs-pTab

Peroxidases are a group of enzymes that catalyze the oxidation of a substrate by H_2O_2-producing water and hydroxyl radical ($^{\bullet}OH$). These catalysts outperform normal enzymes, which quickly denature and lose their activity at temperatures of 40 °C and higher, because of their wide temperature range and rigid structure. High catalytic activity AuNPs-pTab is produced through the synthesis of gold nanoparticles with pullulan. The conversion of glucose into gluconic acid, H_2O_2, and water can be catalyzed by AuNPs-pTab. H_2O_2 can indirectly be used to quantify glucose concentrations by the oxidation of TMB causing the production of blue color. (Figure 0-6) describes the principles of AuNPs-pTab synthesis and glucose sensing.

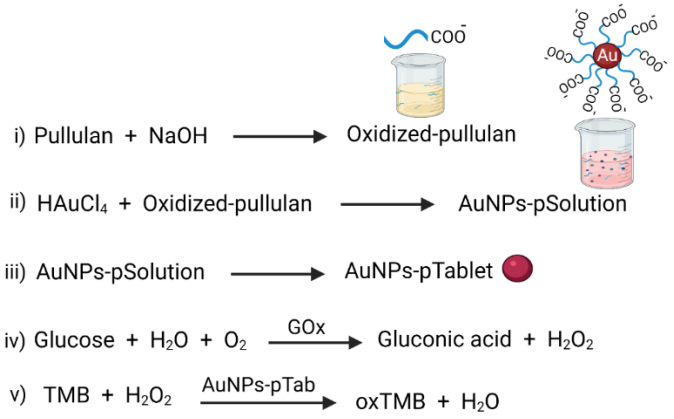

Figure 0-6 *The reaction theory or process linked to glucose detection using synthetically produced AuNPs that are negatively charged. i) pullulan is oxidized when pullulan and NaOH are combined. ii) the emergence of a carboxylate group with a negative charge when gold nanoparticles are introduced to the mixture. iii) From AuNPs-pSol, AuNPs-pTab is formed. iv) the production of H_2O_2 from glucose when water, oxygen, and GOx are present. This process emits also gluconic acid. v) addition of AuNPs-pTab into a solution of TMB and H_2O_2 triggers the oxidation of TMB and the production of water.*

1.22.2 The characterization of the AuNPs-pSol and AuNPs-pTab

Utilizing the catalytic feature of AuNPs, the AuNPs-pTab sensor was created for the colorimetric detection of glucose in saliva. Pullulan that had undergone alkali treatment and gold salt were combined to create AuNPs-pSol in an aqueous phase without the use of external reducing or capping agents (Laksee et al. 2017a). The pullulan chain's alcoholic groups were changed into aldehyde and α-hydroxyketone functionalities via the Nef-Isbell-Richards mechanism, which is NaOH-mediated ring opening of the polymer (Knill and Kennedy 2002). To form AuNPs surrounded by pullulan fragments with carboxyl groups C(=O) OH following oxidation,

tetrahydroauric chloride is used to disintegrate pullulan as an effective reducing agent. Different chlorohydroxyaurate complexes, including $AuCl_4^-$, Au $(OH)_4^-$, $AuCl(OH)_3^-$, $AuCl_2(OH)_2^-$, and $AuCl_3(OH)^-$, were produced in a reaction mixture, leading to the production of AuNPs. The negatively charged carboxylate ions $-COO^-$ frame the AuNPs efficiently and thus act as a capping ligand. In addition to being a reducing and stabilizing agent, the long polymeric chains of pullulan also act as tablet-forming reagents because of the film-forming property of pullulan upon drying(Luís, Ramos, and Domingues 2020; Pan et al. 2021).

AuNPs formation is a quick redox reaction because wined red Au^0 particles have been formed within 3 minutes confirmed by absorbance peak at 520 nm. The peak intensity gradually improved within 40 minutes and remained persistent after 60 minutes as shown in (Figure 0-7 A and B).

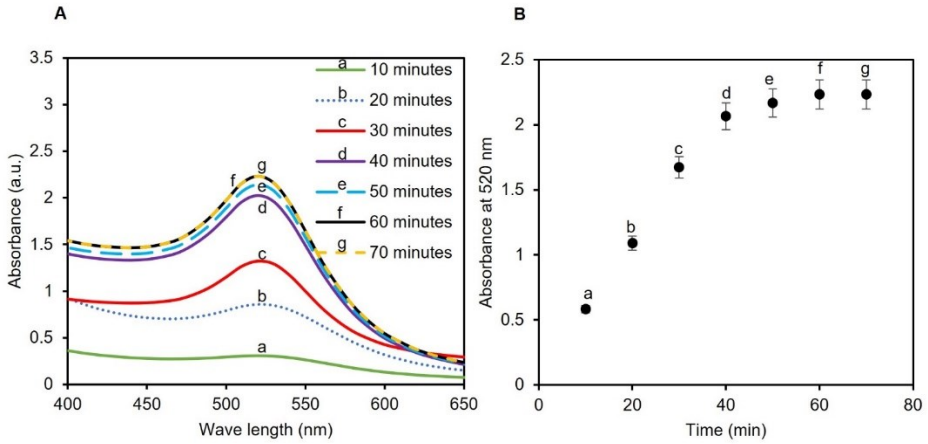

Figure 0-7 A) *AuNPs-pSol reaction development. a) after 10 minutes of adding $HAuCl_4$. b) after 20 minutes. c) after 30 minutes. d) after 40 minutes. e) after 50 minutes. f) after 60 minutes. and g) after 70 minutes.* ***B)*** *Absorbance at 520 nm corresponds to the peak development and particle growth of dAuNPs-pSol showing no change in absorbance was reported after 60 minutes.*

The pH and temperature of the reaction media have a great impact on particle shape and size. The optimal pH is 6.7 which produced a narrow and sharp absorption peak at 520 nm indicating a uniform particle size whereas a weak peak appeared at pH <6.7. On the other hand, AuNPs formation was observed at alkaline pH, but particles get aggregated into a black solution within minutes. The reaction went well at 90 °C whereas a slight decrease in temperature (70 °C) produced a purple color solution indicating the bigger size particles as shown by the absorption peak at 540 nm (Figure 0-8A). Then, the successful synthesis of AuNPs-pSol was followed by AuNPs-pTab formation at ambient conditions and in an oven at 50 °C. Solid tablets were collected and characterized using FTIR, TEM, and DLS analysis.

Finally, the zeta potential of the AuNPs-pTab solution was compared with AuNPs-pSol to see the changes in the particle's surface charge. It is worth mentioning that no change in zeta potential value in both samples which was -9.7 mV indicated the similar reactivity of AuNPs-pTab particles as of AuNPs-pSol. In DLS analysis, the hydrodynamic diameter of AuNPs-pTab and AuNPs-pSol was found to be 80.20 nm with 22% PDI (polydispersity index) and 70.23 nm with 25% PDI, respectively. The size of particles in dry and solution formats was almost similar which indicated our AuNPs-pTab as a potential replacement for AuNPs-pSol. which is presented in (Figure 0-8B).

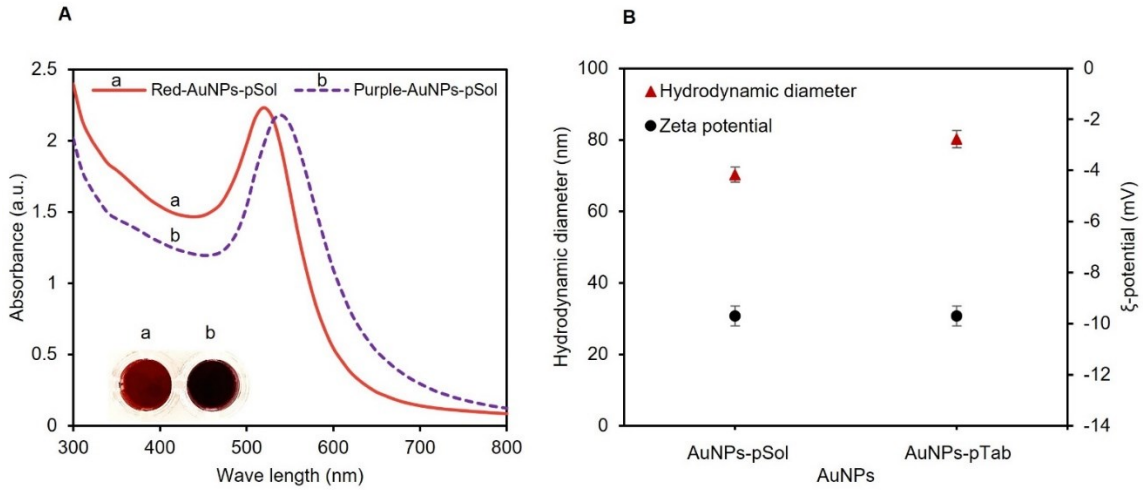

Figure 0-8 A) *The influence of temperature on the particle size formation of AuNPs-pSol. a) the color of the solution was wine-red with a peak at 520 nm specifying smaller size particles. While b) purple color AuNPs-pSol is obtained with a peak at 540 nm signifying larger size particles.* ***B)*** *The hydrodynamic diameter vs the apparent zeta potential for AuNPs-pSol and AuNPs-pTab indicates almost the same features.*

The FTIR spectrum of AuNPs-pTab was related with pristine pullulan and alkali-degraded pullulan which indicated the successful incorporation of pullulan chains throughout AuNPs as shown in (Figure 0-9). The FTIR spectra showed a broad absorption band at 3290 cm^{-1} due to O-H stretching whereas other common absorption peaks in AuNPs-pTab and pristine pullulan were at 2920 and 2910 cm^{-1} respectively related to sp^3 hybridization of C-H stretching. The prominent absorption band at 1620 cm^{-1} was due to the O-H bending of H_2O molecules in alkali-treated pullulan. The absorption at 1360 cm^{-1} was related to C-O-H bending, while the peaks at 751 and 990 cm^{-1} revealed the presence of α-(1,4)-D-glucosidic and α-(1,6)-D-glucosidic bonds respectively in AuNPs-pTab (Y. Wu, He, and Zhou 2022). The FTIR spectrum of AuNPs-pTab displays new absorption bands at 1354 and 1591 cm^{-1} due to symmetrical and asymmetrical stretching vibrations of $-COO^-$ (Prasad et al. 2012).

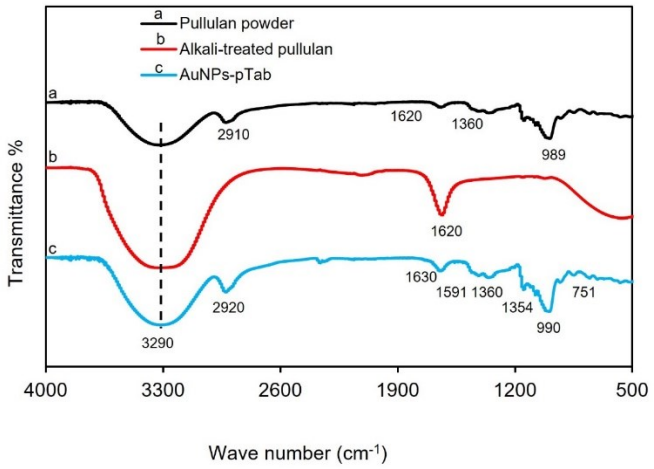

Figure 0-9 *The FTIR analysis of a) Pullulan powder. b) Alkali-treated pullulan. and c) AuNPs-pTab showing the different functional groups.*

The nanoparticle size of AuNPs-pSol and AuNPs-pTab were confirmed by UV-vis spectroscopy showing a peak at 520 nm as shown in (Figure 0-10A). While the size of AuNPs-pTab was confirmed by the TEM image as shown in (Figure 0-10B). The image illustrates an average particle size of 10±1.5 nm with a spherical shape which was also confirmed by the UV-vis absorption peak at 520 nm.

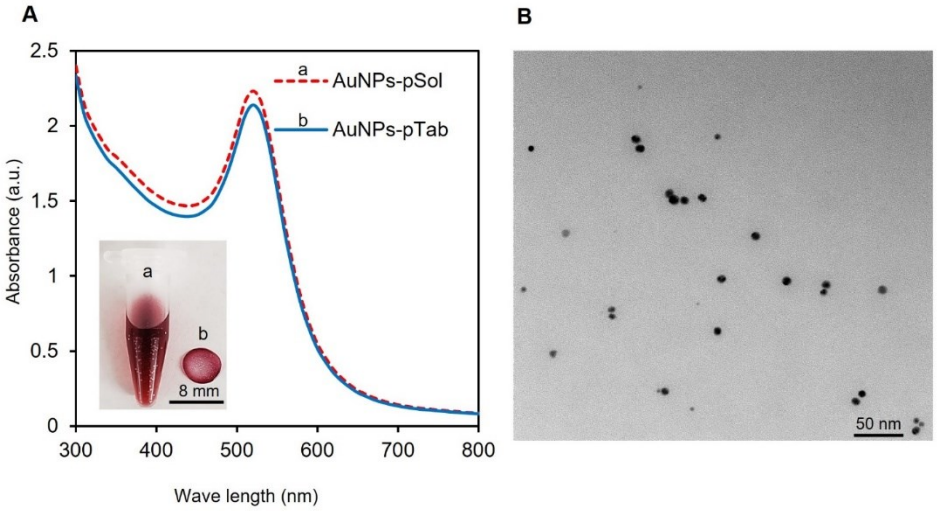

Figure 0-10 A) *The absorption spectra of AuNPs-pSol and AuNPs-pTab show almost the same peak at 520 nm.* ***B)*** *Transmission electron microscopy (TEM) analysis of AuNPs-pTab showing the spherical shape and nanosize of particles.*

Finally, to examine the pAuNPs-Tablet surface morphology and its surroundings in a solid state, high-resolution surface images of the pAuNPs-Tablet were acquired using AFM scanning probe microscopy. The pullulan matrix contained dispersed AuNPs, resulting in a red-colored tablet as

depicted in (Figure 0-11A). The phase trace image in the figure revealed that the mean height of the AuNPs was between 10-30 nm, indicating that they were uniformly distributed and well preserved throughout the exopolysaccharide substance. The largest gold particle in the image had a diameter of 89.40 nm. For a surface roughness and texture description of the pAuNPs-Tablet in 2D and 3D height profiles, refer to (Figure 0-11B, C, and D).

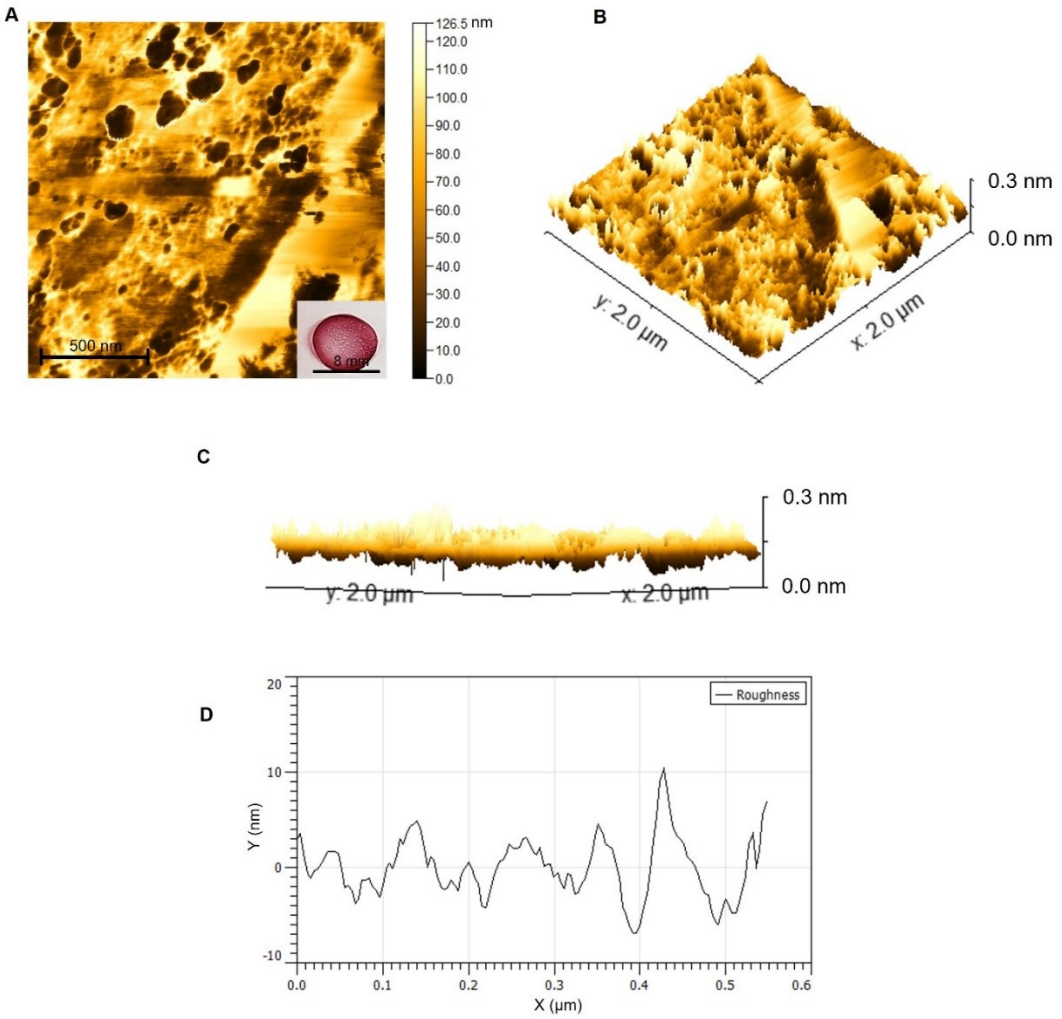

Figure 0-11 *The AFM images of the pAuNPs-Tablet particles show a height trace of the tablet surface.* ***A)*** *2D image of height profile of pAuNPs-Tablet in an amplitude trace;* ***B and C)*** *3D image of height profile of A;* ***D)*** *Height distribution as surface roughness and texture description along the black line area of image A. The average roughness was ~1.8 nm, the average maximum height of the roughness was ~10 nm, the average maximum roughness valley depth was ~6.6 nm, the maximum peak to valley roughness was ~18 nm and the waviness average was ~1.15 nm. The results confirmed that the strong binding between pullulan and AuNPs occurred.*

Benedict's Test, a chemical analysis technique, is used to evaluate how much sugar has been reduced in a solution. A qualitative test called Benedict's Test is frequently used to distinguish

between reducing and non-reducing forms of carbs (sugars and carbohydrates). Sugars that have free aldose or ketose groups are considered reducing sugars because they can give electrons to other molecules that are oxidizing them. Their molecules have a free carbon atom at the end of them. Reducing sugars are present in all monosaccharides as well as some disaccharides, oligosaccharides, and polysaccharides.

Benedict's test is frequently applied to distinguish simple sugars (monosaccharides) from other reducing sugars. It is substituted for Fehling's test. The appearance of a brick-red color brought on by the chemical interaction between Benedict's reagent and reducing sugar serves as the basis for identification. Based on the strength of the reaction mixture, the sugar concentration can be calculated, but its precise value cannot be predicted. As a result, this test is both semi-quantitative and qualitative (Hernández-López et al. 2020).

The principles of Benedict's test are based on the measurement of the pH of the mixture and sample reagents which is raised by the presence of sodium carbonate. Reducing sugars become powerful reducing agents called enediols when exposed to alkaline and hot environments. These enediols change the cupric ions (Cu^{2+}) of the Benedict reagent, which are present as copper sulfate ($CuSO_4$), into cuprous ions (Cu^{+}), carbon dioxide, and water. Red cuprous oxide (Cu_2O), commonly referred to as insoluble copper (I) oxide, is the form in which the cuprous particles are present. Red copper oxides precipitate in this manner (I. Elzagheid 2018). The amount of reducing sugar in the sample affects the color and intensity of the reaction mixture. Then, the amount of reduced sugar in the sample can be calculated based on the hue of this color. The color progressively shifts from green to yellow to orange to brick red as the number of reduced sugar increases.

In this research, the presence of aldehyde -C(=O) H and α-hydroxyketone RCR′(OH)(CO)R) species in treated pullulan was confirmed by Benedict's test which produced green color in degraded pullulan while untreated pullulan showed no color change. Moreso, the Benedict's solution of AuNPs-pSol and AuNPs-pTab turned greenish-brown which was in agreement with previous research as shown in (Figure 0-12) (Amornkitbamrung et al. 2014; Ng and Hashimoto 2020).

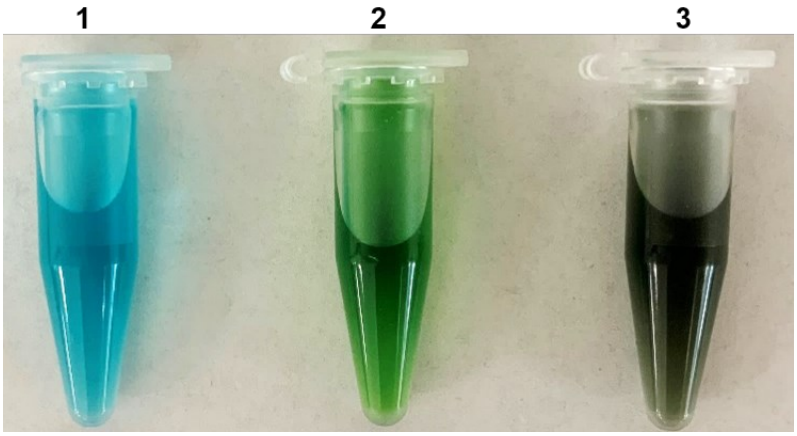

Figure 0-12 *Benedict's test shows the presence or absence of reducing sugars (α-hydroxy ketone and aldehyde functional groups) in pullulan polymer. The Benedict solution did not undergo any color change and remained blue (1) with untreated pullulan showing the absence of reducing sugars. The solution turned green (2) in the case of alkali-treated pullulan indicating the presence of reducing sugars. Benedict's solution shows dark-green color (3) in the presence of AuNPs-pSol or AuNPs-pTab solution.*

1.22.3 The mechanism of glucose assay using AuNPs-pTab sensor

The principle of glucose assay is based on the detection of H_2O_2 which is necessarily produced as a by-product of glucose oxidation in the presence of GOx. In the tablet-based colorimetric test, the peroxidase-mimicking enzymatic activity of AuNPs-pTab was examined studying H_2O_2 as an oxidizing agent and TMB as a peroxidase substrate. Peroxidase is an enzyme used to break up peroxides. Hence, AuNPs-pTab was employed to cleave H_2O_2 to generate $^{\bullet}OH$ radical as a reactive oxygen species (ROS) in the detection system. The H_2O_2-TMB system works well in the acidic condition which was maintained using McIlvaine buffer (Drozd et al. 2016).

The generated $^{\bullet}OH$ radical is unstable due to the presence of an unpaired electron which was stabilized by the interactions with conduction band electrons of AuNPs-pTab. These interactions may contribute to the peroxidase-like catalytic activity of AuNPs-pTab as visualized by the oxidation of TMB (oxTMB) into a blue color product. Moreover, the positive charge on oxTMB may accelerate this process by attracting negatively charged AuNPs-pTab as confirmed by obtaining a low K_m value of Michaelis Menten's kinetics (Yanping Liu et al. 2014).

The peroxidase behavior of AuNPs-pTab was confirmed by adding a stop solution of 1M H_2SO_4 which quickly terminated the oxidation of TMB; hence, the blue color of oxTMB was changed to yellow. This inhibition caused a shift in the absorbance peak from 652 to 450 nm whereas no peak was observed for the TMB-H_2O_2 system without AuNPs-pTab as indicated in (Figure 0-13A).

Hence, the peroxidase-like nanozyme behavior of AuNPs-pTab was confirmed and employed for glucose detection. In addition to this, the catalytic performance of AuNPs-pTab was compared with AuNPs-pSol and absorbance spectra was recorded for both samples using the H_2O_2-TMB system under similar conditions. The peroxidase activity of AuNPs-pTab was 25% higher than AuNPs-pSol as shown by the intense blue color of oxTMB in (Figure 0-13B). This is anticipated by the dehydrated layer of a polymer around the nanoparticles which increases the catalytic activity of the gold in the case of AuNPs-pTab (Machida et al. 2022).

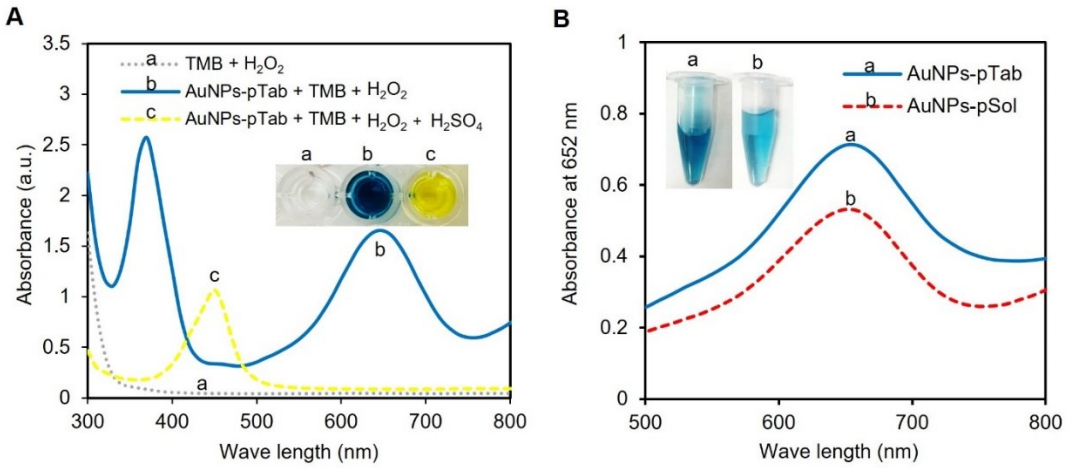

Figure 0-13 *The catalytic activity of AuNPs-pTab and their comparison with AuNPs-pSol.* ***A)*** *The TMB-H_2O_2 solution was colorless and showed no absorption peak in the absence of AuNPs-pTab whereas an intense blue color formed having absorption peak at 652 nm in the presence of AuNPs-pTab. When 1M H_2SO_4 was added in the blue solution, the color turned to yellow having an absorption peak at 450 nm;* ***B)*** *The peroxidase-like activity of AuNPs-pTab was higher than AuNPs-pSol due to having concentrated AuNPs in TMB-H_2O_2 system.*

1.22.4 Optimization of glucose assay using AuNPs-pTab sensor

Glucose detection using the peroxidase-like activity of AuNPs-pTab involves the oxidation of TMB using H_2O_2 under specific conditions because this colorimetric assay is sensitive to pH changes and temperature. Moreover, the concentration of nanozyme and substrate is also important to achieve the best performance of the tablet sensor. In the following section, different reaction parameters were optimized using 1M H_2O_2 for tablet-based glucose assay.

1.22.4.1 Effect of pH

The TMB substrate has two amino groups attached to the benzene ring which are sensitive to acidic conditions, so pH changes have a great impact on the behavior of the enzyme-substrate. The experiment was screened at different acidic pHs from 3.5 to 5.5 using PB solution as illustrated in

(Figure 0-14A). Unreacted TMB was colorless whereas oxidized TMB showed blue color which was confirmed by the absorbance value at 652 nm. The development of the blue color is due to the formation of a charge transfer complex which indicated the peroxidase behavior of AuNPs-pTab and can be quantified using UV-vis spectroscopy. The higher absorbance value was achieved at pH 4.2 while the system remained working till pH 5 whereas the solution turned purple at pH 7, mauve at pH 8, and colorless at pH 9. Therefore, unless stated, pH 4.2 was chosen in the following experiments. The highly acidic conditions or pH <4.2 disfavored the TMB oxidation indicating the inability of AuNPs-pTab to catalyze this reaction. The nanoparticles may not be fully dispersed in highly acidic conditions due to the protonation of carboxylate ions of pullulan. Resultantly, the negative charge on pullulan fragments may neutralize and cannot stabilize the AuNPs efficiently.

1.22.4.2 Effect of temperature

Temperature is an important parameter in enzymatic reactions because the performance of enzymes are sensitive to heat changes and may lose their activity at elevated temperatures (Jeevanandam et al. 2022; Alvarado-Ramírez et al. 2021). Natural enzymes rapidly denature at a temperature above 40 °C (Ashrafi et al. 2021b), however artificial enzymes like AuNPs-pTab can tolerate higher temperatures. So, the effect of temperature on reaction time in the TMB-H_2O_2 system was observed at variable temperature ranges (25-70 °C). It was observed that TMB oxidation leading to the generation of blue color was slower at room temperature and took 30 minutes while the reaction happened quickly (13-15 minutes) with increasing the temperature up to 70 °C. This might be attributed to the faster dissolution of AuNPs-pTab which releases the nanoparticles faster in the solution and increases their energy capacity which decreases the reaction time for the development of blue color (Roper, Ahn, and Hoepfner 2007). However, no further color change was observed in the solution at above 70 °C as displayed in (Figure 0-14B). To confirm this temperature effect, a test tube was placed in the fridge at (4-6 °C). The color development took around 3 hours to turn into blue.

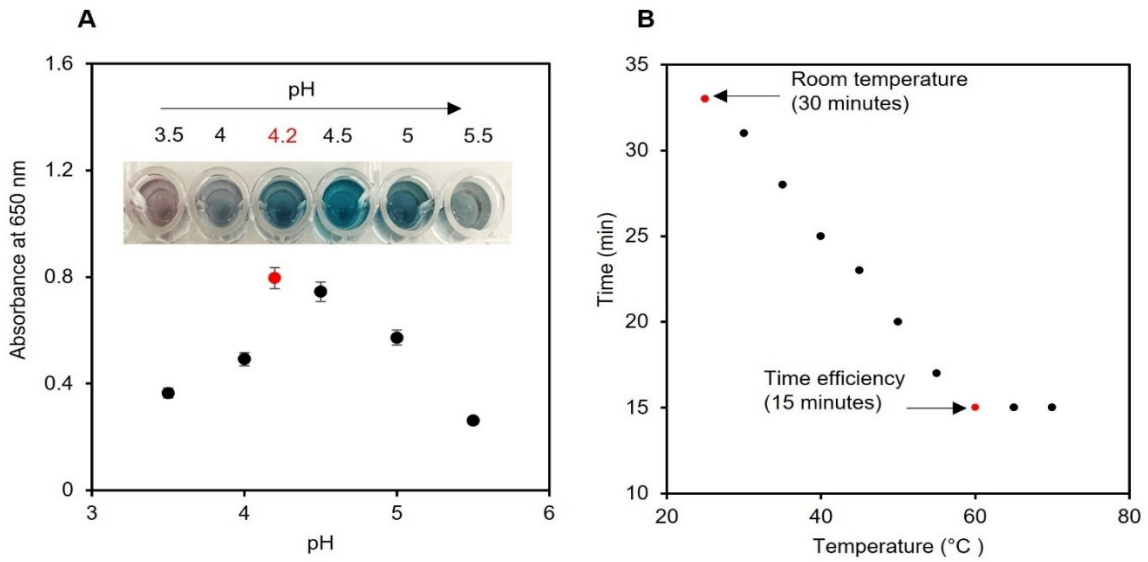

Figure 0-14 *Optimization of pH of TMB and temperature of the reaction condition.* ***A)*** *Effect of pH on the development of blue color;* ***B)*** *Effect of temperature on reaction time for TMB-H_2O_2 system showing the increase in peroxidase activity of AuNPs-pTab with increasing temperature (55-75 °C).*

1.22.4.3 Effect of TMB concentration

Substrate concentration is a crucial parameter in describing the effective collision in substrate-enzyme complex (Reuveni, Urbakh, and Klafter 2014). Increasing substrate concentration can increase the occurrence with which the enzyme and substrate collide according to the Michaelis equation. Five different TMB concentrations including 0.004, 1, 5, 10, and 12 mM were tested using one tablet of AuNPs to find the optimal amount of substrate that could produce an intense blue color. The color intensity was gradually increased with increasing TMB concentration as shown in (Figure 0-15A). The maximum absorbance peak was obtained for 10 mM TMB and a further increase in concentration did not change the intensity of the peak. Hence, 10 mM TMB was used in all the experiments.

1.22.4.4 Effect of the number of AuNPs-pTab

Different numbers of AuNPs-pTab were used to investigate the effect of nanozyme concentration in the catalysis of the H_2O_2-TMB system. Generally, 100 µL of AuNPs-pSol was pipette out to cast one tablet but for the optimization studies, 50 and 75 µL of AuNPs-pSol was also dispensed to get the half and three-quarter tablet. Results showed that the amount of AuNPs-pTab has a direct effect on the development of blue color. Less amount of AuNPs would partially catalyze the reaction and the light blue color developed with 0.75 tablets as indicated in (Figure 0-15B). While

the bluish-black color was developed with two and three tablets indicating an unpreferred color change. Therefore, one tablet was used in all the experiments.

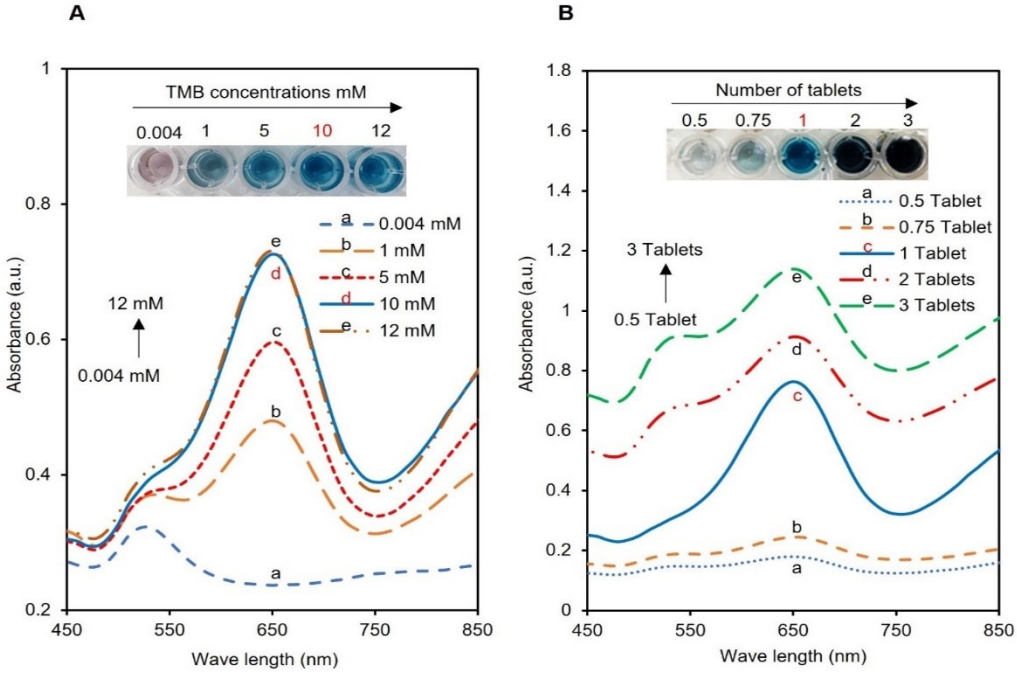

Figure 0-15 *Optimization of TMB concentrations and number of AuNPs-pTabs for the detection of H_2O_2 and glucose.* ***C)*** *The effect of TMB concentrations in the development of blue color having absorbance maximum at 652 nm;* ***D)*** *The effect of a different number of tablets showing deeper blue color with increasing the concentration of AuNPs.*

1.22.5 The reaction kinetics of AuNPs-pTab using Michaelis Menten's model

The kinetic studies for the oxidation of TMB using 1M H_2O_2 and 1 AuNPs-pTab were conducted to see the affinity of the substrate TMB towards AuNPs-pTab. For this purpose, 1, 5, and 12 mM TMB were used. Absorbance at 652 nm was recorded till the maximum time duration and the effect versus time (33 minutes with a one-minute interval) was examined. Of note, the amount of oxidized TMB was increased over time to 30 minutes. After that, the absorbance value was consistent, and no further color change was observed as displayed in (Figure 0-16A). Therefore, a concentration of 10 mM TMB was chosen for the kinetics analysis. Calculating the slopes of initial absorbance over time, yielded a clear steady-state reaction rate at various substrate concentrations. Using a molar absorption coefficient of 39000 M^{-1} cm^{-1}, the Beer-Lambert Law was used to calculate the concentration of TMB-derived oxidation products.

Data presented in (Figure 0-16B) indicated hyperbolic kinetics of Michaelis Menten's model which is the proof of the enzymatic behavior of gold. This model relates the reaction velocity (v)

of an enzyme to its substrate concentrations [S]. At the start, there is almost a direct proportionality between [S] and (v) till the enzyme concentration becomes limiting and a steady state is achieved. Michaelis constant reflects the affinity of an enzyme for its substrate and is distinguishing properties of a particular enzyme towards its substrate. Therefore, the set of parameters of the maximum reaction velocity (v_{max}) and the Michaelis Menten constant (K_m) was then calculated as follows: $K_{m,\ TMB}$ = 0.142 µM, and v_{max} = 0.075x10^{-6} M min^{-1}. Furthermore, kinetic factors are very important for analyzing an enzyme's affinity for its substrate. A high K_m indicates a weak affinity, while a low K_m indicates a strong affinity (D. Yu et al. 2021). The affinity between AuNPs-pTab and TMB was very high which is anticipated by the presence of electrostatic attraction between negatively charged AuNPs-pTab and the substrate TMB. Thus, produce a lower K_m value and a higher attraction.

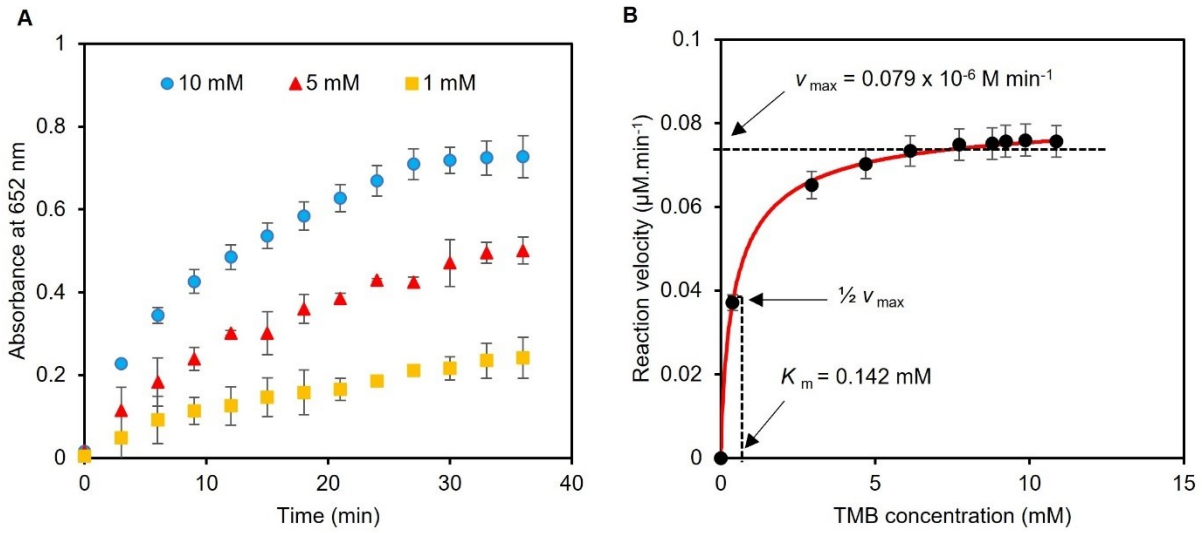

Figure 0-16 *The reaction kinetics study for the TMB-H_2O_2 system involves AuNPs-pTab as a peroxidase catalyst.* ***A)*** *The absorbance at 652 nm was recorded for various TMB concentrations with 1M H_2O_2 over 33 minutes;* ***B)*** *The reaction velocity was evaluated by changing the concentration of TMB substrate with 1M H_2O_2. The points represent real experimental data while the curve was fitted with a non-linear function of the Michaelis–Menten equation.*

1.22.6 Colorimetric detection of glucose using AuNPs-pTab sensor

The colorimetric approach has been utilized to detect glucose using peroxidase mimicking the activity of AuNPs-pTab. The first step of glucose assay involves the oxidation of glucose into gluconic acid which is catalyzed by GOx and produced H_2O_2 as a by-product of this reaction. The detection of the generated H_2O_2 plays a key role in glucose assay because the amount of produced H_2O_2 is directly proportional to the amount of glucose. There is a stoichiometric ratio between glucose and hydrogen peroxide production that shows each mM of glucose produces mM of H_2O_2

(Tao et al. 2009). So, TMB was used to capture the produced H_2O_2 in the second step as indicated by the development of blue color in the H_2O_2-TMB system.

Following the detection principle, H_2O_2 was detected initially in a buffer medium using TMB and one tablet of AuNPs. Various concentrations of H_2O_2 ranging from 5-500 µM were tested to see the effect of H_2O_2 concentration on the oxidation of 10 mM TMB. The blue color intensity of oxTMB was quantified by recording the absorption spectra. There is an obvious increase in λ_{max} at 652 nm with increasing H_2O_2 concentrations. The amount of oxTMB is directly proportional to the amount of H_2O_2 present in the system. Without H_2O_2 (0 µM), no absorbance peak in the spectrum indicated the essential role of H_2O_2 in the oxidation of TMB. A negligible peak appeared using 5 µM H_2O_2 which became higher gradually with increasing the concentration of H_2O_2 until reached a plateau at 500 µM as shown in (Figure 0-17A). However, the absorbance (λ_{max} at 652 nm) remained unchanged by further increasing the concentration of H_2O_2 which indicated that TMB has been completely oxidized. A calibration curve of enzyme mimic activity of AuNPs-pTab was plotted of the original H_2O_2 concentrations on the x-axis and the absorbance at 652 nm on the y-axis which resulted in a hyperbolic curve fitted using the dose-response model as shown in (Figure 0-17B). The relative absorption intensity is linearly proportional to the concentration of H_2O_2 at the first six concentrations as displayed in the inset of (Figure 0-17B) with a LOD of 28.7 µM.

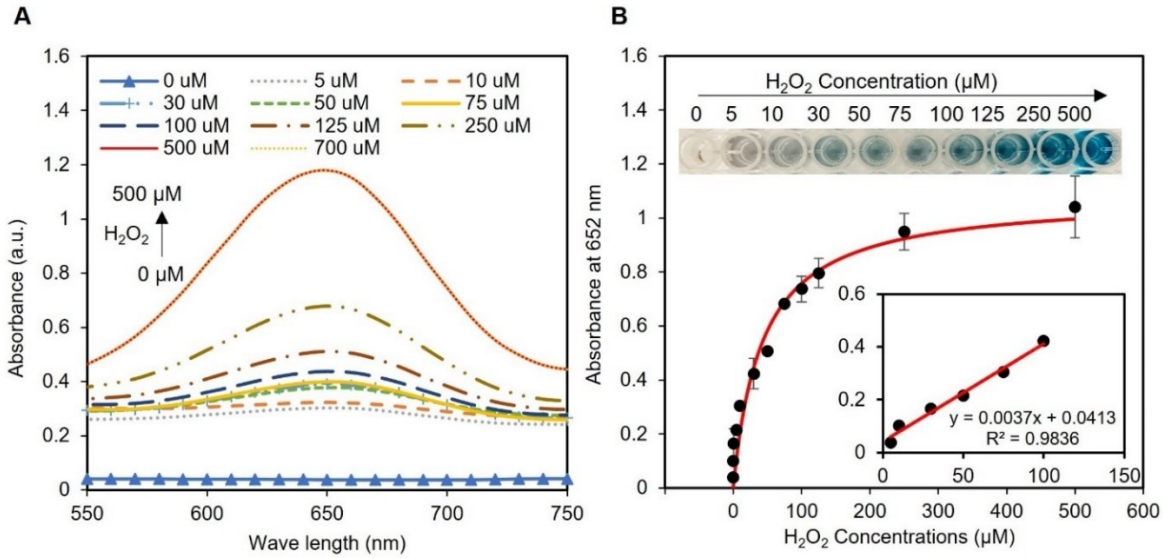

Figure 0-17 *Detection of H_2O_2 using AuNPs-pTab sensor. A) Absorption spectra showing a gradual increase in peak intensity with increasing H_2O_2 concentration; B) The absorbance at 652 nm showing a linear relationship between the first six peak values over-concentration of H_2O_2.*

Next, the peroxidase-mimicking enzymatic activity of AuNPs-pTabs was evaluated for glucose assay using PB as a reaction medium. When glucose concentration was < 5 µM, the solution was colorless indicated by a flat line in the spectrum. The reaction media turned blue progressively with increasing glucose concentrations to 500 µM as shown in (Figure 0-18A). The color change of peroxidase substrate TMB was used to calculate the amount of glucose in the calibration curve which was plotted against relative absorbance intensity at 652 versus the glucose concentration as shown in (Figure 0-18B). At smaller concentrations, the λ_{652} was linearly related to the concentration of glucose. The curve was fitted using a dose-response model and a limit of detection of 38.2 µM was calculated.

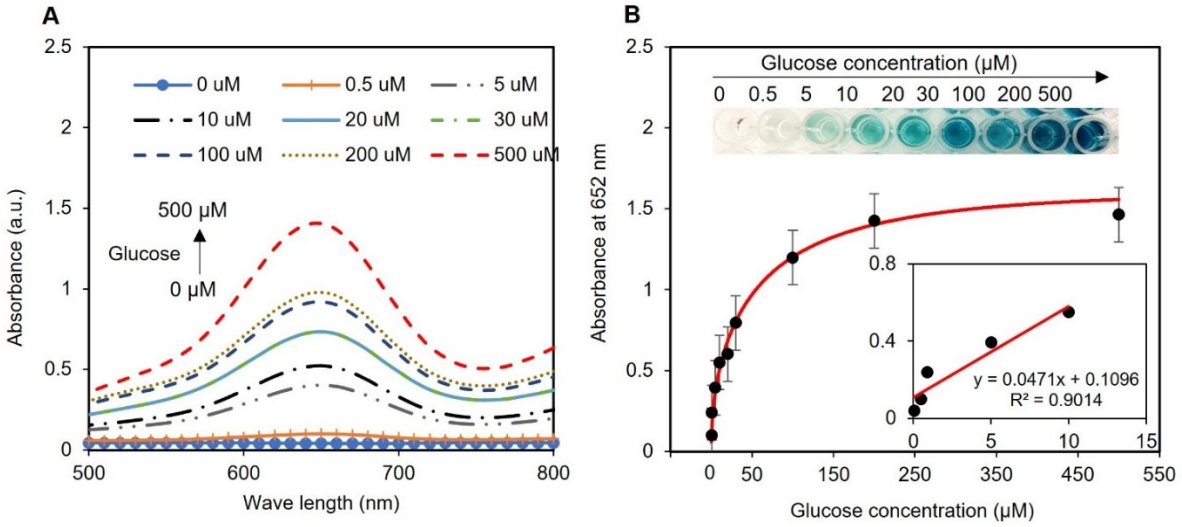

Figure 0-18 *Detection of glucose in buffer using AuNPs-pTab sensor.* ***A)*** *Glucose detection in PB using AuNPs-pTab and the absorption spectra at a variable concentration of glucose (5-500 µM);* ***B)*** *The calibration curve was obtained using an average absorbance of three tests which shows the relationship between the relative absorption intensities versus the concentration of glucose. The linear relationship in the first five concentrations of glucose. The error bars represent the standard deviation of three independent measurements.*

Once the peroxidase behavior of AuNPs-pTab was confirmed for glucose detection in buffer, the same assay was performed in artificial saliva to acquaint with close to real-world situations. In this work, artificial saliva was spiked with different concentrations of glucose (0.5-500 µM), and absorption spectra were recorded which indicated a gradual increase in λ_{652} with increasing glucose concentrations. The calibration curve presents the data between relative absorbance intensity at 652 and glucose concentration as presented in (Figure 0-19A). The absorption spectra linearly correlated to glucose concentration in the first four concentrations of glucose as described in the inset of (Figure 0-19B). The LoD was calculated to be 163.04 µM while the minimum

concentrations of glucose required in saliva for diabetic diagnosis are (201.9 ± 34.9) µM in males and (175.0 ± 22.3) µM in females. Thus, revealing the applicability of our AuNPs-pTab for different glucose levels in artificial saliva samples. Of note, the AuNPs-pTab performance in glucose assay was better in the PB as compared to saliva which may be due to the salivary viscosity that caused less effective molecular collision due to the slow motion of molecules in viscous media, hence affecting the oxidation rate of TMB (Ravikumar, Ramani, and Gayathri 2021). Consequently, a longer time was required to observe the blue color. However, the blue color was obtained in 30 minutes without heat assistance.

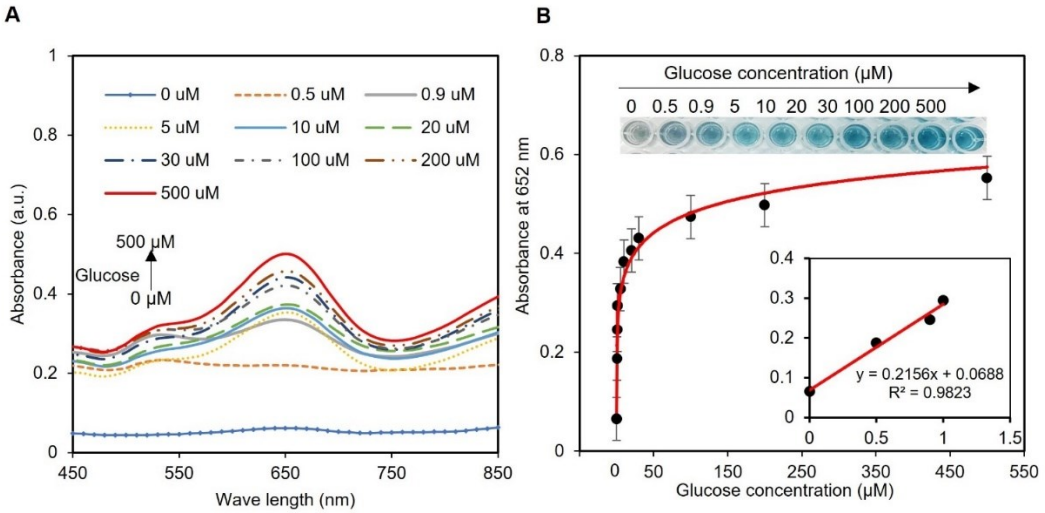

Figure 0-19 *Detection of glucose in an artificial saliva sample.* ***A)*** *Absorption spectra of variable concentration of glucose 0.5-500 µM in artificial saliva;* ***B)*** *The calibration curve showing the relationship between relative absorption intensity (blue color intensity) versus the concentration of glucose. The error bar signifies the standard deviation of three independent measurements. The linear relationship in the first four concentrations of glucose.*

Overall, this newly proposed tablet sensor can efficiently detect glucose as well as H_2O_2 in different media using the catalytic properties of AuNPs. The detection of H_2O_2 is also important not only because of its role in cell balance but also as a signal molecule that controls several vital developments. The presence of H_2O_2 is associated with various diseases such as Parkinson's (J. Yang et al. 2022), Huntington's (Y. F. Wei et al. 2021), Alzheimer's disease (Purwidyantri et al. 2021), and cancer (Ren et al. 2021). Hence our AuNPs-pTab has many potential applications in the disease diagnosis and detection field. Moreover, our approach is portable, low-cost, and user-friendly, which introduces a new platform for the development of POC devices.

1.22.7 Analysis of the interference studies

To investigate the specificity of the AuNPs-pTab sensor towards glucose detection, some other forms of sugars including monosaccharides like fructose, and disaccharides like maltose and lactose were tested in a buffer solution. For this reason, 1 mM of each fructose, maltose, and lactose was incubated with glucose oxidase separately for 15 minutes. Results indicated that there was no obvious color change in the TMB solution and the absorbance peak for fructose, maltose, and lactose was less than glucose. In addition to this, the PB was also tested as an interferent but there was no absorbance recorded against the buffer as shown in (Figure 0-20). This study confirms the specificity of this AuNPs-pTab sensor for the detection of glucose.

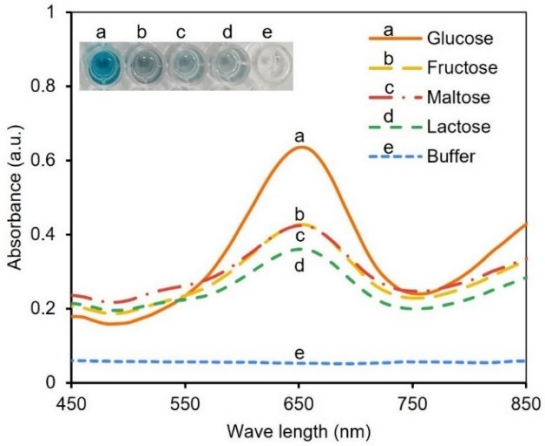

Figure 0-20 *The interference study used glucose, fructose, maltose, lactose, and buffer solution. The higher absorption is detected for glucose which implies the sensor specificity for glucose detection. Testing procedure: 300 uL TMB+330 uL citrate buffer+1 tablet of AuNPs-pTab. In another tube, 20 uL glucose oxidase+(1 mM) of 80 uL (glucose, fructose, maltose, lactose, Mcilvaine buffer) + 200 uL PB (pH 7.4).*

1.22.8 Application of AuNPs-pTab sensor in real saliva samples

Saliva is considered an attractive alternative to blood tests for glucose detection due to its painless and non-invasive sample collection, as well as a reduction in possible interferences. To evaluate the practical applicability of our proposed AuNPs-pTab sensor, glucose detection was performed in real saliva samples. Sample collection was done from two female volunteers between 30 to 40 years old. Before taking the samples, the volunteers were asked to fast for 12 hours to minimize the risk of possible interfering substances, especially ascorbic acid, and lactic acid, which could have a significant impact on the pH of saliva (Chong et al. 2012). The sample was collected according to the literature procedure with some modifications (C. Liu et al. 2015); 1) wash the mouth with water five times, 2) reduce swallowing and hold saliva in the mouth as much as

possible, 3) place the saliva in 1.5 mL test tube. The collected saliva was tested to measure glucose concentration before spiking at absorbance λ_{652} followed by spiking with specific concentrations of glucose as shown in Table 0-1 based on 3 readings. It is worth mentioning that the samples were used without any purification or treatment and stored in test tubes in a well-closed plastic container at 4 °C and used within three days.

Table 0-1 *The results of glucose levels in real saliva samples (n = 3) are presented here.*

Samples	Spiked (µM)	Found (µM)	RSD (%)	Recovery (%)
Non-diabetic	0	85.36 ± 3.67	-	-
Spiked non-diabetic	90	85.61 ± 1.37	1.6%	93.6 - 96.6
Diabetic	0	175.25 ± 0.81	-	-
Spiked diabetic	170	175.64 ± 7.49	4.26%	98.9 - 107.7

The color development of oxTMB was less intense or faint blue in the case of real saliva as compared to artificial saliva and buffer solution. To overcome this issue, the saliva samples were diluted using water using a 1:1 ratio. Resultantly, blue colors varied from faint blue to dark blue, and absorption spectra were measured and presented in (Figure 0-21). To assess the validity of our tablet sensor, the recovery percentage was calculated for real saliva samples including non-diabetic, spiked non-diabetic, diabetic, and spiked diabetic. The % R can help to give an estimation of the amount of glucose available in the real saliva samples with an unknown amount of glucose. While percent standard deviation (%RSD) helps to analyze the precision of the method by calculating the dispersion of the values with the mean. Hence, the calculated %R and %RSD of spiked samples shows that our sensor can be used for glucose detection in real saliva samples.

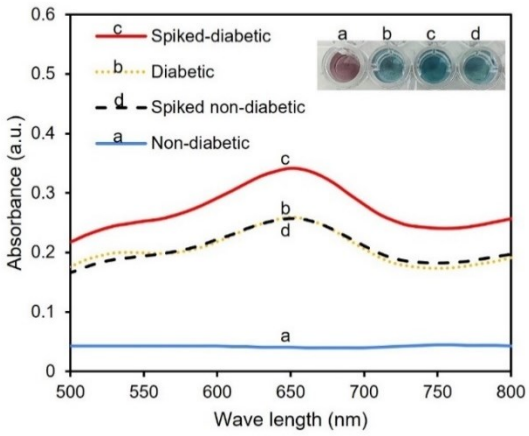

Figure 0-21 *Detection of glucose in real saliva samples. The absorption spectra of different glucose levels in real saliva samples and inset show color change of wells with the presence and absence of glucose.*

1.22.9 Comparison of the performances of AuNPs-pTab and HRP in catalyzing the oxidation of TMB

An assessment test was done to evaluate the performance of AuNPs-pTab (>6 months old tablets) and HRP (freshly prepared) in catalyzing the oxidation of TMB. The obtained results (absorbance at 652) show an almost equal catalytic activity at the lower concentrations of glucose. Whereas at higher concentrations of glucose, the HRP produced greenish-blue color with more absorbance and a higher peak at 652. While a purely blue color was obtained by using AuNPs-pTab which reflected less absorbance. Furthermore, the time was monitored to see which catalyst obtained the faster blue color. HRP gave the blue color in 26 minutes which was faster than AuNPs which took approximately 27 minutes to show results. To evaluate the performance of AuNPs-pTab and HRP, Michaelis Menton's constant (K_m) of enzyme affinity towards TMB substrate was compared. The (K_m) value of the freshly made AuNPs-pTab was 0.142 mM while it was 0.434 mM in the case of HRP. These results confirm the catalytic activity of the fabricated AuNPs-pTab. Furthermore, the performance of the >6 months old AuNPs-pTab and the newly made HRP was plotted and displayed in (Figure 0-22).

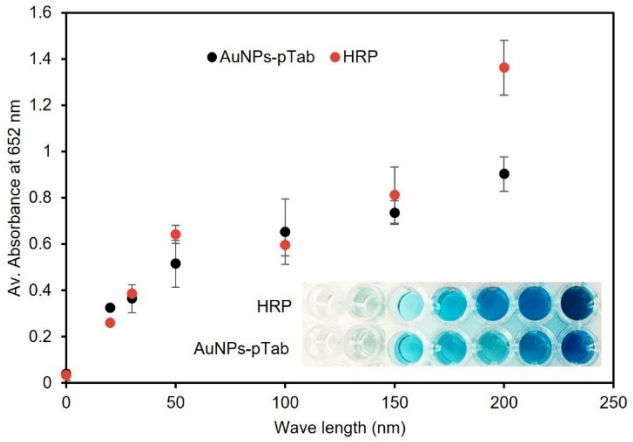

Figure 0-22 *A comparison between peroxidase mimic activity of AuNPs-pTab and horseradish peroxidase (HRP) in catalyzing the TMB-H_2O_2 system. The absorbance at 652 nm shows that the artificial nanozyme AuNPs-pTab (>6 months old tablets) catalytic activity was similar to the natural enzyme HRP. The error bar represents the standard deviation of three independent measurements (n=3).*

1.22.10 The catalytic activity test analysis

The reduction of 4-nitrophenol to 4-aminophenol in the presence of excess $NaBH_4$ was used to test the catalytic efficacy of AuNPs-pTab. It is straightforward to track the development of the reaction using UV-vis spectrophotometric measurements since this reduction process only

produces one kind of product. (Figure 0-23A and B) depicts the absorption band of about 317 nm before the addition of $NaBH_4$ and the band around 400 nm following the addition of $NaBH_4$ solution, which is the typical band for 4-nitrophenol. The solution's color changed from bright yellow (4-nitrophenol) to colorless during this operation (4-aminophenol). The catalytic activity of 4 different portions of AuNPs-pTab (1/4, 1/2, 3/4, and 1) was further examined using the conversion of 4-nitrophenol (yellow color) into 4-aminophenol (colorless) using $NaBH_4$. The conversion was too fast and obtained in 30 seconds when using one tablet of AuNPs-pTab while 60 seconds when using 3/4 tablet. An increase in time for full conversion was noticed in the case of half and a quarter of the tablet indicating a decrease in catalytic activity due to the presence of fewer AuNPs.

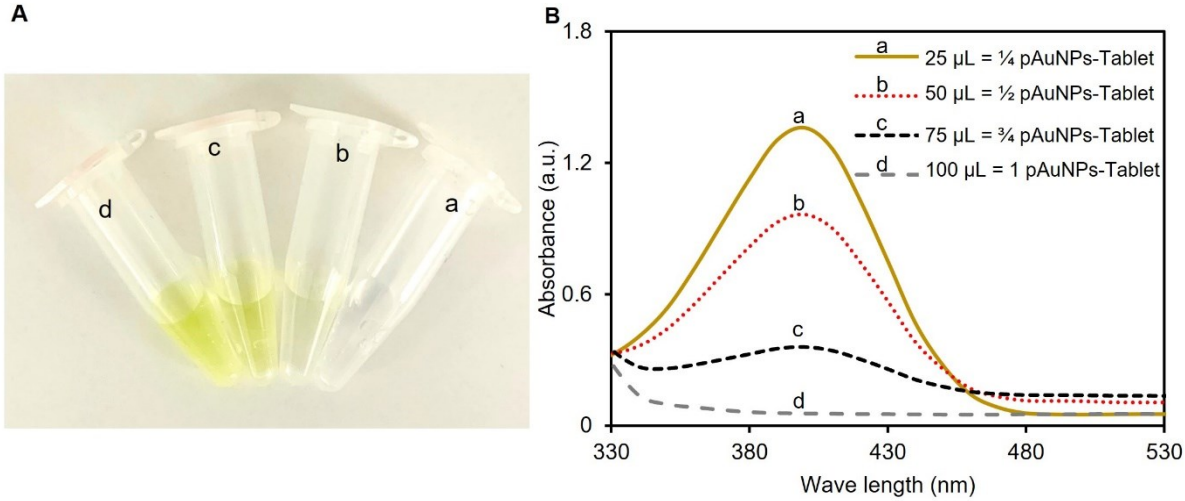

Figure 0-23 *The catalytic activity test for different concentrations of AuNPs-pTab using the conversion of 4-4-nitrophenol (yellow color) into 4-aminophenol (colorless) using sodium borohydride.* ***A)*** *a) quarter tablet, b) half tablet, c) three-quarter tablet, and one tablet of AuNPs-pTab.* ***B)*** *The corresponding absorbance spectra show a high catalytic activity (high conversion of 4-nitrophenol (yellow color) into 4-aminophenol (colorless) in the presence of one tablet of AuNPs-pTab. While the catalytic activity is less when using quarter AuNPs-pTab.*

1.22.11The stability test of AuNPs-pTab

The AuNPs-pTabs were stored at 4 °C but can be stored at room temperature with controlled humidity because the variations in humidity level resulted in sticky tablets. The stability profile of AuNPs-pTab was measured for 16 months by taking an absorbance ratio of 520/650 and compared with AuNPs-pSol. (Figure 0-24) shows that the AuNPs-pTab remained stable for 16 months with a little decrease in stability while a gradual decrease in colloidal dispersity of AuNPs-pSol was observed which is in agreement with the literature findings (Laksee et al. 2017b). Besides being

ultra-stable, the tablet platform has other advantages over AuNPs-pSol such as easy storing and transport as well as the pre-measured mass of AuNPs-pSol in each tablet which eliminates the need for a weighing balance, pipettes, and other labor extensive calibration steps.

The stability of AuNPs-pTab was compared with AuNPs-pSol over 16 months stored at 4 °C. Interestingly, the 16 months old AuNPs-pTab were used to test their catalytic activity by measuring the absorbance at 652 nm using the 1M H_2O_2-TMB system. There was no change in their catalytic activity which makes them an amazing candidate as portable sensors for glucose detection.

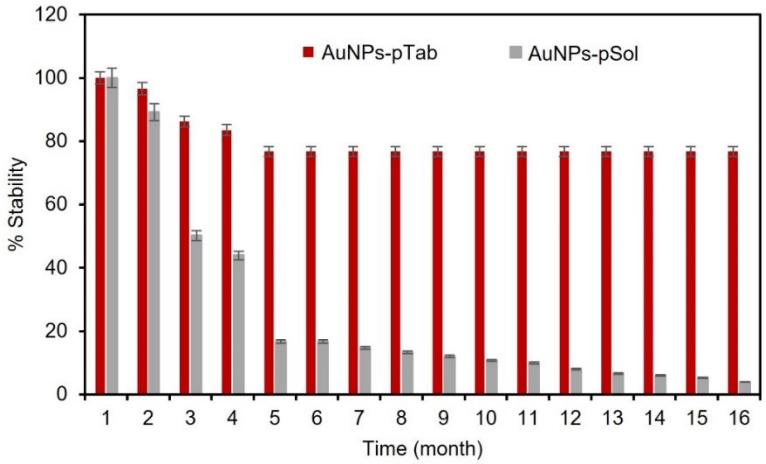

Figure 0-24 *The stability profile of AuNPs-pTab over sixteen months shows a gradual decrease in the stability of AuNPs.*

Chapter 4. Cysteamine Detection

This chapter aims on the experimental procedures carried out for cysteamine detection in human serum and explains in detail the results analyses.

1.23 Chemicals

All reagents and chemicals were analytical grade and used as received. Gold (III) chloride solution (30 wt.% in dilute HCl), Cysteamine (C_2H_7NS), 3,3', 5,5'-tetramethylbenzidine (TMB), Dimethyl sulfoxide (DMSO)(C_2H_6OS), sulfuric acid (H_2SO_4), Trisodium citrate ($C_6H_5Na_3O_7$), sodium phosphate monobasic monohydrate ($NaH_2PO_4 \cdot H_2O$), sodium phosphate dibasic (Na_2HPO_4), hydrogen peroxide (H_2O_2), citric acid ($C_6H_8O_7$), sodium hydroxide (NaOH), sodium borohydride ($NaBH_4$), 4-nitrophenol ($C_6H_5NO_3$), methionine, asparagine, glycine, glutathione, aspartic acid, cysteine, and arginine were purchased from Sigma-Aldrich, USA. Pullulan (average Mw. ~200 kDa) was obtained from Polyscience, Inc, USA. Artificial serum (99.99% purified) was purchased from Biochemzone, USA. Real human serum samples were attained from a clinical lab in Montreal, CA. Deionized water from Sigma Aldrich, USA was used to prepare all solutions. A carbon steel tray (Betty Crocker) was obtained from a local store, in Canada.

1.24 Synthesis and fabrication of pullulan-stabilized gold nanoparticles

The procedure for pullulan capped gold nanoparticles solution synthesis and fabrication of tablets is the same as reported in section 3.2 and 3.3. A summary of the method is presented in (Figure 0-2A).

1.25 Sensing of cysteamine in Phosphate buffer

First, the peroxidase activity of pAuNPs-Tablet was evaluated by investigating its ability to oxidize TMB substrate to a blue-colored product using H_2O_2 as an oxidizing agent. The detection system involved incubation of 300 µL of 50 mM Mcilvaine buffer which is a citrate-phosphate buffer (pH 4), 1 pAuNPs-Tablet (100 µL, 1.2 mg), 300 µL of 10 mM TMB, 100 µL of 1 mM H_2O_2. were incubated at 25 °C for 20 minutes pursued by UV-vis spectroscopic measurements on a 96-well plate reader (Ulti Dent Scientific, Canada) as a function of time. The pH of the Mcilvaine buffer solution was adjusted between 2 and 6 with citric acid or sodium phosphate dibasic using a pH meter (AB200 pH/mV/conductivity made from Fisher Scientific Accumet, Singapore). Reaction conditions such as pAuNPs-Tablet nanozyme concentration, buffer pH, reaction temperature,

TMB concentration, the colloidal ratio of pAuNPs to cast the tablets, and the cysteamine ratio to cause inhibition were optimized. This experiment was followed by the detection of cysteamine concentrations (0-200 µM) in phosphate buffer (PB) (pH 7). In a typical procedure, a stock solution of cysteamine with various concentrations (0-200 µM) was prepared in PB pH 7. Then, 1 pAuNPs-Tablet and 100 µL cysteamine were incubated for 1 min and mixed using vortex (Model# 945FIALUS, 50/60 Hz Fisherbrand, USA) followed by the addition of (300 µL, 10 mM TMB), (300 µL, 50 mM Mcilvaine buffer), and (100 µL, 1 mM H_2O_2). The absorbance was collected at 652 nm after 20 minutes to measure the color intensity of the solution. To determine reaction kinetics, different concentrations of cysteamine (0, 60, and 200 µM) were used with 1 pAuNPs-Tablet. The zero-order rate constants were determined by plotting the maximal absorbance at 652 nm against reaction time (0-30 min). The reaction velocity was calculated using Beer-Lambert Law where the absorbance value of oxidized TMB (oxTMB) was converted into product concentration using the molar extinction coefficient of oxTMB (39,000 $M^{-1}.cm^{-1}$). The Michaelis-Menten's constant (K_m) and initial maximum velocity of the reaction (V_{max}) were calculated using non-linear curve fitting software (CurveExpert Professional, USA). The catalytic activity test was done using the conversion of 4-Nitrophenol (4-NP) (yellow) to 4-Aminophenol (4-AP) (colorless) in the presence of pAuNPs-Tablet with/without cysteamine. The reagents were prepared according to the literature procedure with some mofification (Balakumar et al. 2020). In separate test tubes, 1 mL of 0.1 mM of 4-NP and, 0.5 mL of 0.1 M of $NaBH_4$ were dissolved in deionized distilled water. Next, pAuNPs-Tablet and 100 µL of (0, 60, and 200 µM) cysteamine were incubated and added. UV-vis spectroscopy was used to measure the absorbance values and the kinetics of ratios was monitored based on the color change of the solution at 400 nm (yellow) and 300 nm (colorless). The apparent reaction constant (k_{app}) was calculated using the formula reported by Azzam *et al*. (Azzam et al. 2021) $ln\ (A_t/A_0) = -\ k_{app}*t$

1.26 Sensing of cysteamine in artificial serum

The catalytic activity of pAuNPs-Tablet, which mimics peroxidase, was assessed in an artificial serum solution (pH 6.8) with varying cysteamine concentrations (0-200 µM) as outlined in section 4.2. The limit of detection (LoD) was determined using the formula 3σ/µ, where σ and µ represent the relative standard deviation of absorbance measurements and the slope of the linear calibration plot, respectively.

1.27 Interference study for the colorimetric detection of cysteamine

The effect of potential interferants such as methionine, asparagine, glycine, glutathione, aspartic acid, cysteine, and arginine was studied for our proposed cysteamine assay following the procedure mentioned in section 4.2. All the interferants were used at 100 µM concentration in this experiment.

1.28 Analysis of cysteamine in human serum

To demonstrate the practical application of the pAuNPs-Tablet sensor in real-life conditions, the detection of cysteamine was also conducted in real human serum samples taken from cystinosis patients (pH 6.5-7.0). Furthermore, a spiking test was conducted in actual human serum, and the method was validated by calculating the percent recovery (%R) using the formula reported by Sasikumar *et al*.(Sasikumar and Ilanchelian 2020) *Rate of recovery (%) = (Amount of cysteamine found (µM))/(Amount of cysteamine added (µM))*100%*

1.29 Results and discussion

1.29.1 Mechanism of cysteamine detection using pAuNPs-Tablet

It is well known that the catalytic activity of gold nanoparticles is primarily influenced by their surface charge characteristics(S. Wang et al. 2012). During heterogeneous catalysis, the chemical bonds within the reacting molecules that are adsorbed on the active solid surface are broken and reformed, leading to the eventual release of products back into the liquid or gas phase. As a result, the presence of negatively charged carboxylate groups occupying the gold surface using the pullulan polymer as a labeling/capping agent can have an impact on the catalytic activity of gold nanoparticles. Thus, TMB was chosen in the assay because they have opposite charge characteristics(Yanping Liu et al. 2014). Consequently, pullulan-capped gold nanoparticles, which are negatively charged, attract positively charged amino groups of TMB via electrostatic attraction. These anionic pAuNPs will exhibit a strong affinity to the TMB as a reaction substrate. Therefore, facilitating the charge transfer between pAuNPs and TMB.

The colorimetric test using tablets examined the enzyme-like activity of negatively charged pullulan gold nanoparticles tablet, which mimics peroxidase, by utilizing H_2O_2 as an oxidant and TMB as a substrate. Peroxidase is an enzyme that decomposes H_2O_2. Thus, pAuNPs-Tablet was utilized to decompose H_2O_2 and produce hydroxyl radical ($^{\bullet}OH$), which are reactive oxygen

species (ROS), in the detection system. The acidic conditions required for the TMB-H_2O_2 system were maintained using Mcilvaine buffer. The •OH produced was unstable due to the presence of an unpaired electron, which was stabilized by interacting with the conduction band electrons of pAuNPs-Tablet. These interactions resulted in the peroxidase-like catalytic activity of pAuNPs-Tablet, leading to the oxidation of TMB and the formation of a blue-colored product. However, in the presence of cysteamine, the−SH group of cysteamine attracts to the surface of pAuNPs via electrostatic attraction(Apyari et al. 2012) resulting in the formation of a pAuNPs-Tablet-cysteamine complex. As such, the aggregation of pAuNPs-Tablet in the presence of cysteamine is further examined. It was observed that the presence of cysteamine concentrations (0-400 µM) did not cause any aggregation of pAuNPs-Tablet until the concentration reached 500 µM as displayed in (Figure 0-1). Therefore, a hypothesis of a complex formation rather than an aggregation was suggested to inhibit the catalytic activity of pAuNPs-Tablet.

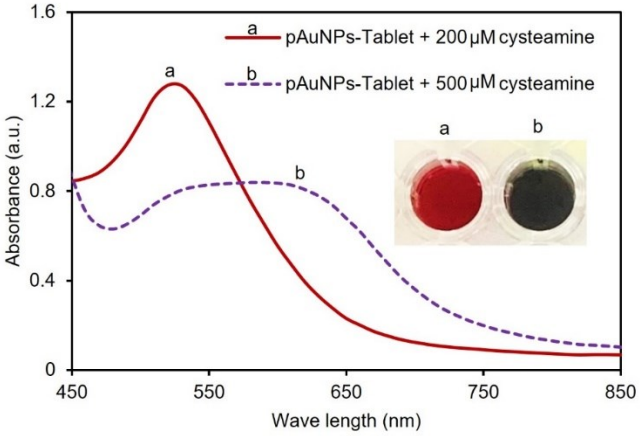

Figure 0-1 *The UV-vis spectra of pAuNPs-Tablet in the presence of (200 and 500 µM) cysteamine. A 200 µM of cysteamine could not cause the aggregation of pAuNPs-Tablet while 500 µM caused the aggregation. Considering the higher concentrations of cysteamine cause aggregation of pAuNPs-Tablet based on LSPR, the peroxidase-like activity method is the resolution for cysteamine detection to achieve lower LoD.*

According to previously reported studies, amino acids act as antioxidants(Wood, Khan, and Moskal 2008) and catalyst poisoning(Say et al. 2022). Furthermore, recent studies have demonstrated that amino acids could interact with the nanozyme where there is a competition between amino acids and the substrates to bind to the surface of the nanozyme(Liyanage et al. 2021). As such, we investigated the capability of cysteamine to inhibit the oxidation of the TMB-H_2O_2 system. According to the above theory, Cysteamine competes with the TMB substrate to bind to the surface of pAuNPs-Tablet causing the formation of a pAuNPs-Tablet-cysteamine complex. This complex should inhibit the blue color development of the solution of pAuNPs-

Tablet and TMB as shown in (Figure 0-2B). Furthermore, in the current case, the catalytic activity of the pAuNPs-Tablet does not improve with time in cases where cysteamine concentration is high enough to block the initial activity 100 and 200 µM. This suggests that cysteamine may act as an inhibitor of the catalytic activity of the pAuNPs-Tablet. Likewise, it was noticed that a blue color formed in the absence of cysteamine exhibiting a high peak at 652 nm. Whereas, in the presence of cysteamine, a flat peak with colorless/grey was detected as recorded by UV-vis spectroscopy.

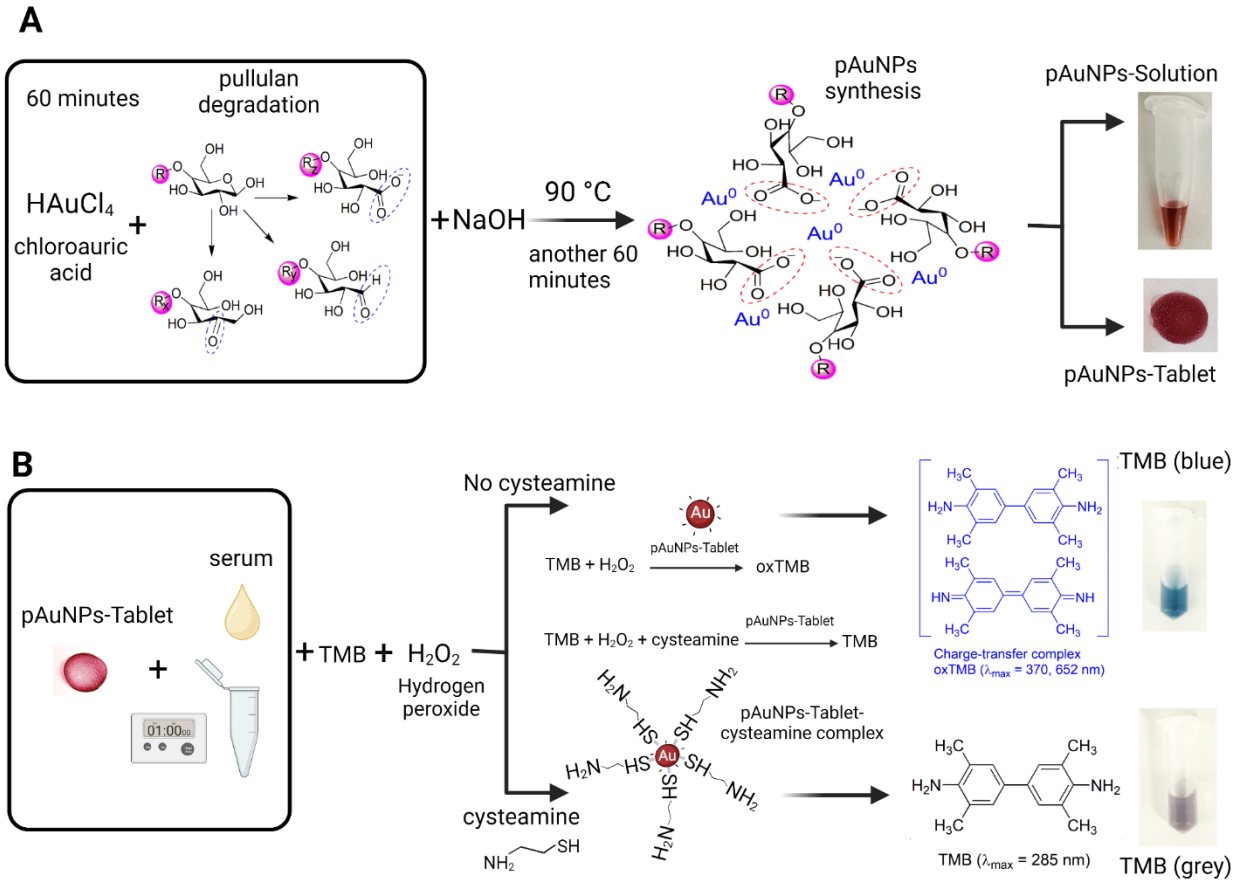

Figure 0-2 *Representation of the synthesis of pAuNPs-Solution/pAuNPs-Tablet and the mechanism of cysteamine detection.* ***A)*** *The production of tablets containing gold nanoparticles stabilized with pullulan (pAuNPs-Tablet) was achieved by using pAuNPs-Solution. To start, pullulan was treated with NaOH-mediated degradation at a temperature of 70 °C for 60 minutes. The next step involved adding a solution of* $HAuCl_4$ *and heating the reaction mixture to 90 °C for another 60 minutes to synthesize the pAuNPs-Solution. Finally, pAuNPs-Solution was pipetted onto a non-stick tray to create the pAuNPs-Tablet. The tablets were then dried for 30 minutes in an oven at 50 °C or left to dry at room temperature for 24 hours.* ***B)*** *The mechanism of peroxidase-like activity inhibition in the presence of cysteamine. In the absence of cysteamine, the active sites of pAuNPs surface are free so that TMB can attach easily to pAuNPs surface. Consequently, the charge transfer from the surface of pAuNPs to the* H_2O_2 *generates the radical* $^{\bullet}OH$ *resulting in the formation of oxidized TMB (oxTMB) (blue color). Upon incubating pAuNPs with cysteamine, a pAuNPs-cysteamine complex is formed which blocks the active sites on the surface of pAuNPs. When TMB is added because the surface is blocked with cysteamine, no charge transfer can leave the surface of pAuNPs causing the inhibition of the formation of oxTMB. Hence, the colorless-grey color will not develop into a blue color.*

1.29.2 Optimization of cysteamine ratio

It is commonly understood that $^{\bullet}OH$ is produced through the reaction of peroxidase-like mimics with H_2O_2, which can facilitate the oxidation of peroxidase substrates. According to the literature, competition between amino acids and the substrate for the surface of nanozyme is the main reason for inhibition(Kalhor and Yahyazadeh 2019). Based on the principles of enzyme kinetics, these inhibitors bind to the natural enzyme with a perceived affinity that is similar to the concentration of the enzyme's active sites. This suggests that when the concentration of the inhibitor increases, there will be a point where the enzyme activity is entirely lost. In the case of nanozymes, the active site is believed to be the surface atoms, which may result in numerous active sites within a single nanozyme particle. Therefore, to completely deactivate a single nanozyme, a high concentration of inhibitor molecules would be necessary to drive the reaction. To further investigate the catalytic mechanism of the peroxidase-like activity of pAuNPs-Tablet, cysteamine was utilized as an inhibitor that formed a stable complex on the surface of pAuNPs-Tablet which inhibits the oxidation of TMB. Based on the above facts, the concentrations and ratios of cysteamine have a significant impact on the quantity of oxTMB in the system. As such, various ratios (25, 50, 75, and 100 µL) of 200 µM cysteamine were employed to assess the inhibition of the catalytic activity of pAuNPs-Tablet. It was observed that the maximum inhibition was achieved using 100 µL of cysteamine. Thus, this ratio was used for the detection of cysteamine as shown in (Figure 0-3).

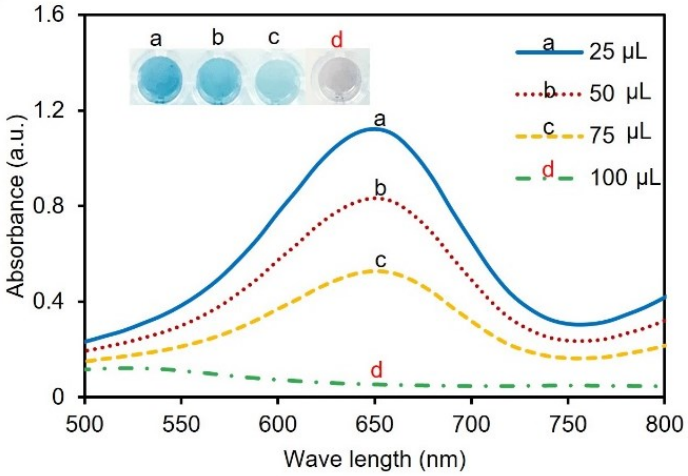

Figure 0-3 *Inhibition effect using various ratios (25, 50, 75, and 100) µL of 200 µM of cysteamine showing the maximum inhibition occurred using 100 µL cysteamine. Hence, this ratio was applied to the rest of the tests.*

1.29.3 Inhibition of the peroxidase-like activity of pAuNPs-Tablet in presence of cysteamine

The peroxidase activity of pAuNPs-Tablet was verified by introducing a 1 M H_2SO_4 stop solution which quickly stopped the oxidation process of TMB and resulted in the formation of a yellow color. The test is based on the hypothesis that the oxTMB (blue color) should be produced in the presence of pAuNPs-Tablet whereas the presence of cysteamine prevents the formation of oxTMB. As a result, a change in the color of oxTMB from blue to yellow by H_2SO_4 can be used as an indicator of the presence of oxTMB. Since introducing cysteamine obstructed the active sites on the surface of pAuNPs-Tablet, oxTMB could not be formed. As a result of this inhibition, the absorbance peak of pAuNPs-Tablet + TMB shifted from 652 to 450 nm, while no peak was observed for the TMB-pAuNPs-Tablet system with cysteamine, as shown in (Figure 0-4). Thus, the yellow color intensity caused by the addition of H_2SO_4 is directly proportional to the amount of oxTMB which was not produced when cysteamine is present.

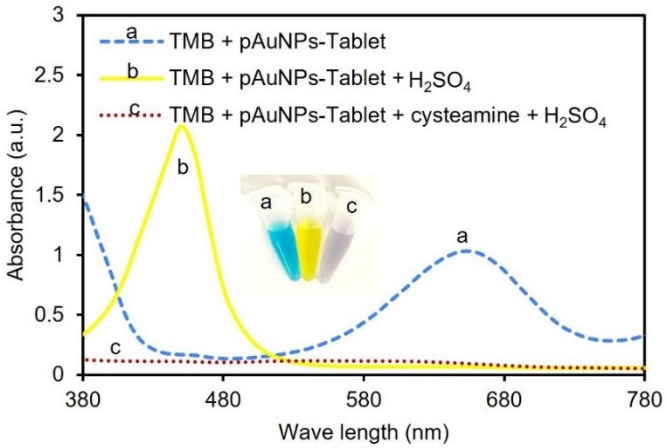

Figure 0-4 *The TMB response in the presence and absence of cysteamine and the effect of using sulfuric acid (H_2SO_4) as a color indication for oxTMB. In the absence of cysteamine and the presence of pAuNPs-Tablet, a high absorbance peak was observed at 652 nm. While no peak was observed when 200 µM of cysteamine was added to the system. The effect of using H_2SO_4 on TMB + pAuNPs-Tablet and TMB + pAuNPs-Tablet + cysteamine. The TMB color was shifted to 450 nm in the system containing TMB + pAuNPs-Tablet. Whereas, adding H_2SO_4 to TMB + pAuNPs-Tablet + cysteamine did not cause any color change since the oxTMB was not presented in the system.*

1.29.4 Reaction kinetics in the presence and absence of cysteamine

To set the assay time, the time for blue color saturation in the absence and presence of cysteamine was measured using UV-vis spectroscopy over a period of 30 minutes. The kinetic study for the oxidation of TMB using 1mM H_2O_2, 1 pAuNPs-Tablet, and (0, 60, and 200 µM) of cysteamine was investigated. The results show a time-dependent kinetic analysis of the catalytic reaction between pAuNPs-Tablet and TMB substrates in both concentrations (0 and 60 µM) of cysteamine.

Based on the findings, the activity using 0 μM cysteamine proceeds rapidly and reaches saturation at 20 minutes as shown in (Figure 0-5A). While using 60 μM cysteamine, the reaction took longer time till saturation ~2 hours. On the other hand, the reaction containing 200 μM of cysteamine showed no color development and remained permanently unchanged. This leads to further investigation of the type of inhibition (reversible or irreversible) to occur in the presence of 60 and 200 μM cysteamine. If we consider the potential influence of the effect of cysteamine concentration on the steady-state kinetics of Michaelis Menten parameters (K_m and V_{max}) of the pAuNPs-Tablet, we should assume to see no alteration in the K_m, as the irreversible binding of 200 μM cysteamine to the pAuNPs-Tablet in the initial phase should not influence the instantaneous binding of substrate molecules to the surface of the pAuNPs. Conversely, considering that a reduced number of liberated surface atoms will be accessible to interact with the substrate, it is expected that the V_{max} for substrate oxidation catalyzed by nanozyme will diminish(Yan Liu et al. 2016). To confirm this theory, K_m and V_{max} were determined in the presence and absence of cysteamine, as illustrated in (Figure 0-5B). Based on this assumption, a decline in the V_{max} of TMB substrates as the concentration of cysteamine is enhanced was noticed, while K_m remains unchanged when using 200 μM cysteamine. Whereas different K_m and V_{max} were obtained using 60 μM cysteamine indicating a reversible inhibition phenomenon. These results lead to the observation that double types of inhibition occurred which is dependent on the concentrations of cysteamine. Overall, in contrast to natural enzymes, where one inhibitor molecule typically leads to the deactivation of a single enzyme molecule by interacting at the active site, in the case of nanozymes, the surface atoms of the nanoparticles perform the same function as the enzyme's active sites(W. Chen et al. 2019). When pAuNPs-Tablet is exposed to low concentrations of cysteamine, it experiences only partial loss of activity as the surface of pAuNPs is not completely blocked. However, higher concentrations of cysteamine lead to a complete loss of catalytic activity. According to enzyme kinetic theory, we observed that the affinity of the nanozyme to its substrate (K_m) remained constant while the catalytic efficiency decreased. This indicates that more than one cysteamine molecule binds to the surface of each pAuNPs-Tablet, obstructing the surface atoms as presented in (Figure 0-5B).

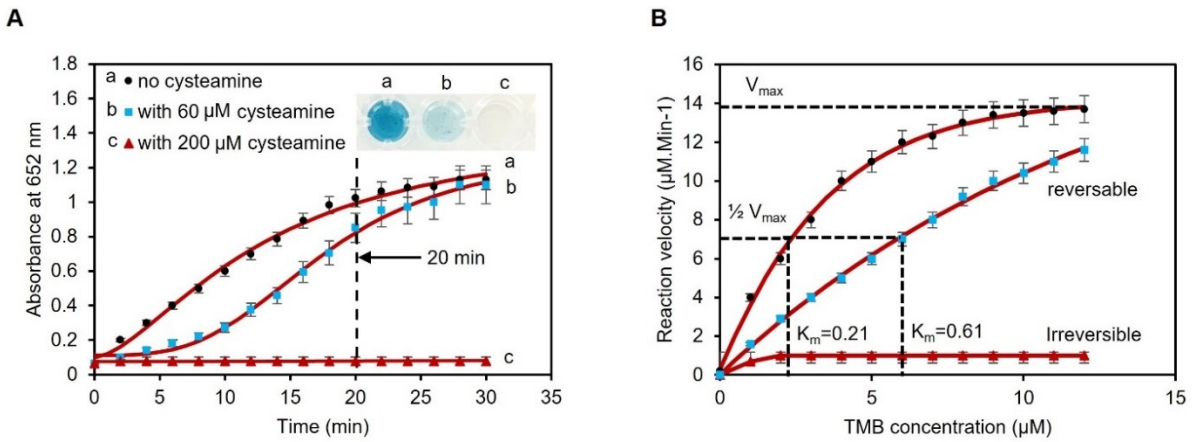

Figure 0-5 *The reaction kinetics in the presence of (0, 60, and 200 µM) of cysteamine.* ***A)*** *The kinetics study shows a detection time of 20 min. The reaction in the absence of cysteamine converted into a complete blue color (higher absorbance) while the solution containing 60 µM cysteamine shows less blue color intensity (less absorbance). On the other hand, no color transformation was achieved using 200 µM cysteamine which confirms the absence of oxTMB.* ***B)*** *Michaelis-Menten parameters were obtained when using (0, 60, and 200 µM) of cysteamine according to three replicas. A reversible (competitive) mechanism (blue squares) was observed when using 60 µM of cysteamine while the inhibition was irreversible (non-competitive) using 200 µM of cysteamine (red triangles).*

To further confirm the reversible/irreversible inhibition of pAuNPs-Tablet by 60 and 200 µM of cysteamine, we employed FTIR spectroscopy after centrifugal and washing of the colloidal pAuNPs-Tablet-cysteamine complex. The results are stated in (Figure 0-6). The FTIR spectrum of the washed pAuNPs exhibited extra peaks arising from the -SH bend and -NH stretch, which were absent in the case of pristine pAuNPs-Tablet.

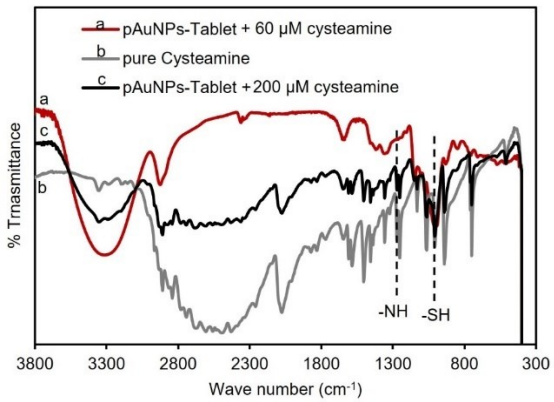

Figure 0-6 *The FTIR analyses after centrifugal and washing of the pAuNPs-Tablet-cysteamine solutions. The FTIR spectrum of the washed pAuNPs-Tablet + 200 µM cysteamine exhibited extra strong peaks arising from the -SH bend and -NH stretch due to the presence of pAuNPs-Tablet-cysteamine complex even after washing the catalyst. The absence of -SH and -NH peaks in the pristine pAuNPs-Tablet + 60 µM cysteamine indicates the pAuNPs-Tablet-cysteamine complex formation is dependent on cysteamine concentration.*

Moreso, the DLS analyses were employed to study the ζ-potential and hydrodynamic diameters of the same colloidal complex as presented in (Figure 0-7). The analyses show a decrease of ζ-potential to -2 mV and an increase in the hydrodynamic diameter of the nanoparticles to 785 nm with PDI% of 46% of the nanoparticles which can be due to the formation of pAuNPs-Tablet-cysteamine complex.

These findings confirm the potent affinity of cysteamine towards the pAuNPs, indicating the establishment of a durable complex between the nanozyme and inhibitor using a concentration of 200 µM. While no pAuNPs-cysteamine complex was observed using a 60 µM concentration of cysteamine resulting in reversible inhibition.

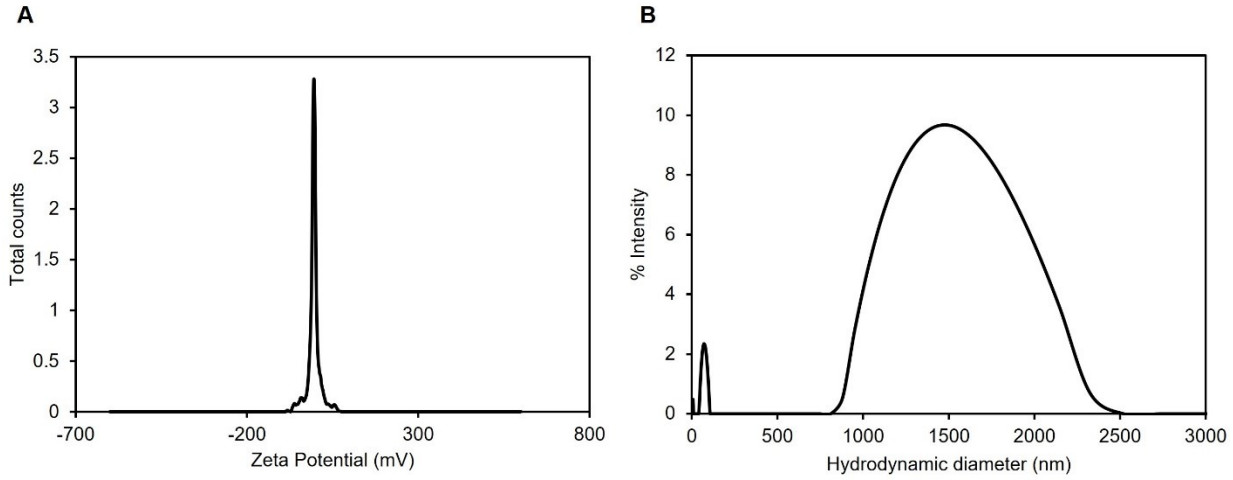

Figure 0-7 *The DLS analyses of the pAuNPs-Tablet-cysteamine complex.* ***A)*** *The ζ-potential analysis displays a decrease in ζ-potential value from-9 to -2 mV.* ***B)*** *An increase in the hydrodynamic diameter from 91.77 nm with PDI% of 24% to 785 nm with 46%, respectively indicating the formation of a complex of nanoparticles.*

Next, we performed the catalytic activity test in the presence and absence of (0, 60, and 200 µM) cysteamine. Briefly, the test is based on studying the conversion of 4-Nitrophenol (4-NP) (yellow) to 4-Aminophenol (4-AP) (colorless) in the presence of a catalyst. As displayed in (Figure 0-8A), a very fast conversion was achieved using (100 µL pAuNPs-Solution =1 pAuNPs-Tablet) while a slow conversion was observed using (25 µL pAuNPs-Solution = quarter tablet).

The catalytic activity in the presence and absence of 200 µM cysteamine is shown in (Figure 0-8B). The conversion of 4-NP into 4-AP was fully completed using pAuNPs-Tablet alone.

While the conversion was blocked in the presence of 200 µM cysteamine as shown in the reaction rate presented in (Figure 0-8C).

Moreso, the Langmuir-Hinshelwood model was used to calculate the apparent reaction constant (k_{app}) as shown in (Figure 0-8D). The k_{app} has a higher value in the case of 0 µM cysteamine while a small value was observed using 200 µM cysteamine suggesting that the pAuNPs-Tablet-cysteamine complex prevented the conversion of 4-NP to 4-AP.

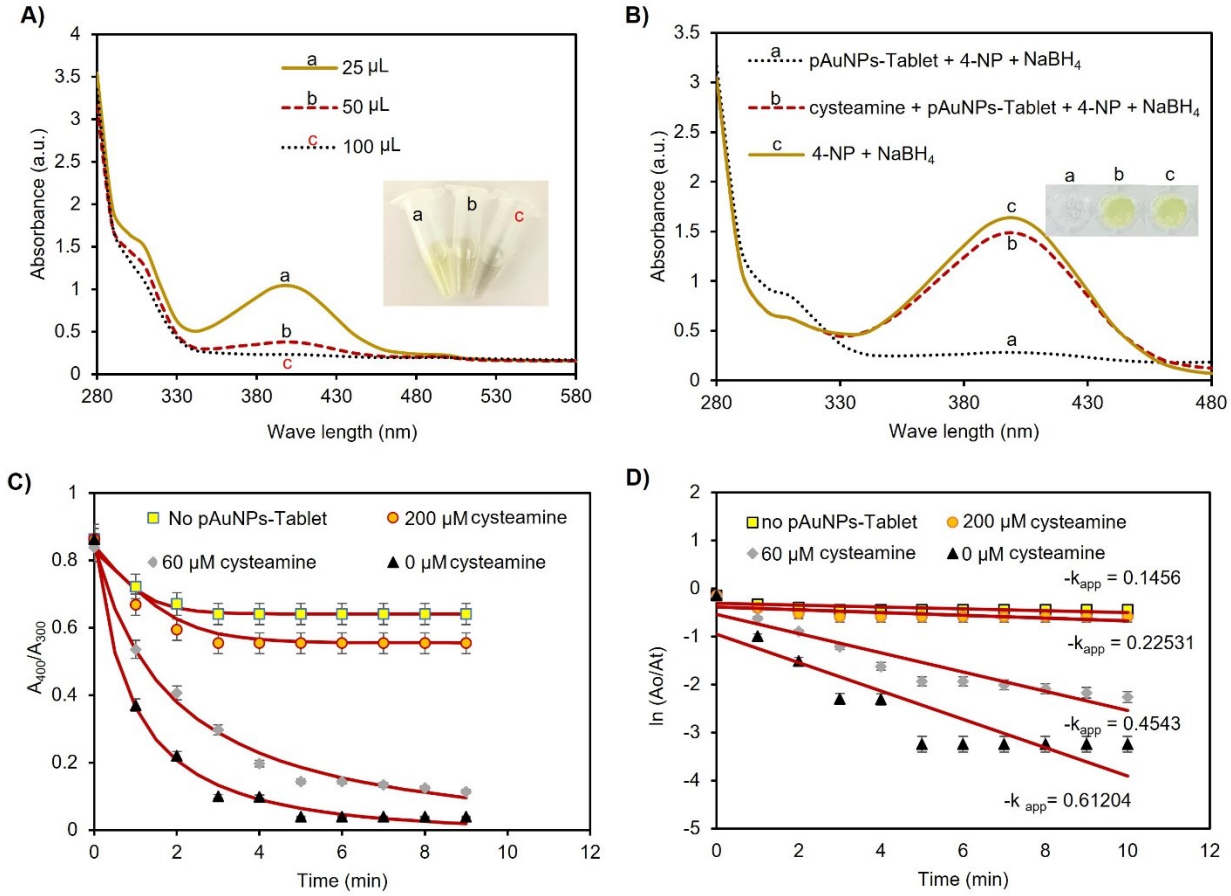

Figure 0-8 *The catalytic activity test using the conversion of 4-Nitrophenol (4-NP) (yellow) to 4-Aminophenol (4-AP) (colorless) in the presence of pAuNPs-Tablet.* ***A)*** *A higher catalytic activity was observed using 100 µM pAuNPs-Solution to cast pAuNPs-Tablet.* ***B)*** *The catalytic activity in the presence and absence of 200 µM cysteamine. The conversion of 4-NP into 4-AP was completed using pAuNPs-Tablet. While the conversion was blocked in the presence of 200 µM cysteamine.* ***C)*** *The reaction rate in the presence of (0, 60, and 200 µM) cysteamine shows a very fast conversion when 0 µM cysteamine. Whereas a slower reaction was noticed in the presence of 60 µM cysteamine. Almost no conversion was achieved in the case of 200 µM cysteamine which was comparable to the color of the blank.* ***D)*** *The Langmuir-Hinshelwood model to calculate the apparent reaction constant (k_{app}) shows a fast reaction in the case of 0 µM cysteamine while a very low (k_{app}) was observed in 200 µM cysteamine indicating that pAuNPs-Tablet-cysteamine complex prevented the conversion of 4-NP to 4-AP.*

1.29.5 Colorimetric detection of cysteamine in buffer and artificial serum

The colorimetric detection of cysteamine has been explored using the peroxidase-mimic activity of pAuNPs-Tablet. The reaction involves the oxidation-mediated TMB by pAuNPs-Tablet in the

presence of H_2O_2. The TMB was used to capture the electron transfer from the catalyst which was indicated by the development of the blue color of the system. This blue color of oxTMB is due to the establishment of a charge transfer complex that cannot form without a peroxidase catalyst. Hence, pAuNPs-Tablet was used as a peroxidase catalyst in cysteamine assay. In initial experiments, cysteamine was detected in 0–200 μM concentrations in a buffer medium using 10 mM TMB. The blue color intensity of oxTMB was quantified by recording the absorption spectra at 652 nm. There is an obvious decrease in λ_{max} at 652 nm with increasing cysteamine concentrations. While higher peaks appeared using 5-40 μM cysteamine which became less gradual with increasing the concentration of cysteamine until a fully flat peak with 200 μM as shown in (Figure 0-9A). However, the absorbance λ_{652} remained unaffected with a further increase in cysteamine concentration indicating the complete blockage of oxidation of TMB substrate.

A calibration curve of enzyme mimic activity of pAuNPs-Tablet was plotted against cysteamine concentrations on the x-axis and change in absorbance (ΔA) values at 652 nm on the y-axis resulting in a hyperbolic curve which was fitted using the Hill model as shown in (Figure 0-9B).

The relative absorption intensity is linearly proportional to the concentration of cysteamine at the first four concentrations as displayed in the inset of (Figure 0-9C) with an LoD of 69 μM. Once the peroxidase behavior of pAuNPs-Tablet was confirmed for cysteamine detection in PB, the same protocols were followed in artificial serum to acquaint with close to real-world situations.

Next, the peroxidase-mimic activity of pAuNPs-Tablet was evaluated using different cysteamine concentrations (0–200 μM) in the artificial serum medium. The lower cysteamine concentrations <40 μM produced the high blue color intensity solution showing a plateau at 652 nm in the UV–vis spectrum. The reaction media turned to the faded blue color progressively with the increase in cysteamine concentrations until 200 μM as shown in (Figure 0-9D). The color of the TMB solution was changed according to cysteamine concentration which was used to calculate the amount of cysteamine in the calibration curve. The curve was plotted considering the relative change in absorbance intensity (ΔA) at 652 nm versus the cysteamine concentrations using a Hill model.

An LoD of 80 μM was calculated in artificial serum as shown in (Figure 0-9E). At lower concentrations, the λ_{652} was linearly proportional to the concentration of cysteamine as displayed in (Figure 0-9F).

In conclusion, our newly proposed pAuNPs-Tablet sensor efficiently detected cysteamine in different media using the peroxidase catalytic property of AuNPs. Cysteamine which contains a thiol group is an essential amino acid that was found to be the only treatment for cystinosis(Gahl 2003). However, abnormal concentrations of cysteamine are implicated in a variety of health conditions. Therefore, it is highly important to report changes in cysteamine concentrations via real-time monitoring. Hence, pAuNPs-Tablet would be a potential platform in the disease diagnostic and detection field. Moreover, the pAuNPs-Tablet sensor is portable, low-cost, user-friendly, and offers colorimetric read-out which presents a good candidate for point-of-care analytical devices.

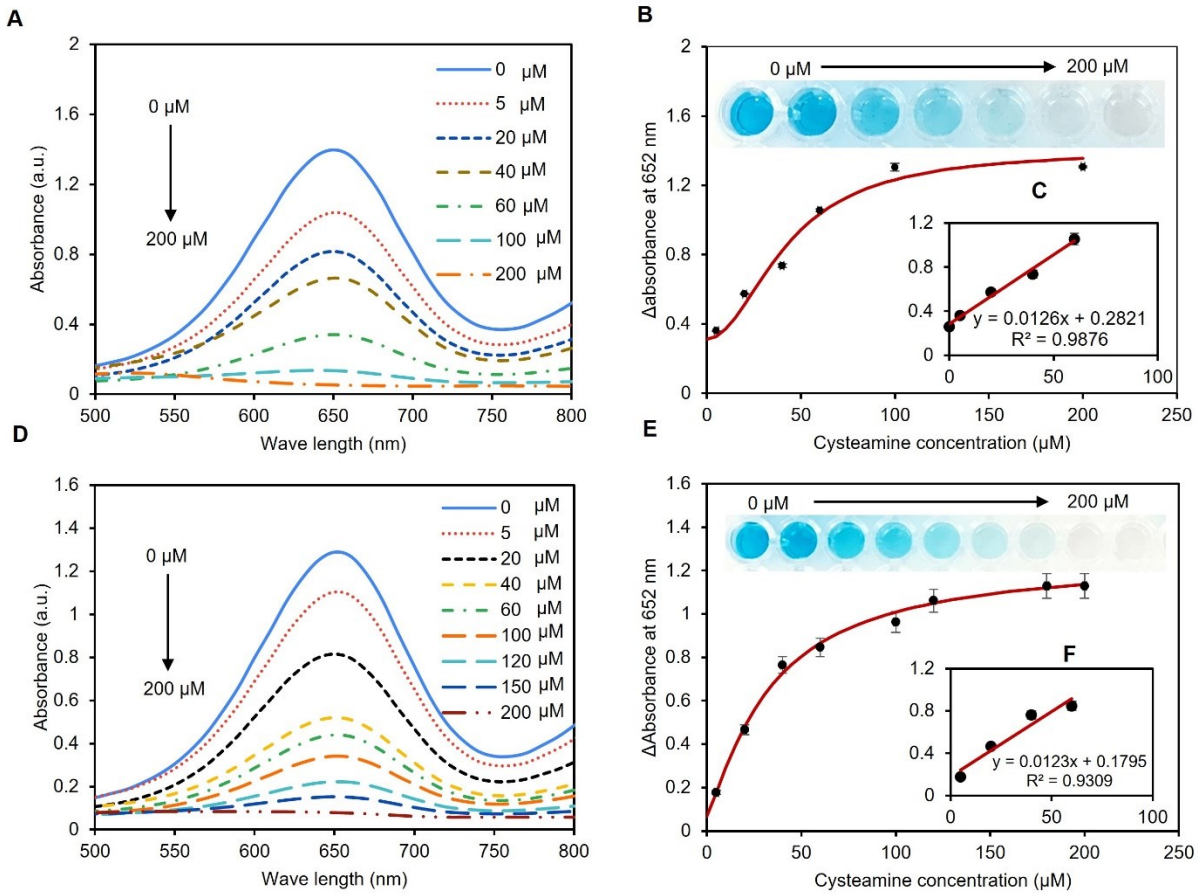

Figure 0-9 *Detection of cysteamine in phosphate buffer and artificial serum.* ***A)*** *UV-vis spectra of TMB in phosphate buffer pH=7 in the presence of a different concentration of cysteamine (0-200 μM).* ***B)*** *The calibration curve was obtained using various concentrations of cysteamine.* ***C)*** *The linear range of the curve shows good linearity between (0-40 μM) of cysteamine. The LoD was calculated using the 3σ/slope method and was found to be 69 μM.* ***D)*** *UV-vis spectra of TMB in artificial serum pH= 6.8 in the presence of a different concentration of cysteamine (0-200 μM).* ***E)*** *The calibration curve was obtained using various concentrations of cysteamine.* ***F)*** *The linear range of the curve shows good linearity between (0-40 μM) of cysteamine. The LoD was measured using the 3σ/slope method where the value was 80 μM. ΔA= ($A_{652\ nm,\ absence}$) -($A_{652\ nm,\ cysteamine}$).*

1.29.6 Selectivity analysis towards cysteamine detection

To investigate the specificity of the pAuNPs-Tablet sensor toward cysteamine detection, other amino acids including methionine, asparagine, glycine, glutathione, aspartic acid, cysteine, and arginine were tested in an artificial serum. For this study, 100 µM of each amino acid was incubated with pAuNPs-Tablet separately for 1 min followed by the addition of TMB and H_2O_2 solutions. There was an obvious change in the TMB color in the presence of other amino acids while the TMB color remain colorless-grey in the presence of cysteamine as illustrated in (Figure 0-10A). Hence, these results confirm the specificity of our pAuNPs-Tablet sensor for the detection of cysteamine.

1.29.7 Determination analysis of cysteamine in human serum

To evaluate the practical suitability of our suggested pAuNPs-Tablet sensor, cysteamine detection was accomplished in human serum samples. Four samples (Sample 1: healthy individual, Sample 2, 3, and 4: cystinosis patients) were donated from a clinical lab, in Montreal, Canada. For the detection of cysteamine, the time of sample collection is critical. Therefore, the samples were collected after 30-60 min of the patients' digestion of 1200 mg of the Cystagon drug (Stachowicz et al. 1998a). It is worth mentioning that the serum samples were used without any treatment and stored in test tubes in well-closed plastic bags at -20 °C and used within three days. The samples were checked for cysteamine levels without spiking as presented in (Figure 0-10B). The findings confirmed the presence of different concentrations of cysteamine. The obtained color development of oxTMB varied from less intense or faint blue in the case of samples 2, 3, and 4 to a very intense blue color as in sample 1.

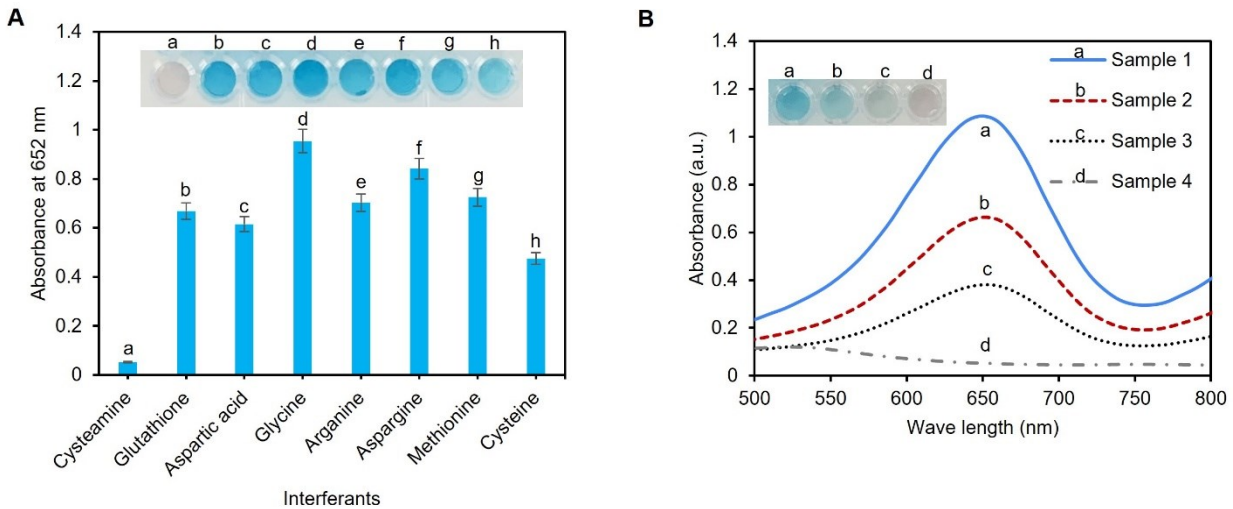

Figure 0-10 *The interference studies and the real sample testing. A) The selectivity of the sensor in the presence of other amino acids shows that other amino acids do not interfere with the sensor specificity for cysteamine. B) UV-vis peaks at 652 nm of the samples before spiking indicating a higher peak for (sample 1: healthy individual) while a decrease in peaks was observed for samples 2,3, and 4 which are samples taken from patients with cystinosis. (n=3).*

Finally, to assess the applicability of the pAuNPs-Tablet for real-world applications, samples 1, 2, and 3 were spiked with cysteamine 100, 60, and 70 µM, respectively. As shown in (Figure 0-11) with the blue squares, red triangles, and green diamonds, the results of the measured intensities for the spiked samples followed the trend in the calibration curves, with the calculated recovery values of 105, 103.8, and 102% for sample 1, 101, 102, and 104 % for the samples 2, and 91, 94, 98% for sample 3, respectively. Likewise, the real samples exhibited outstanding precision, as evidenced by the %RSD measurements of less than 2% for each of the three repeated data points. These results show the applicability of pAuNPs-Tablet as a sensor for complex matrices in real-world applications.

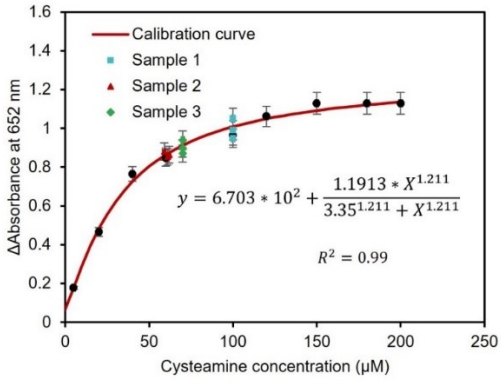

Figure 0-11 *Analytical performance of the tablet-based sensor in real human serum samples. The calibration curve was attained by testing the sensor with the known concentrations of 60, 70, and 100 µM cysteamine in real human serum samples. A Hill function was fit to the whole data with an R2 > 0.99, showing the compatibility of the data with a standard saturation model. Each data point is the mean ± standard deviation of the replications (n = 3).*

Chapter 5. Conclusion and Future Work

In this section, the accomplished objectives briefly explained and sum-up this part with the future research topics.

In Chapter 1, the background, and the motivation of the work to create a glucose sensor that can detect salivary glucose and replace the invasive methods of testing have been highlighted. The background and motivation to establish the cysteamine sensor in serum samples has been discussed.

In Chapter 2, a review of the principles of peroxidase-like activity of different kinds of developed peroxidase nanozyme has been described in detail. A literature review of various nanozymes composed of metal nanoparticles has been discussed. Among these nanozymes, AuNPs synthesis using green methods is a flexible and attractive selection. The various media of human fluids used to monitor glucose levels showed complicated extraction as well as the multistep preparation of samples to produce successful tests. Furthermore, the history of green and chemical synthesis of AuNPs has been reviewed indicating the benefits of using pullulan (all in reducing, stabilizing, and encapsulating agent) as an environmentally friendly procedure over the chemical methods. Other glucose detection platforms using saliva samples have been described. The inhibition of peroxidase like activity in presence of amino acids has been highlighted.

Whereas **Chapter 3** represents the procedures followed to prepare the reagents and buffers that are used for H_2O_2, glucose, and cysteamine detection. Moreso, (AuNPs-pSol) was synthesized using the green synthesis procedure. In the first step, gold (III) salt was reacted with alkali-treated pullulan to synthesize AuNPs-pSol. Pullulan was used exclusively as a reducing/capping/tablet forming agent, hence AuNPs-pTabs were cast from a pre-measured amount of AuNPs-pSol without any additional reagent. The process of AuNPs-pTab formation using various methods of drying has been stated.

Furthermore, Benedicts and catalytic activity reagents were prepared and performed to unveil the presence of reducing sugar. In addition, the chapter discuss the optimization of the experimental condition along with the results obtained from using the peroxidase tablet-based sensor (AuNPs-pTab) for the colorimetric detection of glucose in saliva using the H_2O_2-TMB system. First, different parameters such as temperature, pH, TMB concentrations, and reaction kinetics were examined for glucose assay. AuNPs-pTab sensor was functional over a broad temperature range (25-70 °C) at pH 3. Second, the AuNPs-pTab was explored for the peroxidase-mimic activity to

oxidize TMB in the presence of H_2O_2 as a potential step for glucose detection. Third, Benedict's test indicated that a high amount of reducing sugar existed in AuNPs-pTab. While the catalytic activity test performed using the conversion of 4-nitrophenol to 4-aminophenol by the addition of AuNPs-pTab shows a high catalytic activity which was highly affected by the portion of AuNPs-pTab used in the test. Moreso, the peroxidase activity of AuNPs-pTab was 25% better than AuNPs-pSol and comparable to horseradish peroxidase. Hence, AuNPs-pTab can be a good replacement for natural peroxidase enzymes with enhanced heat tolerance.

In addition, the AuNPs-pTab is ultra-stable which confirmed by evaluating the tablet performance over sixteen months while AuNPs-pSol showed a decreased stability after the first month. Last, this proposed glucose assay showed a LOD of 28.7 μM, 38.2 μM, and 163.04 μM in buffer media, artificial saliva, and real saliva, respectively. The AuNPs-pTab sensor showed excellent performance in terms of high specificity and selectivity toward glucose and H_2O_2 detection. The percent recovery (%R) for real saliva samples was 93.6% and 107.7%.

Chapter 4 demonstrates the catalytic activity of pAuNPs-Tablet as a peroxidase mimic. The tablet nanozymes showed high specificity towards oxidation of positively charged TMB substrate. Different media of phosphate buffer and artificial human serum were tested to quantify the amount of cysteamine. The kinetics analyses using the Michaelis-Menten model were also employed to study the inhibition types. Importantly, this study for the first time establishes cysteamine to exhibit two features as a reversible/irreversible inhibitor to temporarily/permanently block the catalytic activity of pAuNPs-Tablet nanozyme.

Considering that surface atoms function as active positions in nanozymes, it was observed that the cysteamine concentrations had an impact on the suppression of catalytic activity. The specific nature of this interaction allowed the fabrication of a simple colorimetric sensor for cysteamine detection using the pAuNPs-Tablet. As a proof of concept, sulfuric acid was used to confirm the inhibition by quantifying the amount of oxTMB through the formation of yellow color products. This tablet detected low levels of cysteamine concentrations with an LoD of 69.04 and 82.9 μM in phosphate buffer and artificial serum samples, respectively.

Other potential interferants were used for the selectivity of the sensor towards cysteamine among other amino acids. The recovery percentages (%R) in real human samples show the method's validity with values ranging from 91-105% in real human serum samples. All in all, the

combination of gold nanoparticles and pullulan in tablet platforms provides numerous distinctive advantages, including transportability, simple fabrication, low cost, high selectivity and sensitivity, and naked-eye visibility. Our study results provide strong evidence that pAuNPs-Tablet has a high potential for use in the routine clinical diagnosis of cysteamine overdoses in real human serum samples.

Overall, the AuNPs-pTab sensor is simple, portable, inexpensive (estimated cost per one test is $ 0.014 CAD), and offers a colorimetric read-out for H_2O_2, glucose, and cysteamine detection that serves as an attractive platform for POC devices and under RE-ASSURED criteria.

Future work

This research was an examination of the encapsulation of AuNPs for the detection of glucose in real saliva samples and cysteamine in real serum samples in addition, AuNPs-pTab was applied for the detection of glucose and cysteamine which still needs further experimental validation. Generally, an additional exploration into the research can be extended by:

- The sensor can further be developed by using a mobile phone application that analysis the RGB color for fully home-used glucose monitoring. In this way, the sensor can be used without UV-vis spectroscopy. Furthermore, a colorimeter can be used to quantify the amount of glucose and cysteamine instead of UV-vis spectrometer.
- Pullulan is sensitive to high humidity, therefore, studying the effect of humidity on the AuNPs-pTab and increasing the shelf life of AuNPs-pTab in humid areas is needed.
- Exploring the catalytic activity of the larger particle size (540 nm) of AuNPs-pTab as tested it has a great potential to detect H_2O_2 and glucose. By adjusting the temperature and the amount of reducing agent during the synthesis we could obtain other sizes and shapes of AuNPs-pTab which might be beneficial to discover other properties of nanozyme.
- Exploring the AuNPs-pTab abilities for the detection of other biomarkers which are based on the production of H_2O_2 such as cholesterol, creatinine, glutathione, and uric acid.
- Studying the encapsulation of TMB with other buffers using different concentrations of pullulan as well as different polysaccharides which could facilitate the transportation and reduce the number of steps to perform the test.
- Exploring the other features of pullulan capped gold nanoparticles tablet such as oxidase, catalase, superoxide dismutase, and hydrolase. Combining other features in one tablet nanozymes such as glucose oxidase and peroxidase nanozyme in one tablet nanozymes.
- The recyclability of the pullulan capped gold nanoparticles tablet can be further examined. The tablet was recovered up to 5 times using centrifugation method. However, the peroxidase like activity of the tablets decreased 20% each time due to particle lose. This issue leads to the approach of producing beads instead of tablets. Beads have many advantages such as they can catalyze the reaction and produce blue color products without being dissolved in the mixture.

References

Adeniyi, Omotayo, Nnamdi Nwahara, Daniel Mwanza, Tebello Nyokong, and Philani Mashazi. 2021. "Nanohybrid Electrocatalyst Based on Cobalt Phthalocyanine-Carbon Nanotube-Reduced Graphene Oxide for Ultrasensitive Detection of Glucose in Human Saliva." Sensors and Actuators B: Chemical 348 (June): 130723. https://doi.org/10.1016/j.snb.2021.130723.

Aldewachi, H., T. Chalati, M. N. Woodroofe, N. Bricklebank, B. Sharrack, and P. Gardiner. 2018. "Gold Nanoparticle-Based Colorimetric Biosensors." Nanoscale 10 (1): 18–33. https://doi.org/10.1039/C7NR06367A.

Alle, Madhusudhan, Rajkumar Bandi, Garima Sharma, Ramakrishna Dadigala, Seung Hwan Lee, and Jin Chul Kim. 2022. "Gold Nanoparticles Spontaneously Grown on Cellulose Nanofibrils as a Reusable Nanozyme for Colorimetric Detection of Cholesterol in Human Serum." International Journal of Biological Macromolecules 201 (January): 686–97. https://doi.org/10.1016/j.ijbiomac.2022.01.158.

Alvarado-Ramírez, Lynette, Magdalena Rostro-Alanis, José Rodríguez-Rodríguez, Juan Eduardo Sosa-Hernández, Elda M. Melchor-Martínez, Hafiz M N Iqbal, and Roberto Parra-Saldívar. 2021. "Enzyme (Single and Multiple) and Nanozyme Biosensors: Recent Developments and Their Novel Applications in the Water-Food-Health Nexus." Biosensors 11 (11): 410. https://doi.org/10.3390/bios11110410.

Aminabad, Esmaeil Darvish, Ahmad Mobed, Mohammad Hasanzadeh, Mohammad Ali Hosseinpour Feizi, Reza Safaralizadeh, and Farzad Seidi. 2022. "Sensitive Immunosensing of α-Synuclein Protein in Human Plasma Samples Using Gold Nanoparticles Conjugated with Graphene: An Innovative Immuno-Platform towards Early Stage Identification of Parkinson's Disease Using Point of Care (POC) Analysis." RSC Advances 12 (7): 4346–57. https://doi.org/10.1039/D1RA06437A.

Amine, Aziz, Loubna El Harrad, Fabiana Arduini, Danila Moscone, and Giuseppe Palleschi. 2014. "Analytical Aspects of Enzyme Reversible Inhibition." Talanta 118: 368–74. https://doi.org/10.1016/j.talanta.2013.10.025.

Amornkitbamrung, Lunjakorn, Prompong Pienpinijtham, Chuchaat Thammacharoen, and Sanong Ekgasit. 2014. "Palladium Nanoparticles Synthesized by Reducing Species Generated during a Successive Acidic/Alkaline Treatment of Sucrose." Spectrochimica Acta - Part A: Molecular and Biomolecular Spectroscopy 122: 186–92. https://doi.org/10.1016/j.saa.2013.10.095.

"Angewandte Chemie - 2004 - Manea - Nanozymes Gold-Nanoparticle-Based Transphosphorylation Catalysts.Pdf." n.d.

Apyari, Vladimir V., Stanislava G. Dmitrienko, Viktoriya V. Arkhipova, Aydar G. Atnagulov, and Yuri A. Zolotov. 2012. "Determination of Cysteamine Using Label-Free Gold Nanoparticles." Analytical Methods 4 (10): 3193. https://doi.org/10.1039/c2ay25675d.

Arakawa, Takahiro, Yusuke Kuroki, Hiroki Nitta, Prem Chouhan, Koji Toma, Shin ichi Sawada, Shuhei Takeuchi, et al. 2016. "Mouthguard Biosensor with Telemetry System for Monitoring of Saliva Glucose: A Novel Cavitas Sensor." Biosensors and Bioelectronics 84: 106–11. https://doi.org/10.1016/j.bios.2015.12.014.

Ashrafi, Amir M., Zuzana Bytesnikova, Jiri Barek, Lukas Richtera, and Vojtech Adam. 2021a. "A Critical Comparison of Natural Enzymes and Nanozymes in Biosensing and Bioassays." Biosensors and Bioelectronics 192 (April): 113494. https://doi.org/10.1016/j.bios.2021.113494.

Atallah, Carla, Catherine Charcosset, and Hélène Greige-Gerges. 2020. "Challenges for Cysteamine Stabilization, Quantification, and Biological Effects Improvement." Journal of Pharmaceutical Analysis 10 (6): 499–516. https://doi.org/10.1016/j.jpha.2020.03.007.

Azzam, Ahmed B., Ridha Djellabi, Sheta M. Sheta, and S. M. El-Sheikh. 2021. "Ultrafast Conversion of Carcinogenic 4-Nitrophenol into 4-Aminophenol in the Dark Catalyzed by Surface Interaction on BiPO4/g-C3N4nanostructures in the Presence of NaBH4." RSC Advances 11 (31): 18797–808. https://doi.org/10.1039/d1ra02852a.

Balaji, R., Revathi Duraisamy, and M. P. Santhosh Kumar. 2019. "Complications of Diabetes Mellitus: A Review." Drug Invention Today 12 (1): 98–103.

Balakumar, Vellaichamy, Hyungjoo Kim, Ji Won Ryu, Ramalingam Manivannan, and Young A. Son. 2020. "Uniform Assembly of Gold Nanoparticles on S-Doped g-C3N4 Nanocomposite for Effective Conversion of 4-Nitrophenol by Catalytic Reduction." Journal of Materials Science and Technology 40 (March): 176–84. https://doi.org/10.1016/j.jmst.2019.08.031.

Bambo, Mokae Fanuel, Rui Werner Marcedo Krause, and Richard Motlhaletsi Moutloali. 2017. "Facile Method for the Synthesis of Copper Nanoparticles Supported on the Organoclay Material." Journal of Biomaterials and Nanobiotechnology 08 (02): 144–58. https://doi.org/10.4236/jbnb.2017.82010.

Besouw, Martine, Henk Blom, Albert Tangerman, Adriana de Graaf-Hess, and Elena Levtchenko. 2007. "The Origin of Halitosis in Cystinotic Patients Due to Cysteamine Treatment." Molecular Genetics and Metabolism 91 (3): 228–33. https://doi.org/10.1016/j.ymgme.2007.04.002.

Besouw, Martine T.P., Richard Bowker, Jean-paul Dutertre, Francesco Emma, William A Gahl, Marcella Greco, Marc R Lilien, et al. 2011. "Cysteamine Toxicity in Patients with Cystinosis." The Journal of Pediatrics 159 (6): 1004–11. https://doi.org/10.1016/j.jpeds.2011.05.057.

BHOOLA, K. D. 1969. "Protein Inhibitors." Nature 223 (5204): 426–426. https://doi.org/10.1038/223426b0.

Bouazza, Naïm, Jean-Marc Tréluyer, Chris Ottolenghi, Saik Urien, Georges Deschenes, Daniel Ricquier, Patrick Niaudet, and Bernadette Chadefaux-Vekemans. 2011. "Population Pharmacokinetics and Pharmacodynamics of Cysteamine in Nephropathic Cystinosis Patients." Orphanet Journal of Rare Diseases 6 (1): 86. https://doi.org/10.1186/1750-1172-6-86.

Castro, Lucas F. de, Soraia V. de Freitas, Lucas C. Duarte, João Antônio C. de Souza, Thiago R.L.C. Paixão, and Wendell K.T. Coltro. 2019. "Salivary Diagnostics on Paper Microfluidic Devices and Their Use as Wearable Sensors for Glucose Monitoring." Analytical and Bioanalytical Chemistry 411 (19): 4919–28. https://doi.org/10.1007/s00216-019-01788-0.

Cemeroglu, Ayse Pinar, Argun Can, Alan T. Davis, Ozlem Cemeroglu, Lora Kleis, Maala S. Daniel, Jessica Bustraan, and Tracy J. Koehler. 2015. "Fear of Needles in Children with Type 1 Diabetes Mellitus on Multiple Daily Injections and Continuous Subcutaneous Insulin Infusion." Endocrine Practice 21 (1): 46–53. https://doi.org/10.4158/EP14252.OR.

Chakraborty, Pinak, Saurab Dhar, Nitumoni Deka, Kamalesh Debnath, and Suvra Prakash Mondal. 2020. "Non-Enzymatic Salivary Glucose Detection Using Porous CuO Nanostructures." Sensors and Actuators, B: Chemical 302 (June 2019): 127134. https://doi.org/10.1016/j.snb.2019.127134.

Chang, Keke, Shun Wang, Hao Zhang, Qingqian Guo, Xinran Hu, Zhili Lin, Haifeng Sun, Min Jiang, and Jiandong Hu. 2017. "Colorimetric Detection of Melamine in Milk by Using Gold Nanoparticles-Based LSPR via Optical Fibers." PLoS ONE 12 (5): 1–12. https://doi.org/10.1371/journal.pone.0177131.

Chen, Meizi, Xiaowei Cao, Kang Chang, Huanhuan Xiang, and Rong Wang. 2021. "A Novel Electrochemical Non-Enzymatic Glucose Sensor Based on Au Nanoparticle-Modified Indium Tin Oxide Electrode and Boronate Affinity." Electrochimica Acta 368: 137603. https://doi.org/10.1016/j.electacta.2020.137603.

Chen, Qiao, Jia Chen, Cunji Gao, Mingliang Zhang, Junying Chen, and Hongdeng Qiu. 2015. "Hemin-Functionalized WS2 Nanosheets as Highly Active Peroxidase Mimetics for Label-Free Colorimetric Detection of H2O2 and Glucose." Analyst 140 (8): 2857–63. https://doi.org/10.1039/c5an00031a.

Chen, Wenjun, Shunyao Li, Jun Wang, Kai Sun, and Youbin Si. 2019. "Metal and Metal-Oxide Nanozymes: Bioenzymatic Characteristics, Catalytic Mechanism, and Eco-Environmental Applications." Nanoscale. Royal Society of Chemistry. https://doi.org/10.1039/c9nr04771a.

Chen, Zhongwen, Jun Jie Yin, Yu Ting Zhou, Yu Zhang, Lina Song, Mengjie Song, Sunling Hu, and Ning Gu. 2012. "Dual Enzyme-like Activities of Iron Oxide Nanoparticles and Their Implication for Diminishing Cytotoxicity." ACS Nano 6 (5): 4001–12. https://doi.org/10.1021/nn300291r.

Chong, Pei Yi, Li Li Chan, Joon Wah Mak, and Stephen Ambu. 2012. "Evaluation of Escherichia Coli, Streptococcus Pneumonia and Human Glial Cells as Food Source on Modulating the Pathogenic Characteriatics of Acanthamoeba towards BALB/c Mice." Diabetes, Metabolic Syndrome and Obesity: Targets and Therapy 5: 149–54.

Chu, Yizhuo, Ethan Schonbrun, Tian Yang, and Kenneth B. Crozier. 2008. "Experimental Observation of Narrow Surface Plasmon Resonances in Gold Nanoparticle Arrays." Applied Physics Letters 93 (18). https://doi.org/10.1063/1.3012365.

Cui, Xiaoyu, Jinming Li, Yuting Li, Mingyu Liu, Jinglong Qiao, Dong Wang, Hui Cao, Wanli He, Yun Feng, and Zhou Yang. 2022. "Detection of Glucose in Diabetic Tears by Using Gold Nanoparticles and MXene Composite Surface-Enhanced Raman Scattering Substrates." Spectrochimica Acta Part A: Molecular and Biomolecular Spectroscopy 266 (February): 120432. https://doi.org/10.1016/j.saa.2021.120432.

Cui, Yangyang, Hankun Zhang, Jia Zhu, Zhenhua Liao, Song Wang, and Weiqiang Liu. 2022. "Correlations of Salivary and Blood Glucose Levels among Six Saliva Collection Methods." International Journal of Environmental Research and Public Health 19 (7): 4122. https://doi.org/10.3390/ijerph19074122.

Das, Bhaskar, Javier Lou Franco, Natasha Logan, Paramasivan Balasubramanian, Moon Il Kim, and Cuong Cao. 2021. "Nanozymes in Point-of-Care Diagnosis: An Emerging Futuristic Approach for Biosensing." Nano-Micro Letters 13 (1): 193. https://doi.org/10.1007/s40820-021-00717-0.

Deshmukh, Aarti R., Hajer Aloui, and Beom Soo Kim. 2021. "Novel Biogenic Gold Nanoparticles Catalyzing Multienzyme Cascade Reaction: Glucose Oxidase and Peroxidase Mimicking Activity." Chemical Engineering Journal 421 (P2): 127859. https://doi.org/10.1016/j.cej.2020.127859.

Diamai, Siewdorlang, and Devendra P.S. Negi. 2019. "Cysteine-Stabilized Silver Nanoparticles as a Colorimetric Probe for the Selective Detection of Cysteamine." Spectrochimica Acta - Part A: Molecular and Biomolecular Spectroscopy 215 (May): 203–8. https://doi.org/10.1016/j.saa.2019.02.101.

Dill, Ken A. 1997. "Additivity Principles in Biochemistry." Journal of Biological Chemistry. American Society for Biochemistry and Molecular Biology Inc. https://doi.org/10.1074/jbc.272.2.701.

Dong, Jinlai, Lina Song, Jun Jie Yin, Weiwei He, Yihang Wu, Ning Gu, and Yu Zhang. 2014. "Co3O4 Nanoparticles with Multi-Enzyme Activities and Their Application in Immunohistochemical Assay." ACS Applied Materials and Interfaces 6 (3): 1959–70. https://doi.org/10.1021/am405009f.

Drozd, Marcin, Mariusz Pietrzak, Paweł G. Parzuchowski, and Elżbieta Malinowska. 2016. "Pitfalls and Capabilities of Various Hydrogen Donors in Evaluation of Peroxidase-like Activity of Gold Nanoparticles." Analytical and Bioanalytical Chemistry 408 (29): 8505–13. https://doi.org/10.1007/s00216-016-9976-z.

Duong, Hong Dinh, Ok Jae Sohn, and Jong Il Rhee. 2020. "Development of a Ratiometric Fluorescent Glucose Sensor Using an Oxygen-Sensing Membrane Immobilized with Glucose Oxidase for the Detection of Glucose in Tears." Biosensors 10 (8). https://doi.org/10.3390/BIOS10080086.

E, Xiu Tian Feng, Yu Zhang, Ji Jun Zou, Xiangwen Zhang, and Li Wang. 2014. "Shape Evolution in Brust-Schiffrin Synthesis of Au Nanoparticles." Materials Letters 118: 196–99. https://doi.org/10.1016/j.matlet.2013.12.066.

Emma, Francesco, Galina Nesterova, Craig Langman, Antoine Labbé, Stephanie Cherqui, Paul Goodyer, Mirian C. Janssen, et al. 2014. "Nephropathic Cystinosis: An International Consensus Document." Nephrology Dialysis Transplantation. Oxford University Press. https://doi.org/10.1093/ndt/gfu090.

Esfahani, AmirReza R., Zubi Sadiq, Oyejide Damilola Oyewunmi, Seyed Hamid Safiabadi Tali, Ndifreke Usen, Daria Camilla Boffito, and Sana Jahanshahi-Anbuhi. 2021. "Portable, Stable, and Sensitive Assay to Detect Phosphate in Water with Gold Nanoparticles (AuNPs) and Dextran Tablet." The Analyst 146 (11): 3697–3708. https://doi.org/10.1039/D0AN02063J.

Fan, Jia, Jun Jie Yin, Bo Ning, Xiaochun Wu, Ye Hu, Mauro Ferrari, Gregory J. Anderson, Jingyan Wei, Yuliang Zhao, and Guangjun Nie. 2011. "Direct Evidence for Catalase and Peroxidase Activities of Ferritin-Platinum Nanoparticles." Biomaterials 32 (6): 1611–18. https://doi.org/10.1016/j.biomaterials.2010.11.004.

Feng, Jiayu, Pengcheng Huang, Shuizhen Shi, Ke Yu Deng, and Fang Ying Wu. 2017. "Colorimetric Detection of Glutathione in Cells Based on Peroxidase-like Activity of Gold Nanoclusters: A Promising Powerful Tool for Identifying Cancer Cells." Analytica Chimica Acta 967: 64–69. https://doi.org/10.1016/j.aca.2017.02.025.

Fiore, Luca, Benedetta De Lellis, Vincenzo Mazzaracchio, Elena Suprun, Renato Massoud, Bianca Maria Goffredo, Danila Moscone, and Fabiana Arduini. 2022. "Smartphone-Assisted Electrochemical Sensor for Reliable Detection of Tyrosine in Serum." Talanta 237 (April 2021): 122869. https://doi.org/10.1016/j.talanta.2021.122869.

Franzin, Martina, Silvia Rossetto, Rachele Ruoso, Rossella Del Savio, Gabriele Stocco, Giuliana Decorti, and Riccardo Addobbati. 2022. "A New Proof of Evidence of Cysteamine Quantification for Therapeutic Drug Monitoring in Patients with Cystinosis." Orphanet Journal of Rare Diseases 17 (1): 400. https://doi.org/10.1186/s13023-022-02540-1.

Fung, Ka Kei, Cangel Pui Yee Chan, and Reinhard Renneberg. 2009. "Development of Enzyme-Based Bar Code-Style Lateral-Flow Assay for Hydrogen Peroxide Determination." Analytica Chimica Acta 634 (1): 89–95. https://doi.org/10.1016/j.aca.2008.11.064.

Gahl, William A. 2003. "Early Oral Cysteamine Therapy for Nephropathic Cystinosis." European Journal of Pediatrics 162 (0): 38–41. https://doi.org/10.1007/s00431-003-1349-x.

Galant, A. L., R. C. Kaufman, and J. D. Wilson. 2015. "Glucose: Detection and Analysis." Food Chemistry 188: 149–60. https://doi.org/10.1016/j.foodchem.2015.04.071.

Gallego-Villar, L, Luciana Hannibal, J Häberle, B Thöny, T Ben-Omran, G K Nasrallah, Al-N Dewik, W D Kruger, and H J Blom. 2017. "Cysteamine Revisited: Repair of Arginine to Cysteine Mutations." Journal of Inherited Metabolic Disease 40 (4): 555–67. https://doi.org/10.1007/s10545-017-0060-4.

Gao, Lizeng, Jie Zhuang, Leng Nie, Jinbin Zhang, Yu Zhang, Ning Gu, Taihong Wang, et al. 2007. "Intrinsic Peroxidase-like Activity of Ferromagnetic Nanoparticles." Nature Nanotechnology 2 (9): 577–83. https://doi.org/10.1038/nnano.2007.260.

Gibrat, C., and F. Cicchetti. 2011. "Potential of Cystamine and Cysteamine in the Treatment of Neurodegenerative Diseases." Progress in Neuro-Psychopharmacology and Biological Psychiatry 35 (2): 380–89. https://doi.org/10.1016/j.pnpbp.2010.11.023.

Golamari, Uma Maheswara R., Meenakshi Sundari Subramaniyan Natarajan, Annam Lakshmanan, and Rajeswari K. Balakrishnan. 2019. "Correlation between Salivary Glucose and Blood Glucose Levels in Diabetic and Non-Diabetic Individuals." International Journal of Advances in Medicine 6 (4): 1220. https://doi.org/10.18203/2349-3933.ijam20193274.

Guan, Huanan, Yan Song, Bolin Han, Dezhuang Gong, and Na Zhang. 2020. "Colorimetric Detection of Cholesterol Based on Peroxidase Mimetic Activity of GoldMag Nanocomposites." Spectrochimica Acta - Part A: Molecular and Biomolecular Spectroscopy 241: 118675. https://doi.org/10.1016/j.saa.2020.118675.

Guler, Muhammet, Vedat Turkoglu, and Mehmet Riza Kivanc. 2017. "A Novel Enzymatic Glucose Biosensor and Nonenzymatic Hydrogen Peroxide Sensor Based on (3-Aminopropyl) Triethoxysilane Functionalized Reduced Graphene Oxide." Electroanalysis 29 (11): 2507–15. https://doi.org/10.1002/elan.201700417.

H Moubasher, S Wahsh. 2014. "Pullulan Production from Aureobsidium Pullulans by Continuous Culture ." Basic Research J of Microbiology 1 (February): 11–15.

Hammami, Inès, Nadiyah M. Alabdallah, Amjad Al Jomaa, and Madiha Kamoun. 2021. "Gold Nanoparticles: Synthesis Properties and Applications." Journal of King Saud University - Science 33 (7): 101560. https://doi.org/10.1016/j.jksus.2021.101560.

Hayek, Ayman A. Al, Asirvatham A. Robert, Saleha Babli, Khuloud Almonea, and Mohamed A. Al Dawish. 2017. "Fear of Self-Injecting and Self-Testing and the Related Risk Factors in Adolescents

with Type 1 Diabetes: A Cross-Sectional Study." Diabetes Therapy 8 (1): 75–83. https://doi.org/10.1007/s13300-016-0221-8.

Hayek, Ayman A. Al, Asirvatham A. Robert, and Mohamed A. Al Dawish. 2017. "Evaluation of FreeStyle Libre Flash Glucose Monitoring System on Glycemic Control, Health-Related Quality of Life, and Fear of Hypoglycemia in Patients with Type 1 Diabetes." Clinical Medicine Insights: Endocrinology and Diabetes 10. https://doi.org/10.1177/1179551417746957.

Hernández-López, Alejandro, Daniel A. Sanchez Felix, Zenaida Zuñiga Sierra, Itzel García Bravo, Tzvetanka D. Dinkova, and Alma X. Avila-Alejandre. 2020. "Quantification of Reducing Sugars Based on the Qualitative Technique of Benedict." ACS Omega 5 (50): 32403–10. https://doi.org/10.1021/acsomega.0c04467.

Hirai, Hidefumi, and Noboru Yakura. 2001. "Protecting Polymers in Suspension of Metal Nanoparticles." Polymers for Advanced Technologies 12 (11–12): 724–33. https://doi.org/10.1002/pat.95.

Hu, Lianzhe, Yali Yuan, Ling Zhang, Jianming Zhao, Saadat Majeed, and Guobao Xu. 2013. "Copper Nanoclusters as Peroxidase Mimetics and Their Applications to H2O2 and Glucose Detection." Analytica Chimica Acta 762: 83–86. https://doi.org/10.1016/j.aca.2012.11.056.

I. Elzagheid, Mohamed. 2018. "Laboratory Activities to Introduce Carbohydrates Qualitative Analysis to College Students." World Journal of Chemical Education 6 (2): 82–86. https://doi.org/10.12691/wjce-6-2-1.

Iles, Alice H., Peijun J.W. He, Ioannis N. Katis, Panagiotis P. Galanis, Anto J.U.K. John, Paul Elkington, Robert W. Eason, and Collin L. Sones. 2022. "Semi-Quantitative Detection of Inflammatory Biomarkers Using a Laser-Patterned Multiplexed Lateral Flow Device." Talanta 237 (August 2021): 122944. https://doi.org/10.1016/j.talanta.2021.122944.

Jahanshahi-Anbuhi, Sana, Kevin Pennings, Vincent Leung, Meng Liu, Carmen Carrasquilla, Balamurali Kannan, Yingfu Li, Robert Pelton, John D. Brennan, and Carlos D.M. Filipe. 2014a. "Pullulan Encapsulation of Labile Biomolecules to Give Stable Bioassay Tablets." Angewandte Chemie - International Edition 53 (24): 6155–58. https://doi.org/10.1002/anie.201403222.

Jeevanandam, Jaison, Puja Patel, Kumar Ponnuchamy, Saikumar Manchala, Caleb Acquah, and Michael K. Danquah. 2022. "Biocatalytic Nanomaterials as an Alternative to Peroxidase Enzymes." In Nanomaterials for Biocatalysis, 513–42. Elsevier. https://doi.org/10.1016/B978-0-12-824436-4.00009-5.

Jiang, Cuifeng, Cong Zhang, Juan Song, Xiaojie Ji, and Wei Wang. 2021. "Cytidine-Gold Nanoclusters as Peroxidase Mimetic for Colorimetric Detection of Glutathione (GSH), Glutathione Disulfide (GSSG) and Glutathione Reductase (GR)." Spectrochimica Acta. Part A, Molecular and Biomolecular Spectroscopy 250 (April): 119316. https://doi.org/10.1016/j.saa.2020.119316.

Jiang, Cuifeng, Jing Zhu, Zhao Li, Juhua Luo, Jinshan Wang, and Yu Sun. 2017a. "Chitosan-Gold Nanoparticles as Peroxidase Mimic and Their Application in Glucose Detection in Serum." RSC Advances 7 (70): 44463–69. https://doi.org/10.1039/c7ra08967h.

Jiang, Yinghua, Ning Liu, Jinrui Han, Yadan Li, Pierce Spencer, Samuel J. Vodovoz, Ming Ming Ning, et al. 2021. "Diabetes Mellitus/Poststroke Hyperglycemia: A Detrimental Factor for TPA Thrombolytic Stroke Therapy." Translational Stroke Research 12 (3): 416–27. https://doi.org/10.1007/s12975-020-00872-3.

Jin, Shunru, Cui Wu, Zunzhong Ye, and Yibin Ying. 2019. "Designed Inorganic Nanomaterials for Intrinsic Peroxidase Mimics: A Review." Sensors and Actuators, B: Chemical 283 (November 2018): 18–34. https://doi.org/10.1016/j.snb.2018.10.040.

Jing, Wenjie, Fanbo Kong, Sijia Tian, Mincong Yu, Yunchao Li, Louzhen Fan, and Xiaohong Li. 2021. "Glucose Oxidase Decorated Fluorescent Metal-Organic Frameworks as Biomimetic Cascade Nanozymes for Glucose Detection through the Inner Filter Effect." Analyst 146 (13): 4188–94. https://doi.org/10.1039/d1an00847a.

Johnston, Lucy, Gonglei Wang, Kunhui Hu, Chungen Qian, and Guozhen Liu. 2021. "Advances in Biosensors for Continuous Glucose Monitoring Towards Wearables." Frontiers in Bioengineering and Biotechnology 9 (August). https://doi.org/10.3389/fbioe.2021.733810.

Jurysta, Cedric, Nurdan Bulur, Berrin Oguzhan, Ilhan Satman, Temel M. Yilmaz, Willy J. Malaisse, and Abdullah Sener. 2009. "Salivary Glucose Concentration and Excretion in Normal and Diabetic Subjects." Journal of Biomedicine & Biotechnology 2009: 430426. https://doi.org/10.1155/2009/430426.

Kalhor, Hamid R., and Amin Yahyazadeh. 2019. "Investigating the Effects of Amino Acid-Based Surface Modification of Carbon Nanoparticles on the Kinetics of Insulin Amyloid Formation." Colloids and Surfaces B: Biointerfaces 176 (April): 471–79. https://doi.org/10.1016/j.colsurfb.2019.01.033.

Kalra, Sanjay, Biranchi Narayan Jena, and Rajiv Yeravdekar. 2018. "Emotional and Psychological Needs of People with Diabetes." Indian Journal of Endocrinology and Metabolism 22 (5): 696–704. https://doi.org/10.4103/ijem.IJEM_579_17.

Kap, Özlem, Volkan Kılıç, John G. Hardy, and Nesrin Horzum. 2021. "Smartphone-Based Colorimetric Detection Systems for Glucose Monitoring in the Diagnosis and Management of Diabetes." Analyst 146 (9): 2784–2806. https://doi.org/10.1039/d0an02031a.

Khor, Sook Mei, Joonhwa Choi, Phillip Won, and Seung Hwan Ko. 2022. "Challenges and Strategies in Developing an Enzymatic Wearable Sweat Glucose Biosensor as a Practical Point-Of-Care Monitoring Tool for Type II Diabetes." Nanomaterials 12 (2). https://doi.org/10.3390/nano12020221.

Kim, Jayoung, Alan S. Campbell, Berta Esteban Fernández de Ávila, and Joseph Wang. 2019. "Wearable Biosensors for Healthcare Monitoring." Nature Biotechnology 37 (4): 389–406. https://doi.org/10.1038/s41587-019-0045-y.

Kim, Yejin, and Dong Hee Na. 2019. "Simultaneous Determination of Cysteamine and Cystamine in Cosmetics by Ion-Pairing Reversed-Phase High-Performance Liquid Chromatography." Toxicological Research 35 (2): 161–65. https://doi.org/10.5487/TR.2019.35.2.161.

Kimling, J., M. Maier, B. Okenve, V. Kotaidis, H. Ballot, and A. Plech. 2006. "Turkevich Method for Gold Nanoparticle Synthesis Revisited." Journal of Physical Chemistry B 110 (32): 15700–707. https://doi.org/10.1021/jp061667w.

Knill, Charles J., and John F. Kennedy. 2002. "Degradation of Cellulose under Alkaline Conditions." Carbohydrate Polymers 51 (3): 281–300. https://doi.org/10.1016/S0144-8617(02)00183-2.

Konar, Suraj, B. N.Prashanth Kumar, Madhusudan Kr Mahto, Dipanjan Samanta, Md Abdus Salam Shaik, Manisha Shaw, Mahitosh Mandal, and Amita Pathak. 2019. "N-Doped Carbon Dot as

Fluorescent Probe for Detection of Cysteamine and Multicolor Cell Imaging." Sensors and Actuators, B: Chemical 286 (May): 77–85. https://doi.org/10.1016/j.snb.2019.01.117.

Laksee, Sakchai, Songchan Puthong, Thapong Teerawatananond, Tanapat Palaga, and Nongnuj Muangsin. 2017a. "Highly Efficient and Facile Fabrication of Monodispersed Au Nanoparticles Using Pullulan and Their Application as Anticancer Drug Carriers." Carbohydrate Polymers 173: 178–91. https://doi.org/10.1016/j.carbpol.2017.05.101.

Lan, Jianming, Wenming Xu, Qiping Wan, Xi Zhang, Jia Lin, Jinghua Chen, and Jianzhong Chen. 2014. "Colorimetric Determination of Sarcosine in Urine Samples of Prostatic Carcinoma by Mimic Enzyme Palladium Nanoparticles." Analytica Chimica Acta 825: 63–68. https://doi.org/10.1016/j.aca.2014.03.040.

Lee, Kar Xin, Kamyar Shameli, Yen Pin Yew, Sin-Yeang Teow, Hossein Jahangirian, Roshanak Rafiee-Moghaddam, and Thomas J. Webster. 2020. "Recent Developments in the Facile Bio-Synthesis of Gold Nanoparticles (AuNPs) and Their Biomedical Applications." International Journal of Nanomedicine 15: 275–300. https://doi.org/10.2147/IJN.S233789.

Lépinay, Sandrine, Khémara Kham, Marie Claude Millot, and Benjamin Carbonnier. 2012. "In-Situ Polymerized Molecularly Imprinted Polymeric Thin Films Used as Sensing Layers in Surface Plasmon Resonance Sensors: Mini-Review Focused on 2010-2011." Chemical Papers. https://doi.org/10.2478/s11696-012-0134-6.

Li, Fan, Tianshuang He, Sihao Wu, Zoujun Peng, Ping Qiu, and Xiaomin Tang. 2021. "Visual and Colorimetric Detection of Uric Acid in Human Serum and Urine Using Chitosan Stabilized Gold Nanoparticles." Microchemical Journal 164 (November 2020): 105987. https://doi.org/10.1016/j.microc.2021.105987.

Li, Li, and Baoxin Li. 2009. "Sensitive and Selective Detection of Cysteine Using Gold Nanoparticles as Colorimetric Probes." The Analyst 134 (7): 1361–65. https://doi.org/10.1039/b819842j.

Li, Rong Sheng, Hai Liu, Bin Bin Chen, Hong Zhi Zhang, Cheng Zhi Huang, and Jian Wang. 2016a. "Stable Gold Nanoparticles as a Novel Peroxidase Mimic for Colorimetric Detection of Cysteine." Analytical Methods 8 (11): 2494–2501. https://doi.org/10.1039/c6ay00367b.

Li, Wei, Xing Zhi, Jingjing Yang, Jinli Zhang, and Yan Fu. 2016. "Colorimetric Detection of Cysteine and Homocysteine Based on an Oligonucleotide-Stabilized Pd Nanozyme." Analytical Methods 8 (25): 5111–16. https://doi.org/10.1039/c6ay01097k.

Liang, Ling, Yuhao Xiong, Yan Duan, Weiyuan Zuo, Li Liu, Fanggui Ye, and Shulin Zhao. 2022. "Colorimetric Detection of Creatinine Based on Specifically Modulating the Peroxidase-Mimicking Activity of Cu-Fenton System." Biosensors and Bioelectronics 206 (January): 114121. https://doi.org/10.1016/j.bios.2022.114121.

Lien, Chia Wen, Ying Chieh Chen, Huan Tsung Chang, and Chih Ching Huang. 2013. "Logical Regulation of the Enzyme-like Activity of Gold Nanoparticles by Using Heavy Metal Ions." Nanoscale 5 (17): 8227–34. https://doi.org/10.1039/c3nr01836a.

Lin, Yu Li, I. Chen Chang, Hung Hsiang Liou, Chih Hsien Wang, Yu Hsien Lai, Chiu Huang Kuo, and Bang Gee Hsu. 2021. "Serum Indices Based on Creatinine and Cystatin C Predict Mortality in Patients with Non-Dialysis Chronic Kidney Disease." Scientific Reports 11 (1): 1–10. https://doi.org/10.1038/s41598-021-96447-9.

Liu, Chengcheng, Yongjie Sheng, Yanhong Sun, Junkui Feng, Shijin Wang, Jin Zhang, Jiacui Xu, and Dazhi Jiang. 2015. "A Glucose Oxidase-Coupled DNAzyme Sensor for Glucose Detection in Tears and Saliva." Biosensors and Bioelectronics 70: 455–61. https://doi.org/10.1016/j.bios.2015.03.070.

Liu, Songqin, Dónal Leech, and Huangxian Ju. 2003. "Application of Colloidal Gold in Protein Immobilization, Electron Transfer, and Biosensing." Analytical Letters 36 (1): 1–19. https://doi.org/10.1081/AL-120017740.

Liu, Yan, Yinping Xiang, Ding Ding, and Rong Guo. 2016. "Structural Effects of Amphiphilic Protein/Gold Nanoparticle Hybrid Based Nanozyme on Peroxidase-like Activity and Silver-Mediated Inhibition." RSC Advances 6 (113): 112435–44. https://doi.org/10.1039/C6RA23773H.

Liu, Yanping, Cunwen Wang, Ning Cai, Sihui Long, and Faquan Yu. 2014. "Negatively Charged Gold Nanoparticles as an Intrinsic Peroxidase Mimic and Their Applications in the Oxidation of Dopamine." Journal of Materials Science 49 (20): 7143–50. https://doi.org/10.1007/s10853-014-8422-x.

Liu, Yingshuai, Lingli Lei, and Zeying Zhang. 2017. "An Ultrasensitive Colorimetric Immunoassay Based on Glucose Oxidase Catalyzed Cascade Formation of Blue–Black Iodine–Starch Complex." Sensors and Actuators, B: Chemical 248: 195–200. https://doi.org/10.1016/j.snb.2017.03.142.

Liu, Yuanjun, Guoxing Zhu, Jing Yang, Aihua Yuan, and Xiaoping Shen. 2014. "Peroxidase-like Catalytic Activity of Ag3PO4 Nanocrystals Prepared by a Colloidal Route." PLoS ONE 9 (10): 3–9. https://doi.org/10.1371/journal.pone.0109158.

Liyanage, Piyumi, Pabudi Weerathunge, Mandeep Singh, Vipul Bansal, and Rajesh Ramanathan. 2021. "L-Cysteine as an Irreversible Inhibitor of the Peroxidase-Mimic Catalytic Activity of 2-Dimensional Ni-Based Nanozymes." Nanomaterials 11 (5): 1285. https://doi.org/10.3390/nano11051285.

Luís, Ângelo, Ana Ramos, and Fernanda Domingues. 2020. "Pullulan Films Containing Rockrose Essential Oil for Potential Food Packaging Applications." Antibiotics 9 (10): 1–20. https://doi.org/10.3390/antibiotics9100681.

Lv, Jie, Shuangling Wang, Cong Zhang, Yulong Lin, Yan Fu, and Meng Li. 2020. "ATP Induced Alteration in the Peroxidase-like Properties of Hollow Prussian Blue Nanocubes: A Platform for Alkaline Phosphatase Detection." Analyst 145 (14): 5032–40. https://doi.org/10.1039/d0an00405g.

Machida, Masato, Yurika Tokudome, Akihide Maeda, Tetsuya Sato, Hiroshi Yoshida, Junya Ohyama, Kenji Fujii, and Naoya Ishikawa. 2022. "A Comparative Study of Various Transition Metal Overlayer Catalysts for Low-Temperature NH3 Oxidation under Dry and Wet Conditions." Catalysis Today 384–386 (June 2021): 70–75. https://doi.org/10.1016/j.cattod.2021.06.023.

Maji, Swarup Kumar, Amit Kumar Dutta, Supriya Dutta, Divesh N. Srivastava, Parimal Paul, Anup Mondal, and Bibhutosh Adhikary. 2012. "Single-Source Precursor Approach for the Preparation of CdS Nanoparticles and Their Photocatalytic and Intrinsic Peroxidase like Activity." Applied Catalysis B: Environmental 126: 265–74. https://doi.org/10.1016/j.apcatb.2012.07.005.

Marin, Marco, Maria Vesna Nikolic, and Jasmina Vidic. 2021. "Rapid Point-of-Need Detection of Bacteria and Their Toxins in Food Using Gold Nanoparticles." Comprehensive Reviews in Food Science and Food Safety 20 (6): 5880–5900. https://doi.org/10.1111/1541-4337.12839.

Naveen Prasad, Sanjana, Pabudi Weerathunge, Md Nurul Karim, Samuel Anderson, Sabeen Hashmi, Pyria D. Mariathomas, Vipul Bansal, and Rajesh Ramanathan. 2021. "Non-Invasive Detection of Glucose in Human Urine Using a Color-Generating Copper NanoZyme." Analytical and Bioanalytical Chemistry 413 (5): 1279–91. https://doi.org/10.1007/s00216-020-03090-w.

Ng, James S., and Michinao Hashimoto. 2020. "Fabrication of Paper Microfluidic Devices Using a Toner Laser Printer." RSC Advances 10 (50): 29797–807. https://doi.org/10.1039/d0ra04301j.

Ogony, Joshua, Suneetha Mare, Wei Wu, and Nuran Ercal. 2006. "High Performance Liquid Chromatography Analysis of 2-Mercaptoethylamine (Cysteamine) in Biological Samples by Derivatization with N-(1-Pyrenyl) Maleimide (NPM) Using Fluorescence Detection." Journal of Chromatography B: Analytical Technologies in the Biomedical and Life Sciences 843 (1): 57–62. https://doi.org/10.1016/j.jchromb.2006.05.027.

Orenius, Tage, LicPsych, Hanna Säilä, Katriina Mikola, and Leena Ristolainen. 2018. "Fear of Injections and Needle Phobia Among Children and Adolescents: An Overview of Psychological, Behavioral, and Contextual Factors." SAGE Open Nursing 4: 1–8. https://doi.org/10.1177/2377960818759442.

Oyewunmi, Oyejide Damilola, Seyed Hamid Safiabadi-Tali, and Sana Jahanshahi-Anbuhi. 2020. "Dual-Modal Assay Kit for the Qualitative and Quantitative Determination of the Total Water Hardness Using a Permanent Marker Fabricated Microfluidic Paper-Based Analytical Device." Chemosensors 8 (4): 97. https://doi.org/10.3390/chemosensors8040097.

Packard, Chris, M. John Chapman, Mahendra Sibartie, Ulrich Laufs, and Luis Masana. 2021. "Intensive Low-Density Lipoprotein Cholesterol Lowering in Cardiovascular Disease Prevention: Opportunities and Challenges." Heart 107 (17): 1369–75. https://doi.org/10.1136/heartjnl-2020-318760.

Pan, Xihao, Siyao Cheng, Cheng Zhang, Yingzhi Jiao, Xiangpeng Lin, Wei Dong, and Xiaoliang Qi. 2021. "Mussel-Inspired Magnetic Pullulan Hydrogels for Enhancing Catalytic Degradation of Antibiotics from Biomedical Wastewater." Chemical Engineering Journal 409 (September 2020): 128203. https://doi.org/10.1016/j.cej.2020.128203.

Pasomsub, E., S. P. Watcharananan, K. Boonyawat, P. Janchompoo, G. Wongtabtim, W. Suksuwan, S. Sungkanuparph, and A. Phuphuakrat. 2021. "Saliva Sample as a Non-Invasive Specimen for the Diagnosis of Coronavirus Disease 2019: A Cross-Sectional Study." Clinical Microbiology and Infection 27 (2): 285.e1-285.e4. https://doi.org/10.1016/j.cmi.2020.05.001.

Pezhhan, Hamzeh, Morteza Akhond, and Mojtaba Shamsipur. 2020a. "Histidine Capped-Gold Nanoclusters Mediated Fluorescence Detection of Glucose and Hydrogen Peroxide Based on Glucose Oxidase-Mimicking Property of Gold Nanoparticles via an Inner Filter Effect Mechanism." Journal of Luminescence 228 (July): 117604. https://doi.org/10.1016/j.jlumin.2020.117604.

Piani, Federica, Arrigo F.G. Cicero, and Claudio Borghi. 2021. "Uric Acid and Hypertension: Prognostic Role and Guide for Treatment." Journal of Clinical Medicine 10 (3): 1–15. https://doi.org/10.3390/jcm10030448.

Prajapati, Vipul D., Girish K. Jani, and Simin M. Khanda. 2013. "Pullulan: An Exopolysaccharide and Its Various Applications." Carbohydrate Polymers 95 (1): 540–49. https://doi.org/10.1016/j.carbpol.2013.02.082.

Prasad, P., G. S. Guru, H. R. Shivakumar, and K. Sheshappa Rai. 2012. "Investigation on Miscibility of Sodium Alginate/Pullulan Blends." Journal of Polymers and the Environment 20 (3): 887–93. https://doi.org/10.1007/s10924-012-0427-4.

Purwidyantri, Agnes, Ya Chung Tian, Gardin Muhammad Andika Saputra, Briliant Adhi Prabowo, Hui Ling Liu, Chia Ming Yang, and Chao Sung Lai. 2021. "Gold Nanoframe Array Electrode for Straightforward Detection of Hydrogen Peroxide." Chemosensors 9 (2): 1–13. https://doi.org/10.3390/chemosensors9020037.

Qiao, Juan, and Li Qi. 2021. "Recent Progress in Plant-Gold Nanoparticles Fabrication Methods and Bio-Applications." Talanta 223 (Pt 2): 121396. https://doi.org/10.1016/j.talanta.2020.121396.

Qin, Xiaoxiao, Jiajing Liu, Zhong Zhang, Jinhua Li, Li Yuan, Zhiyang Zhang, and Lingxin Chen. 2021. "Microfluidic Paper-Based Chips in Rapid Detection: Current Status, Challenges, and Perspectives." TrAC - Trends in Analytical Chemistry 143: 116371. https://doi.org/10.1016/j.trac.2021.116371.

Qiu, Yunfeng, Zhuo Ma, and Pingan Hu. 2014. "Environmentally Benign Magnetic Chitosan/Fe3O4 Composites as Reductant and Stabilizer for Anchoring Au NPs and Their Catalytic Reduction of 4-Nitrophenol." Journal of Materials Chemistry A 2 (33): 13471–78. https://doi.org/10.1039/c4ta02268h.

Rahman, Md Aminur, Pankaj Kumar, Deog Su Park, and Yoon Bo Shim. 2008. "Electrochemical Sensors Based on Organic Conjugated Polymers." Sensors 8 (1): 118–41. https://doi.org/10.3390/s8010118.

Ramasamy, Mohankandhasamy, Jin-Hyung Lee, and Jintae Lee. 2017. "Direct One-Pot Synthesis of Cinnamaldehyde Immobilized on Gold Nanoparticles and Their Antibiofilm Properties." Colloids and Surfaces. B, Biointerfaces 160 (December): 639–48. https://doi.org/10.1016/j.colsurfb.2017.10.018.

Raoof, Jahan Bakhsh, Reza Ojani, and Fereshteh Chekin. 2009. "Immobilization of 1,2-Naphthoquinone-4-Sulfonic Acid on Gold Electrode: Application for Cysteamine Detection Using Michael Addition." Journal of Materials Science 44 (10): 2688–93. https://doi.org/10.1007/s10853-009-3352-8.

Raveendran, Sindhu, Binod Parameswaran, Sabeela Beevi Ummalyma, Amith Abraham, Anil Kuruvilla Mathew, Aravind Madhavan, Sharrel Rebello, and Ashok Pandey. 2018. "Applications of Microbial Enzymes in Food Industry." Food Technology and Biotechnology 56 (1): 16–30. https://doi.org/10.17113/ftb.56.01.18.5491.

Ravikumar, Dhanalakshmi, Pratibha Ramani, and R. Gayathri. 2021. "Estimation of Salivary PH, Viscosity, Flow Rate in Children with and without Early Childhood Caries – an Observational Study." Journal of Pharmaceutical Research International 33: 54–60. https://doi.org/10.9734/jpri/2021/v33i30a31614.

Ren, Mingguang, Dejun Dong, Qingyu Xu, Jingfen Yin, Shoujuan Wang, and Fangong Kong. 2021. "A Biotin-Guided Two-Photon Fluorescent Probe for Detection of Hydrogen Peroxide in Cancer Cells Ferroptosis Process." Talanta 234 (April): 122684. https://doi.org/10.1016/j.talanta.2021.122684.

Reuveni, Shlomi, Michael Urbakh, and Joseph Klafter. 2014. "Role of Substrate Unbinding in Michaelis-Menten Enzymatic Reactions." Proceedings of the National Academy of Sciences of the United States of America 111 (12): 4391–96. https://doi.org/10.1073/pnas.1318122111.

Robinson, Savarimuthu, and Nagaraj Dhanlaksmi. 2017. "Photonic Crystal Based Biosensor for the Detection of Glucose Concentration in Urine." Photonic Sensors 7 (1): 11–19. https://doi.org/10.1007/s13320-016-0347-3.

Roper, D. Keith, W. Ahn, and M. Hoepfner. 2007. "Microscale Heat Transfer Transduced by Surface Plasmon Resonant Gold Nanoparticles." Journal of Physical Chemistry C 111 (9): 3636–41. https://doi.org/10.1021/jp064341w.

Rossini, Eduardo Luiz, Maria Izabel Milani, Liliane Spazzapam Lima, and Helena Redigolo Pezza. 2021. "Paper Microfluidic Device Using Carbon Dots to Detect Glucose and Lactate in Saliva Samples." Spectrochimica Acta. Part A, Molecular and Biomolecular Spectroscopy 248 (March): 119285. https://doi.org/10.1016/j.saa.2020.119285.

Rotureau, E., E. Dellacherie, and A. Durand. 2006. "Viscosity of Aqueous Solutions of Polysaccharides and Hydrophobically Modified Polysaccharides: Application of Fedors Equation." European Polymer Journal 42 (5): 1086–92. https://doi.org/10.1016/j.eurpolymj.2005.11.019.

Sadiq, Zubi, Seyed Hamid Safiabadi Tali, Hasti Hajimiri, Muna Al-Kassawneh, and Sana Jahanshahi-Anbuhi. 2023. "Gold Nanoparticles-Based Colorimetric Assays for Environmental Monitoring and Food Safety Evaluation." Critical Reviews in Analytical Chemistry, January, 1–36. https://doi.org/10.1080/10408347.2022.2162331.

Sadiq, Zubi, Seyed Hamid Safiabadi Tali, and Sana Jahanshahi-Anbuhi. 2022. "Gold Tablets: Gold Nanoparticles Encapsulated into Dextran Tablets and Their PH-Responsive Behavior as an Easy-to-Use Platform for Multipurpose Applications." ACS Omega 7 (13): 11177–89. https://doi.org/10.1021/acsomega.1c07393.

Sasikumar, Thangarasu, and Malaichamy Ilanchelian. 2020. "A Simple Assay for Direct Visual and Colorimetric Sensing Application of Cysteamine Using Au@Ag Core-Shell Nanoparticles." Optical Materials 109 (November): 110237. https://doi.org/10.1016/j.optmat.2020.110237.

Say, Zafer, Melike Kaya, Çağıl Kaderoğlu, Yusuf Koçak, Kerem Emre Ercan, Abel Tetteh Sika-Nartey, Ahsan Jalal, et al. 2022. "Unraveling Molecular Fingerprints of Catalytic Sulfur Poisoning at the Nanometer Scale with Near-Field Infrared Spectroscopy." Journal of the American Chemical Society 144 (19): 8848–60. https://doi.org/10.1021/jacs.2c03088.

Sellami, Kheireddine, Annabelle Couvert, Noureddine Nasrallah, Rachida Maachi, Mahmoud Abouseoud, and Abdeltif Amrane. 2022. "Peroxidase Enzymes as Green Catalysts for Bioremediation and Biotechnological Applications: A Review." Science of the Total Environment 806: 150500. https://doi.org/10.1016/j.scitotenv.2021.150500.

Serafín, V., P. Hernández, L. Agüí, P. Yáñez-Sedeño, and J. M. Pingarrón. 2013. "Electrochemical Biosensor for Creatinine Based on the Immobilization of Creatininase, Creatinase and Sarcosine Oxidase onto a Ferrocene/Horseradish Peroxidase/Gold Nanoparticles/Multi-Walled Carbon Nanotubes/Teflon Composite Electrode." Electrochimica Acta 97: 175–83. https://doi.org/10.1016/j.electacta.2013.03.005.

Shabnam, Taheriniya, and Zahra Behboodi. 2016. "Comparing Green Chemical Methods and Chemical Methods for The." International Journal of Pharmaceutical Sciences and Research 7 (12): 4927–32. https://doi.org/10.13040/IJPSR.0975-8232.7(12).4927-32.

Shah, Monic, Vivek Badwaik, Yogesh Kherde, Hitesh Kumar Waghwani, Tulsi Modi, and Zoraida P Aguilar. 2014. "Table of Contents 1.," no. 8: 1320–44.

Shivakumar, Anantharaman, Jashmitha BG, and Dhruvaraj MR. 2017. "Role of Peroxidase in Clinical Assays: A Short Review." Journal of Clinical Nutrition & Dietetics 03 (02): 1–7. https://doi.org/10.4172/2472-1921.100048.

Shu, Tong, Lei Su, Jianxing Wang, Chenzhong Li, and Xueji Zhang. 2015. "Chemical Etching of Bovine Serum Albumin-Protected Au25 Nanoclusters for Label-Free and Separation-Free Detection of Cysteamine." Biosensors and Bioelectronics 66 (April): 155–61. https://doi.org/10.1016/j.bios.2014.10.073.

Singh, Gagandeep, Deepak Bains, Harupjit Singh, Navneet Kaur, and Narinder Singh. 2019. "Polydentate Aromatic Nanoparticles Complexed with Cu2+ for the Detection of Cysteamine Using a Smartphone as a Portable Diagnostic Tool." ACS Applied Nano Materials 2 (9): 5841–49. https://doi.org/10.1021/acsanm.9b01297.

Song, Yujun, Konggang Qu, Chao Zhao, Jinsong Ren, and Xiaogang Qu. 2010. "Graphene Oxide: Intrinsic Peroxidase Catalytic Activity and Its Application to Glucose Detection." Advanced Materials 22 (19): 2206–10. https://doi.org/10.1002/adma.200903783.

Stachowicz, M, B Lehmann, A Tibi, P Prognon, V Daurat, and D Pradeau. 1998a. "Determination of Total Cysteamine in Human Serum by a High-Performance Liquid Chromatography with Fluorescence Detection." Journal of Pharmaceutical and Biomedical Analysis. Vol. 17. Journal of Pharmaceutical and Biomedical Analyses.

Sun, Jingwei, Yuexiang Lu, Liuying He, Jiawei Pang, Fengyi Yang, and Yueying Liu. 2020a. "Colorimetric Sensor Array Based on Gold Nanoparticles: Design Principles and Recent Advances." TrAC - Trends in Analytical Chemistry 122: 115754. https://doi.org/10.1016/j.trac.2019.115754.

Tang, Junqi, Xuewen Fu, Quanhong Ou, Kunpeng Gao, Shi Qing Man, Jie Guo, and Yingkai Liu. 2018. "Hydroxide Assisted Synthesis of Monodisperse and Biocompatible Gold Nanoparticles with Dextran." Materials Science and Engineering C 93 (November 2017): 759–67. https://doi.org/10.1016/j.msec.2018.08.045.

Tang, Junqi, Kunpeng Gao, Quanhong Ou, Xuewen Fu, Shi-Qing Man, Jie Guo, and Yingkai Liu. 2018. "Calculation Extinction Cross Sections and Molar Attenuation Coefficient of Small Gold Nanoparticles and Experimental Observation of Their UV–Vis Spectral Properties." Spectrochimica Acta Part A: Molecular and Biomolecular Spectroscopy 191 (February): 513–20. https://doi.org/10.1016/j.saa.2017.10.047.

Tao, Zhimin, Ryan A. Raffel, Abdul Kader Souid, and Jerry Goodisman. 2009. "Kinetic Studies on Enzyme-Catalyzed Reactions: Oxidation of Glucose, Decomposition of Hydrogen Peroxide and Their Combination." Biophysical Journal 96 (7): 2977–88. https://doi.org/10.1016/j.bpj.2008.11.071.

Tian, Kun, Saji Alex, Gene Siegel, and Ashutosh Tiwari. 2015. "Enzymatic Glucose Sensor Based on Au Nanoparticle and Plant-like ZnO Film Modified Electrode." Materials Science and Engineering C 46: 548–52. https://doi.org/10.1016/j.msec.2014.10.064.

Treuel, Lennart, Marcelina Malissek, Stefan Grass, Jörg Diendorf, Dirk Mahl, Wolfgang Meyer-Zaika, and Matthias Epple. 2012. "Quantifying the Influence of Polymer Coatings on the Serum Albumin

Corona Formation around Silver and Gold Nanoparticles." Journal of Nanoparticle Research 14 (9): 1102. https://doi.org/10.1007/s11051-012-1102-3.

Tseng, Chao Wei, Hsiang Yu Chang, Jia Yaw Chang, and Chih Ching Huang. 2012. "Detection of Mercury Ions Based on Mercury-Induced Switching of Enzyme-like Activity of Platinum/Gold Nanoparticles." Nanoscale 4 (21): 6823–30. https://doi.org/10.1039/c2nr31716h.

Uryupina, O. Ya, V. V. Vysotskii, V. V. Matveev, A. V. Gusel'nikova, and V. I. Roldughin. 2011. "Production of Gold Nanoparticles in Aqueous Solutions of Cellulose Derivatives." Colloid Journal 73 (4): 551–56. https://doi.org/10.1134/S1061933X1103015X.

Vallabani, N. V.Srikanth, Ajay S. Karakoti, and Sanjay Singh. 2017. "ATP-Mediated Intrinsic Peroxidase-like Activity of Fe3O4-Based Nanozyme: One Step Detection of Blood Glucose at Physiological PH." Colloids and Surfaces B: Biointerfaces 153 (May): 52–60. https://doi.org/10.1016/j.colsurfb.2017.02.004.

Walther, Raoul, Anna K. Winther, Anne Sofie Fruergaard, Wouter van den Akker, Lise Sørensen, Signe Maria Nielsen, Morten T. Jarlstad Olesen, et al. 2019. "Identification and Directed Development of Non-Organic Catalysts with Apparent Pan-Enzymatic Mimicry into Nanozymes for Efficient Prodrug Conversion." Angewandte Chemie 131 (1): 284–88. https://doi.org/10.1002/ange.201812668.

Wang, Junjun, Lin Xu, Yang Lu, Kuang Sheng, Wei Liu, Cong Chen, Yang Li, Biao Dong, and Hongwei Song. 2016. "Engineered IrO2@NiO Core∑shell Nanowires for Sensitive Nonenzymatic Detection of Trace Glucose in Saliva." Analytical Chemistry 88 (24): 12346–53. https://doi.org/10.1021/acs.analchem.6b03558.

Wang, Sheng, Wei Chen, Ai-Lin Liu, Lei Hong, Hao-Hua Deng, and Xin-Hua Lin. 2012. "Comparison of the Peroxidase-Like Activity of Unmodified, Amino-Modified, and Citrate-Capped Gold Nanoparticles." ChemPhysChem 13 (5): 1199–1204. https://doi.org/10.1002/cphc.201100906.

Wang, Yuedan, Xing Qing, Quan Zhou, Yang Zhang, Qiongzhen Liu, Ke Liu, Wenwen Wang, et al. 2017. "The Woven Fiber Organic Electrochemical Transistors Based on Polypyrrole Nanowires/Reduced Graphene Oxide Composites for Glucose Sensing." Biosensors and Bioelectronics 95 (April): 138–45. https://doi.org/10.1016/j.bios.2017.04.018.

Wei, Ting-Yen, Yun Fu, Kuo-Hsuan Chang, Kun-Ju Lin, Yu-Jen Lu, and Chao-Min Cheng. 2018. "Point-of-Care Devices Using Disease Biomarkers To Diagnose Neurodegenerative Disorders." Trends in Biotechnology 36 (3): 290–303. https://doi.org/10.1016/j.tibtech.2017.11.004.

Wei, Yong Feng, Xuan Wang, Wen Jing Shi, Ru Chen, Liyao Zheng, Zi Zhou Wang, Kun Chen, and Liqian Gao. 2021. "A Novel Methylenemalononitrile-BODIPY-Based Fluorescent Probe for Highly Selective Detection of Hydrogen Peroxide in Living Cells." European Journal of Medicinal Chemistry 226: 113828. https://doi.org/10.1016/j.ejmech.2021.113828.

Wood, Paul L., M. Amin Khan, and Joseph R. Moskal. 2008. "Mechanism of Action of the Disease-Modifying Anti-Arthritic Thiol Agents d-Penicillamine and Sodium Aurothiomalate: Restoration of Cellular Free Thiols and Sequestration of Reactive Aldehydes." European Journal of Pharmacology 580 (1–2): 48–54. https://doi.org/10.1016/j.ejphar.2007.10.066.

World Health Organization. 2016. "Global Report on Adult Learning Executive Summary." World Organization Health, 3.

Wu, Jiangjiexing, Xiaoyu Wang, Quan Wang, Zhangping Lou, Sirong Li, Yunyao Zhu, Li Qin, and Hui Wei. 2019a. "Nanomaterials with Enzyme-like Characteristics (Nanozymes): Next-Generation Artificial Enzymes (II)." Chemical Society Reviews 48 (4): 1004–76. https://doi.org/10.1039/c8cs00457a.

Wu, Ying, Lihua He, and Hejun Zhou. 2022. "Preparation of Hydrophobically Modified Carboxylated Pullulan Nanoparticles for Evaluating the Effect of Hydrophobic Substitution on the Properties and Functions of Nanoparticles." Materials Technology 37 (10): 1467–77. https://doi.org/10.1080/10667857.2021.1956230.

Xiao, Hua Ming, Xian Wang, Quan Lan Liao, Shuai Zhao, Wei Hua Huang, and Yu Qi Feng. 2019. "Sensitive Analysis of Multiple Low-Molecular-Weight Thiols in a Single Human Cervical Cancer Cell by Chemical Derivatization-Liquid Chromatography-Mass Spectrometry." Analyst 144 (22): 6578–85. https://doi.org/10.1039/c9an01566c.

Yan, Zhengquan, Hua Yuan, Qi Zhao, Lin Xing, Xiaoyu Zheng, Weiguo Wang, Yulei Zhao, Yang Yu, Lei Hu, and Wenli Yao. 2020. "Recent Developments of Nanoenzyme-Based Colorimetric Sensors for Heavy Metal Detection and the Interaction Mechanism." The Analyst 145 (9): 3173–87. https://doi.org/10.1039/D0AN00339E.

Yang, Jiapei, Lei Wang, Yue Su, Lingyue Shen, Xihui Gao, Leilei Shi, and Xinyuan Zhu. 2022. "Color-Convertible Fluorescent Nanoprobe for Parkinson's Disease Diagnosis." Chemical Engineering Journal 429 (August 2021): 132368. https://doi.org/10.1016/j.cej.2021.132368.

Yang, Ya Chun, and Wei Lung Tseng. 2016. "1,4-Benzenediboronic-Acid-Induced Aggregation of Gold Nanoparticles: Application to Hydrogen Peroxide Detection and Biotin-Avidin-Mediated Immunoassay with Naked-Eye Detection." Analytical Chemistry 88 (10): 5355–62. https://doi.org/10.1021/acs.analchem.6b00668.

Ying, Shuaixuan, Zhenru Guan, Polycarp C. Ofoegbu, Preston Clubb, Cyren Rico, Feng He, and Jie Hong. 2022. "Green Synthesis of Nanoparticles: Current Developments and Limitations." Environmental Technology & Innovation 26 (May): 102336. https://doi.org/10.1016/j.eti.2022.102336.

Yu, Dan, Gundeep Kaur, Robert M. Blumenthal, Xing Zhang, and Xiaodong Cheng. 2021. "Enzymatic Characterization of Three Human RNA Adenosine Methyltransferases Reveals Diverse Substrate Affinities and Reaction Optima." Journal of Biological Chemistry 296 (motif IV): 100270. https://doi.org/10.1016/j.jbc.2021.100270.

Yu, Lihong, Yuehong Pang, Zhenglian Mo, Yuying Huang, and Xiaofang Shen. 2021. "Coordination Array for Accurate Colorimetric Sensing of Multiple Heavy Metal Ions." Talanta 231 (January): 122357. https://doi.org/10.1016/j.talanta.2021.122357.

Yuan, Yawen, Yishi Wang, Hua Wang, and Shifeng Hou. 2019. "Gold Nanoparticles Decorated on Single Layer Graphene Applied for Electrochemical Ultrasensitive Glucose Biosensor." Journal of Electroanalytical Chemistry 855 (November 2018): 113495. https://doi.org/10.1016/j.jelechem.2019.113495.

Zafar, Hima, Asma Channa, Varun Jeoti, and Goran M. Stojanović. 2022. "Comprehensive Review on Wearable Sweat-Glucose Sensors for Continuous Glucose Monitoring." Sensors 22 (2): 1–35. https://doi.org/10.3390/s22020638.

Zhang, Hua, Xiaotong Li, Qunyan Zhu, and Zhenxin Wang. 2022. “The Recent Development of Nanomaterials Enhanced Paper-Based Electrochemical Analytical Devices.” Journal of Electroanalytical Chemistry 909 (February): 116140. https://doi.org/10.1016/j.jelechem.2022.116140.

Zhang, Jin, William Hodge, Cindy Hutnick, and Xianbin Wang. 2011. “Noninvasive Diagnostic Devices for Diabetes through Measuring Tear Glucose.” Journal of Diabetes Science and Technology 5 (1): 166–72. https://doi.org/10.1177/193229681100500123.

Zhang, Jingjing, Zhe Shen, Yu Xiang, and Yi Lu. 2016. “Integration of Solution-Based Assays onto Lateral Flow Device for One-Step Quantitative Point-of-Care Diagnostics Using Personal Glucose Meter.” ACS Sensors 1 (9): 1091–96. https://doi.org/10.1021/acssensors.6b00270.

Zhang, Liding, Ying Su, Xiaohan Liang, Kai Cao, Qingming Luo, and Haiming Luo. 2023. “Ultrasensitive and Point-of-Care Detection of Plasma Phosphorylated Tau in Alzheimer’s Disease Using Colorimetric and Surface-Enhanced Raman Scattering Dual-Readout Lateral Flow Assay.” Nano Research 16 (2): 1–11. https://doi.org/10.1007/s12274-022-5354-4.

Zhang, Suxia, Nü Wang, Huijun Yu, Yaming Niu, and Changqing Sun. 2005. “Covalent Attachment of Glucose Oxidase to an Au Electrode Modified with Gold Nanoparticles for Use as Glucose Biosensor.” Bioelectrochemistry 67 (1): 15–22. https://doi.org/10.1016/j.bioelechem.2004.12.002.

Zhang, Wenjun, Yunqing Du, and Ming L. Wang. 2015. “On-Chip Highly Sensitive Saliva Glucose Sensing Using Multilayer Films Composed of Single-Walled Carbon Nanotubes, Gold Nanoparticles, and Glucose Oxidase.” Sensing and Bio-Sensing Research 4 (June): 96–102. https://doi.org/10.1016/j.sbsr.2015.04.006.

Zhao, Hui, Yuming Dong, Pingping Jiang, Guangli Wang, and Jingjing Zhang. 2015. “Highly Dispersed CeO2 on TiO2 Nanotube: A Synergistic Nanocomposite with Superior Peroxidase-like Activity.” ACS Applied Materials and Interfaces 7 (12): 6451–61. https://doi.org/10.1021/acsami.5b00023.

Zheng, Jie, Min Zhu, Jiao Kong, Zimu Li, Jianming Jiang, Yachao Xi, and Fang Li. 2022. “Microfluidic Paper-Based Analytical Device by Using Pt Nanoparticles as Highly Active Peroxidase Mimic for Simultaneous Detection of Glucose and Uric Acid with Use of a Smartphone.” Talanta 237 (October 2021): 122954. https://doi.org/10.1016/j.talanta.2021.122954.

Zheng, Xufeng, Fanrou Zhang, Kun Wang, Wei Zhang, Yige Li, Yue Sun, Xiaolin Sun, et al. 2021. “Smart Biosensors and Intelligent Devices for Salivary Biomarker Detection.” TrAC - Trends in Analytical Chemistry 140: 116281. https://doi.org/10.1016/j.trac.2021.116281.

Zou, Hongyan, Tong Yang, Jing Lan, and Chengzhi Huang. 2017. “Use of the Peroxidase Mimetic Activity of Erythrocyte-like Cu1.8S Nanoparticles in the Colorimetric Determination of Glutathione.” Analytical Methods 9 (5): 841–46. https://doi.org/10.1039/c6ay03034c.

Appendix

First, in this section, further experiments and characterization of the materials used in the synthesis have been examined. Furthermore, the effect of the concentration of the produced solution of AuNPs-pTab was extensively studied to analyze the impact of gold concentration on the peroxidase and catalytic activity of gold metal. Moreso, the assessment of using different concentrations of pullulan in the direct synthesis of AuNPs-pTab was included. Evaluation of the oven temperature and humidity in AuNPs-pTab formation were highlighted. The attempts to encapsulate the chromogenic substrate (TMB) + McIlvaine buffer were added to the study. Finally, the formulas used for calculation and some software procedure used in this work were listed at the end of this section.

A1. Studying the difference between Alkali-treated and untreated pullulan

Pullulan solution color was highly affected by the addition of NaOH. It was found that heating pullulan solution alone at 90 °C for 30 min remained colorless until treated with NaOH where the color turned yellow as shown in (Figure A1-1).

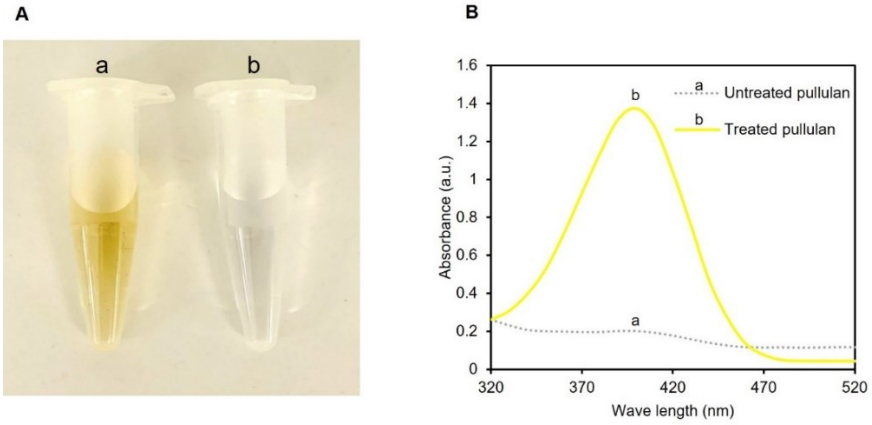

Figure A1-1 *The difference between Alkali-treated and untreated pullulan solution. A) a) treated pullulan solution with NaOH. b) Pullulan solution alone. B) The absorbance spectra for a) Alkali treated pullulan (yellow color) absorption band at 400 nm. b) non-alkali treated pullulan (colorless) has an absorption band of 298 nm.*

A2. Evaluation of AuNPs-pSol concentration on peroxidase-like activity for glucose detection

The peroxidase-like activity of two concentrations of AuNPs-pSol was evaluated for glucose detection. It was found that the high concentration of AuNPs-pSol (~22 nM) produced more blue color intensity when performing the glucose test while 6.5 times less than the original AuNPs-pSol

concentration (~3.3 nM) produced less blue color as shown in (Figure A2-1). However, the peroxidase-like activity of AuNPs-pTab still appeared in the solution color turning into blue even though the solution concentration was decreased. The results were measured at 652 nm after 30 min of the test at room temperature using UV-vis spectroscopy.

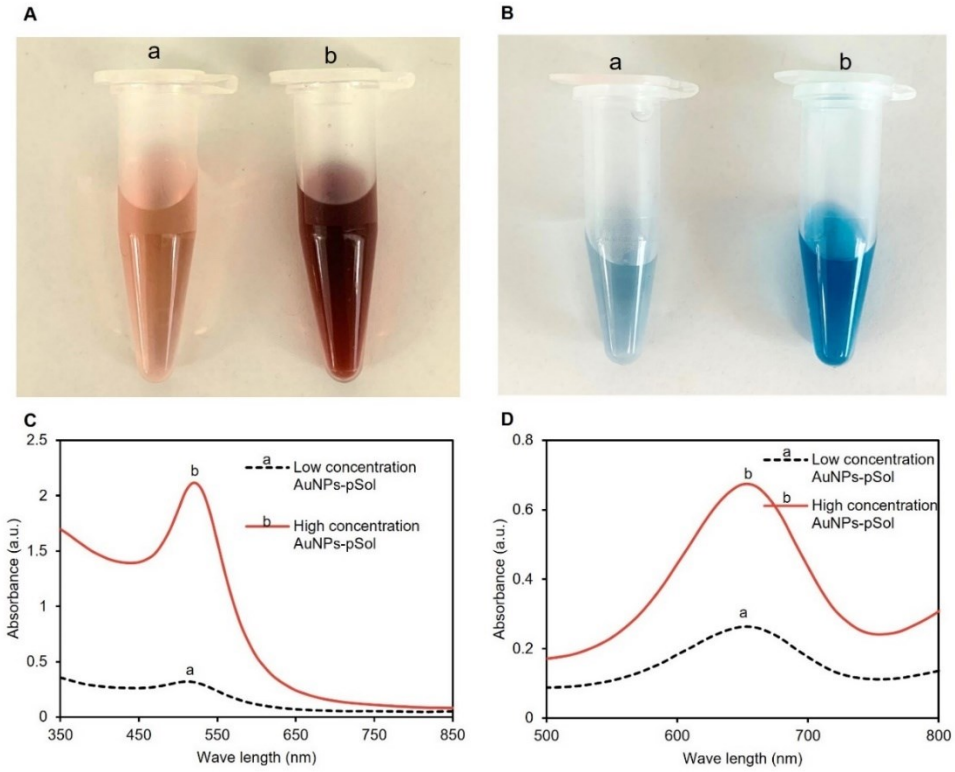

Figure A2-1 *The effect of pullulan AuNPs concentration on the peroxidase-like activity.* ***A)*** *The concentration in a) is 6.5 times less than the concentration in b).* ***B)*** *The corresponding peroxidase activity of AuNPs-pTab: a) low concentration. b) high concentration.* ***C)*** *The corresponding UV-vis spectroscopy measurement for picture A shows a higher peak at 520 nm due to the higher concentration than of AuNPs-pSol depicted in b.* ***D)*** *The corresponding UV-vis spectroscopy measurement for picture B shows a higher peak at 652 nm due to the higher concentration of AuNPs-pSol when performing the glucose detection.*

A3. Fabrication of AuNPs-pTab using 1 and 2% of pullulan (wt/v)

Synthesis of AuNPs-pSol using 1 and 2% of pullulan (wt/v). The results present that successful solutions were obtained following the same mentioned method. Many attempts were done to produce red (unaggregated) tablets. However, casting the 1 and 2% AuNPs-pTab didn't end successfully were the obtained tablets were fragile and stuck on the tray after drying. Furthermore, the AuNPs-pTab formed using 1% pullulan (wt/v) were fully aggregated (blue color) while

partially (purple color) aggregated AuNPs-pTab were observed in the case of using 2% pullulan (wt/v) as indicated in absorption at 520 nm and displayed in (Figure A3-1).

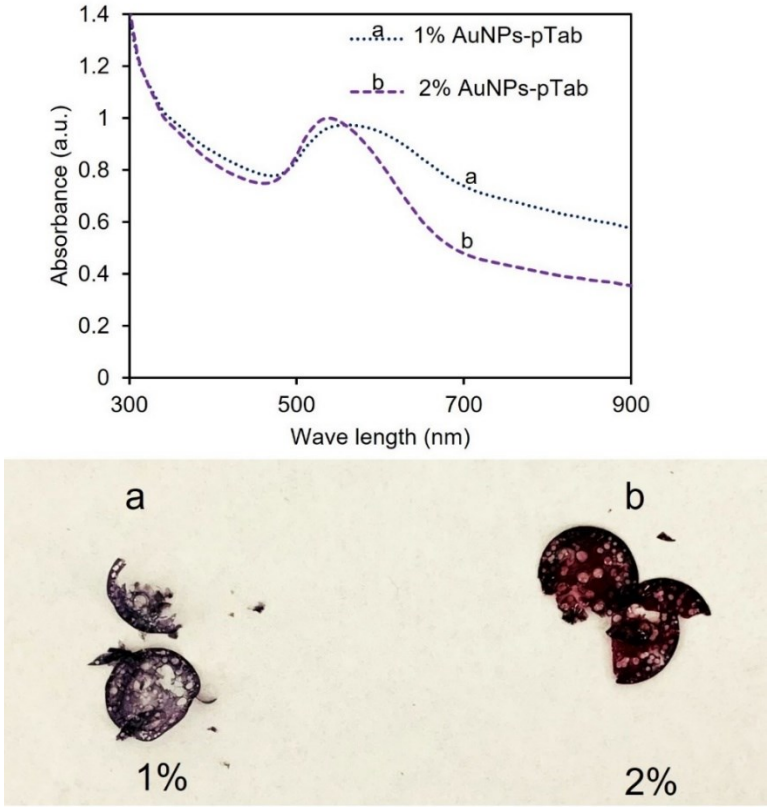

Figure A3-1 *Fabrication of AuNPs-pTab using 1 and 2% pullulan (wt/v). a) synthesis of AuNPs-pSol using 1% of pullulan (wt/v) produced an aggregated (blue color) and very delicate AuNPs-pTab. b) synthesis of AuNPs-pSol using 2% pullulan (wt/v) formed a partially aggregated (purple color) AuNPs-pTab indicating this pullulan concentration is not enough to produce good properties tablets.*

A4. Studying the effect of oven temperature in AuNPs-pTab formation

The effect of temperature on AuNPs-pTab formation was extensively studied. It was observed that when increasing the oven temperature above 60 °C, the tablets appeared to have a hollow center with bubbles which diminish from their rigidity indicating this temperature was not suitable for tablet drying as shown in (Figure A4-1). Furthermore, partial aggregation in some tablets of AuNPs-pTab was noticed using the UV-vis spectroscopy after dissolving the AuNPs-pTab in water producing inconsistency of tablet production. Therefore, monitoring the temperature while fabricating AuNPs-pTab has a great influence on their last properties.

Figure A4-1 *The effect of using high temperature in AuNPs-pTab formation. indicating fragile tablets.*

A5. Examining the effect of humidity in AuNPs-pTab

The effect of humidity on AuNPs-pTab was further examined. The test was based on placing the tablets on plastic or glass surfaces in a humid area with water vapor (closed box with a cup of boiling water inside) for 6 h. The results indicated that the AuNPs-pTab in both cases were stuck on the surface indicating that humidity has a great influence on AuNPs-pTab as displayed in (Figure A5-1).

Figure A5-1 *The effect of humidity on AuNPs-pTab. Humidity has a great influence on AuNPs-pTab where water vapor caused the tablets to stick to the surface.*

A6. Fabrication of AuNPs-pTab using 5% and 6% pullulan (wt/v)

Trials of using different concentrations of pullulan (5 and 6%) to produce higher enzymatic activity of AuNPs-pTab. It was obvious that using 5% and 6% pullulan in the synthesis process produces low catalytic activity tablets which were clear from the absence of the blue color in the corresponding solution when used for glucose detection. Even though a blue color was formed within 5 h of the test, the time was an issue, so these concentrations were excluded from the glucose essay. This slow color formation was anticipated by the existence of pullulan polymer (thicker layer) around the AuNPs which hinders the catalytic activity (Hirai and Yakura 2001)(Treuel et al. 2012) as shown in (Figure A6-1).

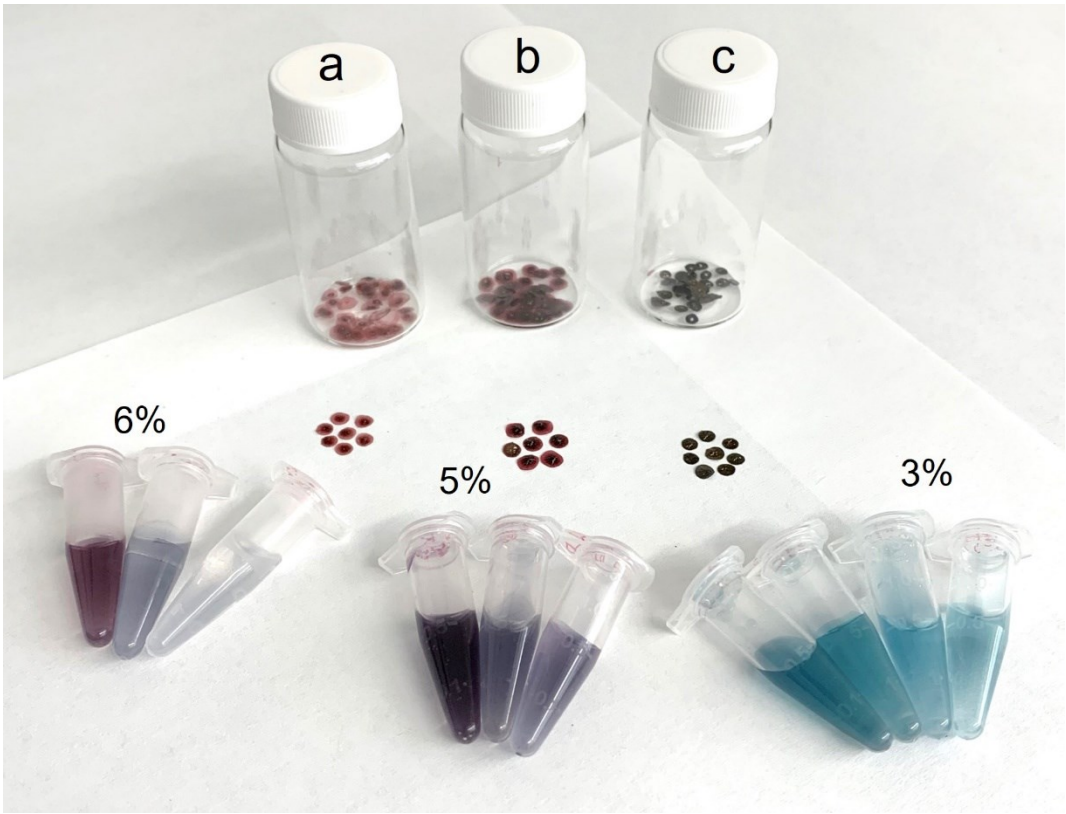

Figure A6-1 *The synthesis of AuNPs-pTab using different concentrations of pullulan (5, 6, and 3%) to examine the peroxidase/enzymatic activity of these tablets for glucose detection. No peroxidase-like activities were observed in the case of using: a) 5% of pullulan (middle of picture) and b) 6% of pullulan (left of picture), while high enzymatic activity was observed in c) 3% of pullulan (right of picture).*

A7. Encapsulation of TMB and McIlvaine buffer

To make the glucose assay easier to operate and transportable. Many trials to encapsulate the TMB + McIlvaine buffer was performed using 3% pullulan (wt/v). 1 mL of TMB working solution was mixed with 3% pullulan powder and vortexed till completely dissolved. The mixture was cast into tablets in a un sticky tray and placed in an oven at 60 °C. The tablets were checked every 15 min to make sure it is fully dried. Unexpectedly, the formed tablets were yellow in color and stuck on the tray even after 2 h of drying in the oven as shown in (Figure A7-1). Thus, this encapsulation method was not successful, and more studies should be done to make the tablet drier and can be taken out easily from the tray.

Figure A7-1 *Encapsulation of TMB and McIlvaine buffer using 3% pullulan (wt/v). The formed tablets were sticky after fully drying indicating the failure of the encapsulation method.*

A.8 List of formulas and software

The following formulas were used in the calculation:

- Beer's Lambert law:

$$A = \varepsilon c l ,$$

where A is the absorbance, ε is the molar extension coefficient of TMB, l is the path length.

- Michaelis Menten's model was plotted by calculating the concentration of TMB from Beer's Lambert law. Then, the reaction rate was obtained using:

$$Reaction\ Rate = \frac{Change\ in\ concentration}{Change\ in\ time} \ ,$$

$$v_0 = v_{max}\frac{[S]}{K_m} + [S] \ ,$$

where v_0 is the initial velocity, v_{max} is the maximum velocity, [S] is the substrate concentration, and K_m is the Michaelis Menten's constant.

- The percent recovery R% was calculated according to the following formula:

$$R\% = \left(\frac{Concentration\ found}{concentration\ spiked}\right) \times 100\% \ .$$

- To calculate the Relative Standard Deviation RSD%, the mean and the standard deviation (SD) should be calculated first:

$$SD = \frac{\sqrt{(\text{concentration 1 found} - \text{the mean})^2 + (\text{concentration 2 found} - \text{the mean})^2 + \cdots}}{\text{n}-1}$$

$$RSD\% = \frac{SD}{the\ mean} \times 100$$

IC_{50} calculation:

To determine the IC_{50} of a substance, a dose-response curve is generated and the interaction between the substance and inhibitor is analyzed at varying concentrations. The IC_{50} values for specific inhibitors are then calculated by identifying the concentration required to reduce 50% of the maximum response from the substance, as shown on the dose-response curve. Typically, a higher level of inhibition at a fixed concentration of inhibitory substances indicates a lower drug response and, consequently, a smaller IC_{50} value.

To calculate the IC_{50} value, follow the steps:

1. generate the dose-response curve for the analyte vs. Absorbance (X vs. Y) in Excel. Use the "Log" function for the X-axis values. The resulting curve should demonstrate an S-shape.

2. use the following formula to obtain the value for IC_{50} by inserting the values for Y and X from the curve. While the Hill coefficient can be found in the curve fitting software.

$$Y = Min + \frac{Max - Min}{\left(1 + X^{IC50}\right)^{Hill\ coefficient}},$$

where Min and Max are displayed in the following figure.

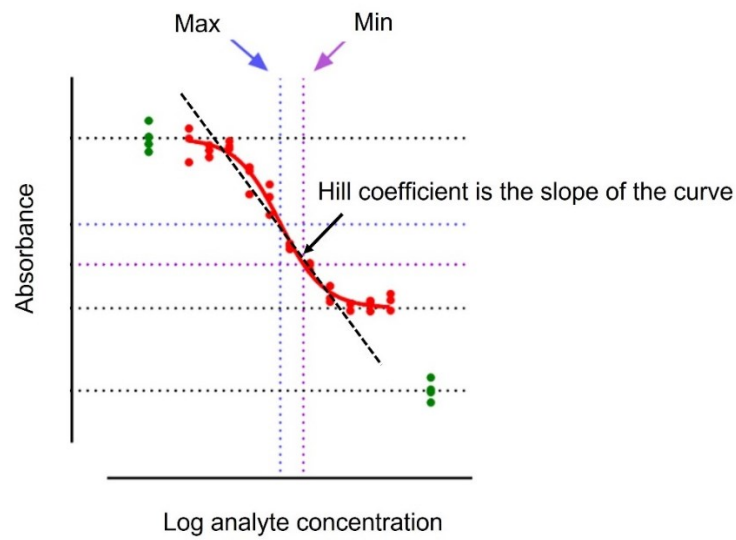

The best curve fitting software that can be used is “Curve Fit Professional”.

LoD calculation:

Several methods can be used:

A) The easiest and most straightforward method is using the regression function in Excel.

1. Go to Data > Data analyses > regression > A window will open asking to select X, and Y. A sheet will appear as shown below.

2. Use the values for standard error (SE) and Slope from the sheet and apply them to the formula (LoD = 3*SD/slope) to calculate the LoD. Standard deviation (SD)=SE*SQRT(N) were SQRT(N) is the square root of number of readings.

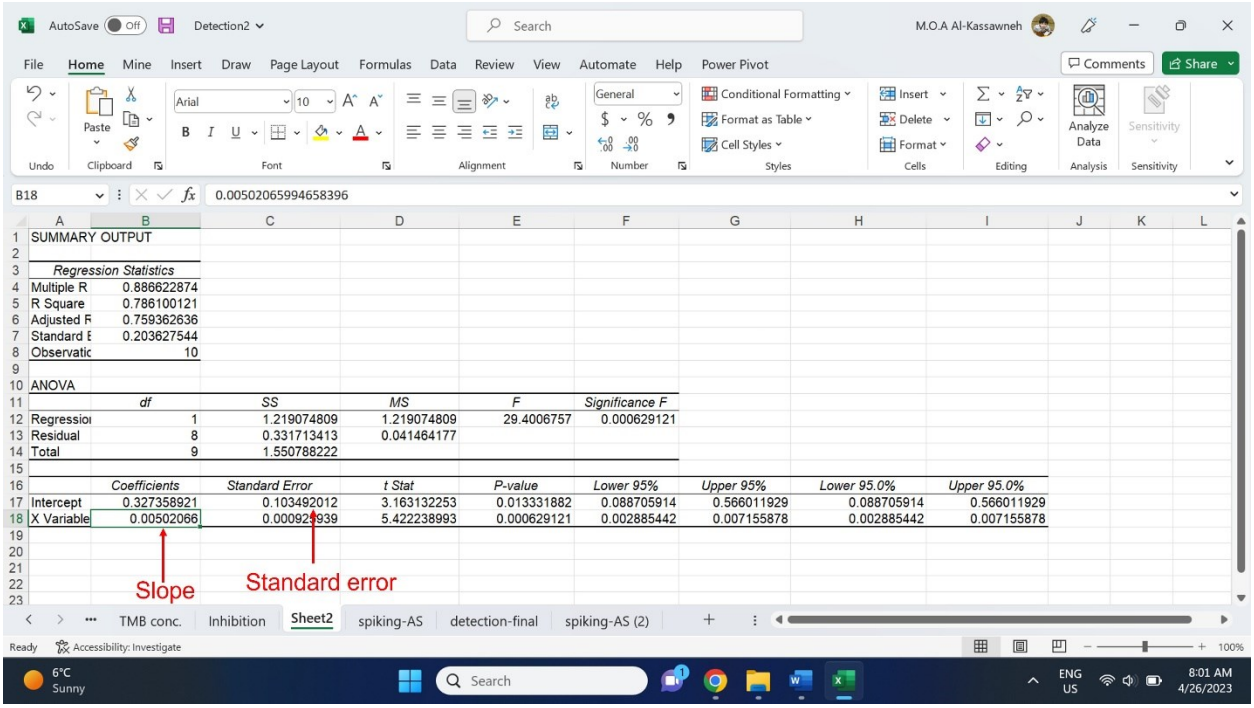

SUMMARY OUTPUT								
Regression Statistics								
Multiple R	0.886622874							
R Square	0.786100121							
Adjusted R	0.759362636							
Standard E	0.203627544							
Observatic	10							
ANOVA								
	df	*SS*	*MS*	*F*	*Significance F*			
Regressioı	1	1.219074809	1.219074809	29.4006757	0.000629121			
Residual	8	0.331713413	0.041464177					
Total	9	1.550788222						
	Coefficients	*Standard Error*	*t Stat*	*P-value*	*Lower 95%*	*Upper 95%*	*Lower 95.0%*	*Upper 95.0%*
Intercept	0.327358921	0.103492012	3.163132253	0.013331882	0.088705914	0.566011929	0.088705914	0.566011929
X Variable	0.00502066	0.000929939	5.422238993	0.000629121	0.002885442	0.007155878	0.002885442	0.007155878

B) Using the STDEV.S and SLOPE functions in Excel. Choose a place to insert your data. Press "= STDEV.S" then take the average. Press "=Slope". You will have the values for the SD and Slope which can be applied in the same formula (LoD = 3*SD/slope).

To use ImageJ to calculate the color intensity and measure the particle size.

A) To measure the color intensity:

1. Upload ImageJ software.

2. Go to File > Open > Image. An icon will appear asking to upload a photo. Choose the picture that you want to calculate the color intensity. Then, the selected image will appear. You can enlarge the pictures to facilitate the next step.

3. In the bar available in ImageJ, choose the type of cut to be used in the area for color intensity.
4. Afterward, go to Analyze> Histogram. An icon will appear showing a graph for RGB color values. Choose "Live" then press "RGB".

5. You can press many times to take the RGB color values for the colors Red, Green, and Blue. Note down the "Mean" values for each color. These values can be used to plot a curve by inserting analyte concentration vs color Intensity.

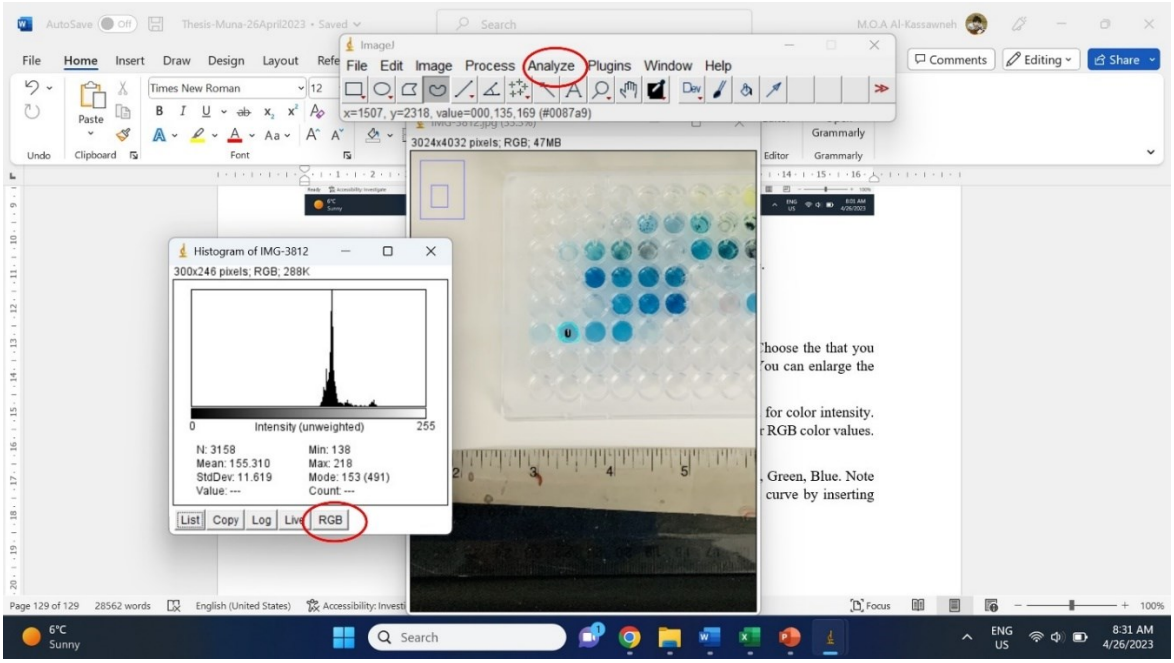

B) To calculate the particle size diameter:

1. Go to File> New> choose the TEM image that you want.
2. Enlarge the picture and maintain the same size or the diameter will be different each time.
3. From the bar, choose the line and draw a line inside the particle to measure the diameter.
4. Press Ctrl+M. The diameter will appear in another window.
5. Count the whole particle's diameter in the picture following the same procedure.
6. Take these values into Excel and calculate the average using the average function in Excel.

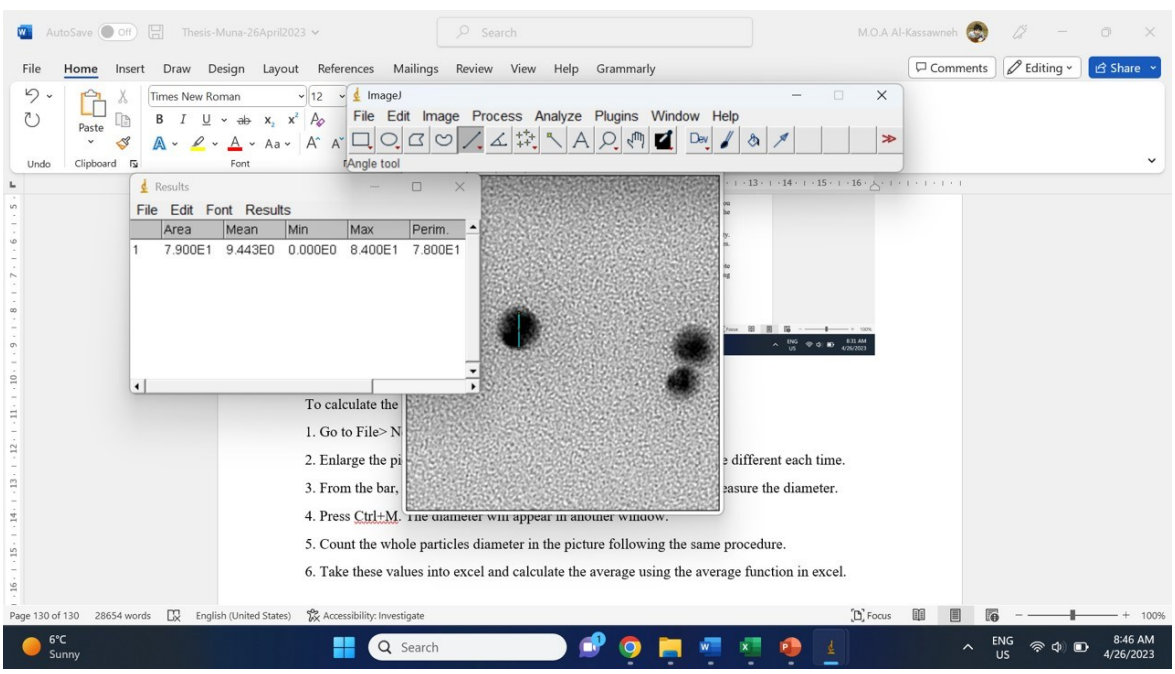

To use InkScape to change the image's scale bar without affecting the image's resolution, follow the steps:

1. Download the InkScape software.

2. Choose “File”>” Open” by choosing the image you want to insert the scale bar on or drag an image into the software.

3. On the left-hand side of the software, draw a square or any shape according to what you want.

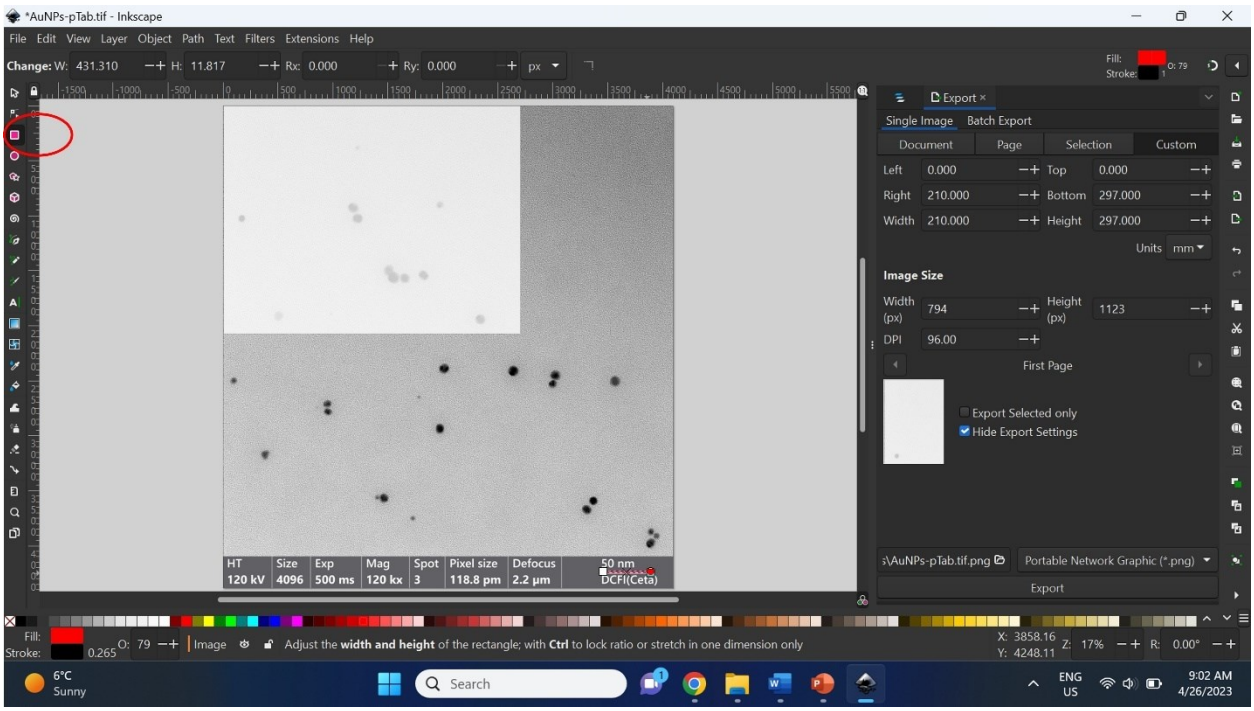

4. Select the square and employ “Fill and Stroke” from “Object” on the top of the software. Then, reduce the color intensity from the down bar part to see through the image.

5. On the left side of the vertical bars. Choose the red square icon to draw a line that matches the scale bar and add it to the image. You can choose any color you want.

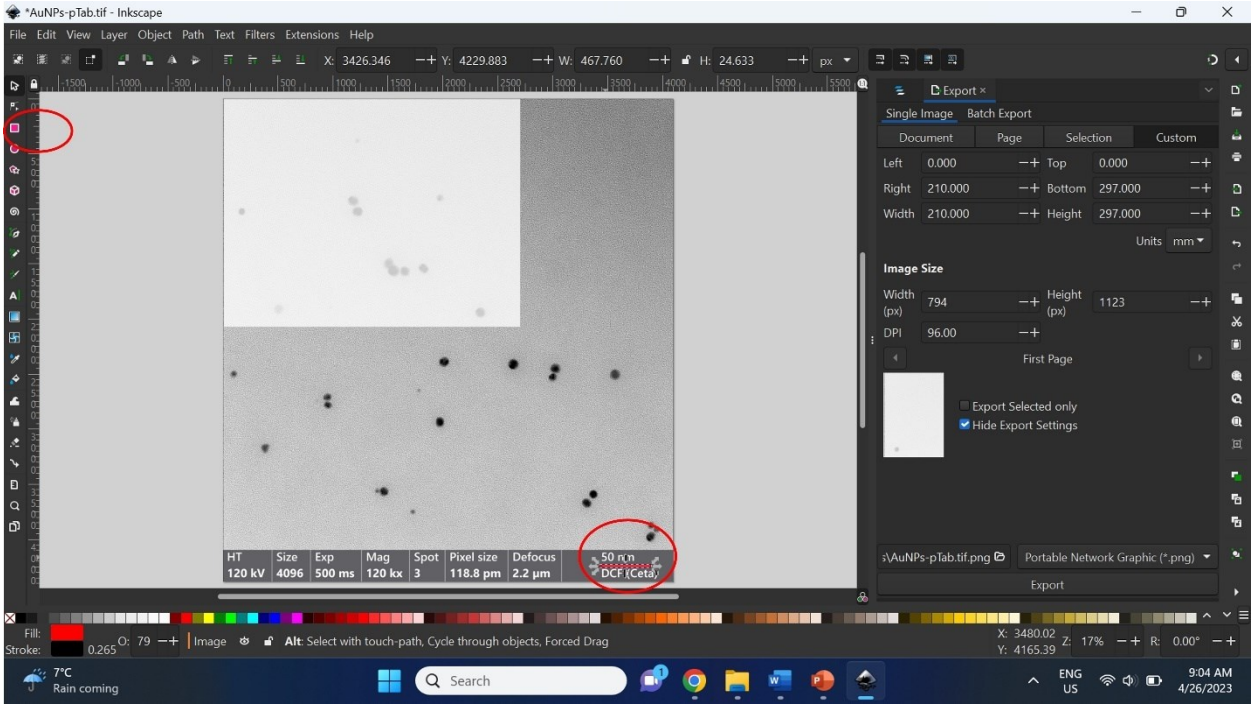

6. Move the transparent triangle and change the color to black by selecting the transparent square and choosing the icon in red from the upper-left part of the software as appeared in the following picture.

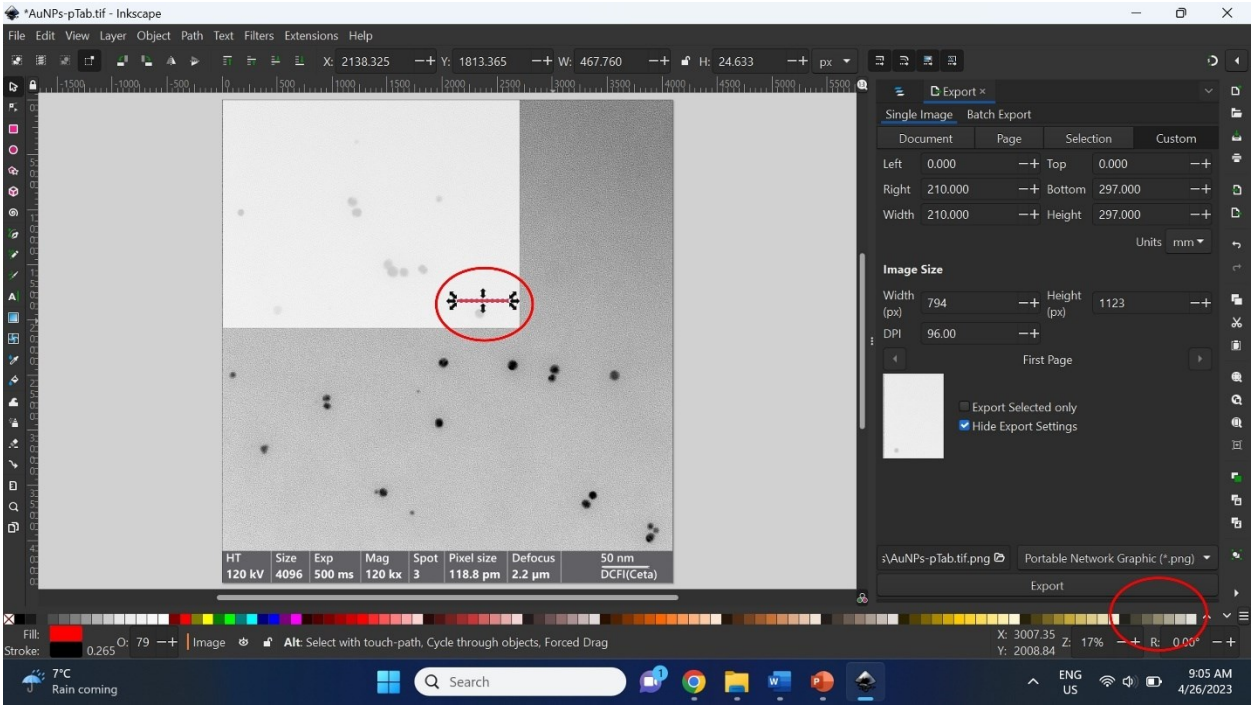

7. Go to “Group” > “Clip” > “Set Clip”. Or press Ctrl + G to group the picture.

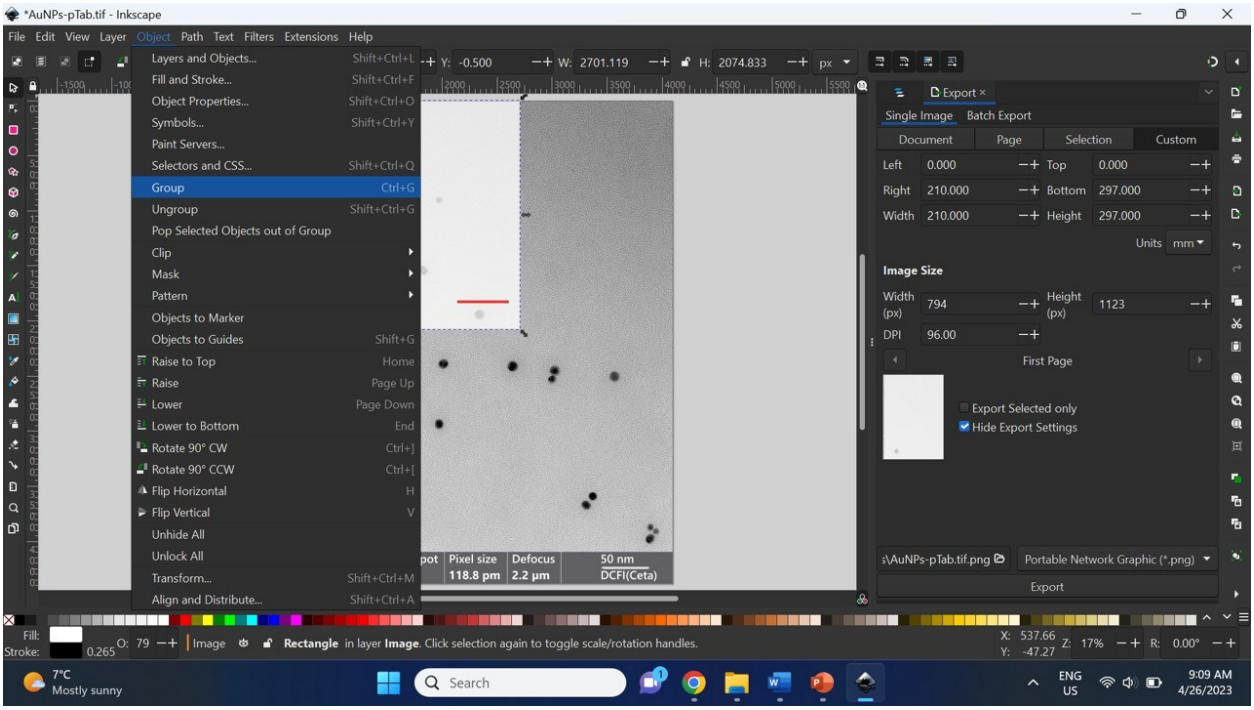
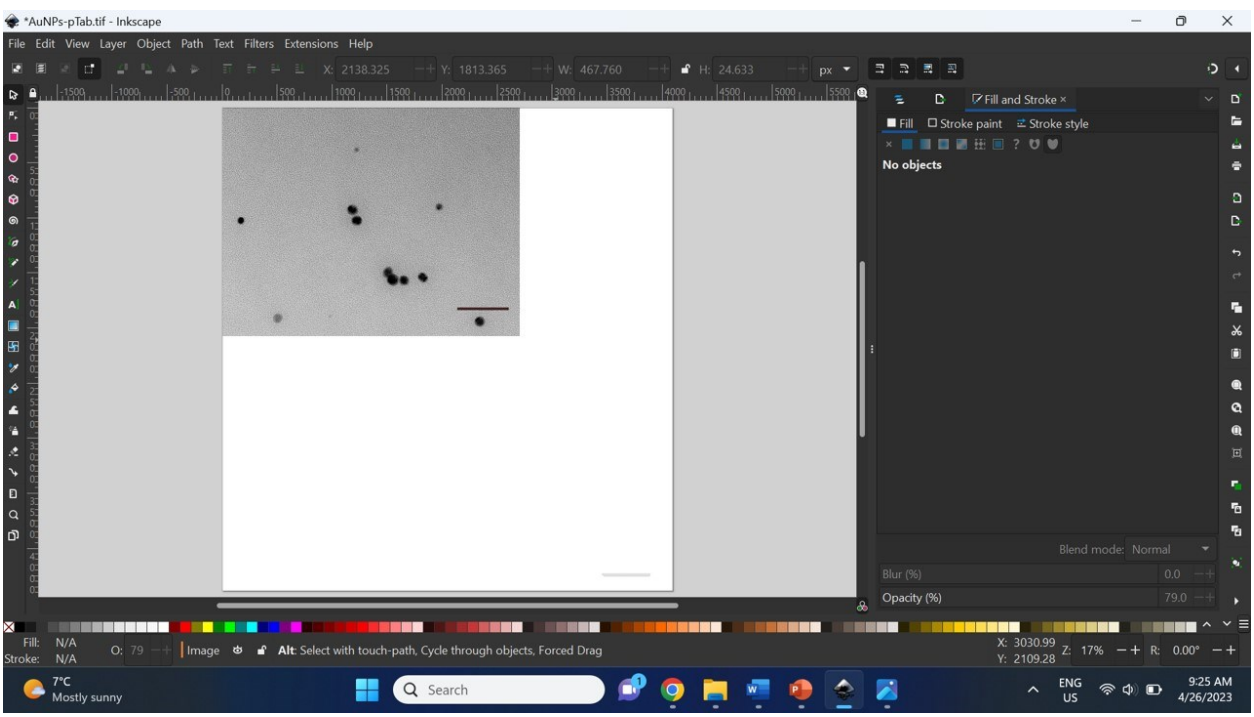
8. Save the modification and export the picture with the scale bar. You can increase/decrease the picture as much as you want without affecting the scale bar.